KINEMATICS OF DELİCE-KOZAKLI FAULT ZONE (NORTH CENTRAL ANATOLIA, TURKEY)

A THESIS SUBMITTED TO
THE GRADUATE SCHOOL OF NATURAL AND APPLIED SCIENCES
OF
MIDDLE EAST TECHNICAL UNIVERSITY

BY

BÜLENT TOKAY

IN PARTIAL FULFILLMENT OF THE REQUIREMENTS
FOR
THE DEGREE OF MASTER OF SCIENCE
IN
DEPARTMENT OF GEOLOGICAL ENGINEERING

AUGUST 2015

I hereby declare that all information in this document has been obtained and presented in accordance with academic rules and ethical conduct. I also declare that, as required by these rules and conduct, I have fully cited and referenced all material and results that are not original to this work.

Name, Last name : Tokay Bülent

Signature:

ABSTRACT

KINEMATICS OF DELİCE-KOZAKLI FAULT ZONE (NORTH CENTRAL ANATOLIA, TURKEY)

Tokay, Bülent

M.Sc., Department of Geological Engineering
Supervisor : Prof. Dr. Erdin Bozkurt
Co-supersivor: Prof. Dr. Nuretdin Kaymakcı

August 2015, 99 pages

The Central Anatolian Crystalline Complex (CACC) forms a part of Alpine orogenic belt in Turkey and incorporates three major massifs and several basins that developed during extension commenced by the Late Cretaceous. They were deformed during subsequent collision of Anatolide-Tauride Platform and Pontides. The deformation of the region has resulted in the break-up of the CACC along major deformation (fault) zones. The present study aims to test existence of one of these fault zones, namely Delice-Kozaklı fault zone.

Several structures are mapped and their geometric analyses are carried out. The structures include: (i) a syncline with axis trending in 070º; (ii) syncline and anticline with axes trending in 160º; (iii) approximately NW−SE-trending plunging fold sets; (iv) E−W-trending anticline and syncline; (v) NW−SE-trending overturned folds; (vi) a NW−SE-trending (130º) and NNW−SSE-trending right-lateral strike-slip faults and (vii) WNW−ESE-trending north-verging reverse faults. Several fault plane data has been collected from the basement rocks and basin infill for kinematic analysis. Paleostress analysis and the stratigraphic data suggests two deformation phases: (1) NW−SE compression that lasted by middle Oligocene and (2) a post-Oligocene NNE−SSW compression that gave rise to a dextral transpressional deformation.

The common results of the geometric and kinematic analyses of the structural data argues for the existence of the Delice-Kozaklı fault zone and that the study area has stayed within same deformation zone during NW−SE and then NNE−SSW compressional phases.

Keywords: Delice-Kozaklı fault zone, Çiçekdağ Basin, structural analysis, kinematic analysis, deformation zone.

ÖZ

DELİCE-KOZAKLI FAY ZONU'NUN KİNEMATİĞİ (KUZEY ORTA ANADOLU, TÜRKİYE)

Tokay, Bülent

Yüksek Lisans, Jeoloji Mühendisliği Bölümü
Tez Yöneticisi : Prof. Dr. Erdin Bozkurt
Ortak Tez Yöneticisi: Prof. Dr. Nuretdin Kaymakcı

Ağustos 2015, 99 sayfa

Alpin orojenez kuşağında yeralan Orta Anadolu Kristalin Kompleksi, üç ana masifi ve birçok havzayı barındırmaktadır. Bu havza ve masifler, Geç Kratese'den beri açılma süresinde gelişmiş, sonrasında Anatolid-Torid ile Pontid çarpışmasının devamı ile deforme olup, evrimleşmiştir. Bölgenin deformasyonu Orta Anadolu Kristalin Kompleksi'nin parçalanmasına ve ana deformasyon zonların oluşmasına neden olmuştur. Bu çalışma, bahsedilen bu zonlardan biri olan Delice-Kozaklı fay zonu'nun varlığını test etmeyi amaçlamaktadır.

Çalışma alanlarında gözlemlenen ana yapıların geometrik analiz yapılmıştır. Bu yapılar: (i) 070º uzanımlı senklinal, (ii) 160º yönelimli antiklinal ve senklinal, (iii) yaklaşık olarak KB−GD doğrultulu dalımlı kıvrım grupları, (iv) D−B uzanımlı antiklinal ve senklinaller, (v) KB−GD doğrultulu yatık kıvrımlar, (vi) KB−GD (130º) ve KKB−GGD doğrultulu sağ-yanal atımlı faylar ve (vii) BKB−DGD doğrultulu ters faylar olarak sıralanabilirler. Temel ve basen dolgusu birimlerden ölçülen çok sayıdaki fay düzlemi verilerinin kinematik analiler gerçekleştirilmiştir. Paleostres analizlerin stratigrafik veriler ile desteklendiği bu çalışmada iki deformasyon evresi tanımlanmıştır: orta Oligosen'e kadar etkin olan KB–GD sıkışmalı rejim ile takip eden dönemde gelişen Oligosen sonrası gelişen ve sağ yönlü transpresyonel deformasyona neden olan KKD–GGB sıkışmalı rejim.

Geometrik ve kinematik analizlerden elde edilen sonuçlar Delice-Kozaklı fay zonu'nun varlığını desteklerken, KB–GD ve KKD–GGB sıkışmalı rejimler süresince çalışma alanlarının aynı deformasyon zonu içinde kaldığını savlamaktadır.

Anahtar Sözcükler: Delice-Kozaklı fay zonu, Çiçekdağ Havzası, yapısal analiz, kinematik analiz, deformasyon zonu

To my brothers,

Mesut and Ramazan

ACKNOWLEDGEMENT

I have to thank my supervisor, Erdin Bozkurt, for all his support. He created facilities to ease my doing for the study whenever I requested. His constructive and critical comments on what I had done provided me to revise and improve my works and thoughts. I am also grateful to him for his patience which created a floor I can study independently.

I am particularly indebted to Nuretdin Kaymakcı for supporting my field study in each aspects. Hadn't he gave opportunities technically and scientifically, I could not have written this thesis.

Special thanks go to Côme Lefebvre for all helpful discussions in the field as well as wherever I wanted him to evaluate my opinions. He always encouraged me how to approach any problems broadly and like a mentor helped me ever since we met.

I would like to thank Jure Žalohar for his leading discussions and contributing suggestions on the analysis of stress and strain based on fault-slip data.

I thank my brother, Ramazan Tokay, for his assisting me as a non-geologist without complaining about hell-like temperature during the field studies he could attend.

I am profoundly grateful to my wife Merve for supporting me ever in every aspects throughout my study.

The thesis was supported by CD-CAT (Continental Dynamics: Central Anatolian Tectonics) Project which is funded by NSF (National Science Foundation). The award number is **1109762**.

TABLE OF CONTENTS

LIST OF FIGURES

FIGURES

CHAPTER 1

INTRODUCTION

1.1 Purpose and Scope

Post-Paleozoic evolution of Turkey is dominated by continental fragments that rifted-off from the northern margin of Gondwana during closure of the Paleotethys. The late Paleozoic to Triassic rifting and drifting of continental blocks gave way to the opening of the Neotethys. The continental blocks include Pontides in the north and was collided and amalgamated to the southern Eurasian margin possibly during the early Mesozoic (Okay *et al.*, 2015). The southern continental blocks include the Taurides and its metamorphic equivalents collectively known as Anatolides (Ketin, 1966). In central Anatolia, they comprise Kırşehir Block, which has a triangular geometry (Figure 1a) and is surrounded in the north by Pontides whereas proper Tauride units in the west, south and east; the latter is also known as Taurus Limestone Axis and comprises five isopic zones geographically from north to south they include Bozkır, Aladağ, Geyikdağı, Bolkardağı, Antalya and Alanya units (Özgül 1984). Except for the Antalya and Alanya units, all other units are transported over the Geyikdağı unit, form north to south during the Late Cretaceous (Özgül, 1976 & 1984). Among these, Bozkır unit forms structurally the highest nappes. A small part of the Kırşehir Block is the main concern of this thesis and therefore detailed description of other units lies outside the interest of this thesis.

Kırşehir Block (KB), as being part of Anatolides, is characterized by crystalline rocks and uncoformably overlaying upper Cretaceous to Recent cover units (Özgül 1984). The crystalline units of KB include: (1) relatively high-grade metamorphic rocks collectively known as Central Anatolian Metamorphics (CAM), (2) unmetamorphosed ophiolitic rocks tectonically above the CAM, collectively known as Central Anatolian Ophiolites (CAO), and (3) large igneous batholiths of granitoids and syenitoids that intrude the CAM and CAO. All of these rock units are named the Central Anatolian Crystalline Complex (CACC, Göncüoğlu *et al.*, 1991) and are nonconformably overlain by a thick upper Cretaceous to Recent sedimentary sequence that exposes within the Çiçekdağı and Ayhan-Büyükkışla basins. These basins developed directly above the CACC and is surrounded and nonconformably overlain by major central successor Anatolian basins (terminology after Ingersoll, 2012) that include Çankırı, Sivas, Ulukışla and Tuzgölü basins (Gürer & Aldanmaz, 2002; Kaymakcı *et al.*, 2009) (Figure 1).

Recent paleomagnetic studies indicate that the Kırşehir Block was originally a NNE-SSW-trending linear tectonic block that is dissected by two crustal scale transfer faults. Along these structures, pieces of Kırşehir Block underwent translational and rotational deformation that gave way to its present-day triangular geometry (Lefebvre *et al.*, 2013) (Figure 1b & c).

The fragments of the Kırşehir Block from north to south comprise Kırşehir-Kırıkkale block (KKB), Akdağ-Yozgat block (AYB) and Ağaçören-Avanos block (AAB) (Lefebvre *et al.*, 2013; Figure 1.1). Structurally, the Ağaçöre-Avanos block is separated from the Kırşehir-Kırıkkale block by Savcılı thrust zone which possibly controlled the evolution of the Ayhan-Büyükkışla basin during the segmentation and further evolution of these tectonic blocks. However, the bounding structure of the Kırşehir-Kırıkkale and the Akdağ-Yozgat blocks is not obvious. It is possibly due to a fact that this structure is covered by thick upper Miocene deposits. This zone, however, corresponds to a well-marked lineament running from the cetral part of Çankırı Basin (Kaymakcı *et al.* 2009) to central eastern margin of the Kırşehir Block. Lefebvre *et al.* (2013) named it as Delice-Kozaklı fault zone (DKFZ) and speculated that it is responsible from the translation and clockwise rotation of the Akdağ-Yozgat block. It is obvious that an important role is attributed to the DKFZ albeit no field evidence is yet documented to support its existence.

The main purpose of this study is therefore to test the hypothesis (cf. Lefebvre *et al.*, 2013) about the existence of the Delice-Kozaklı fault zone.

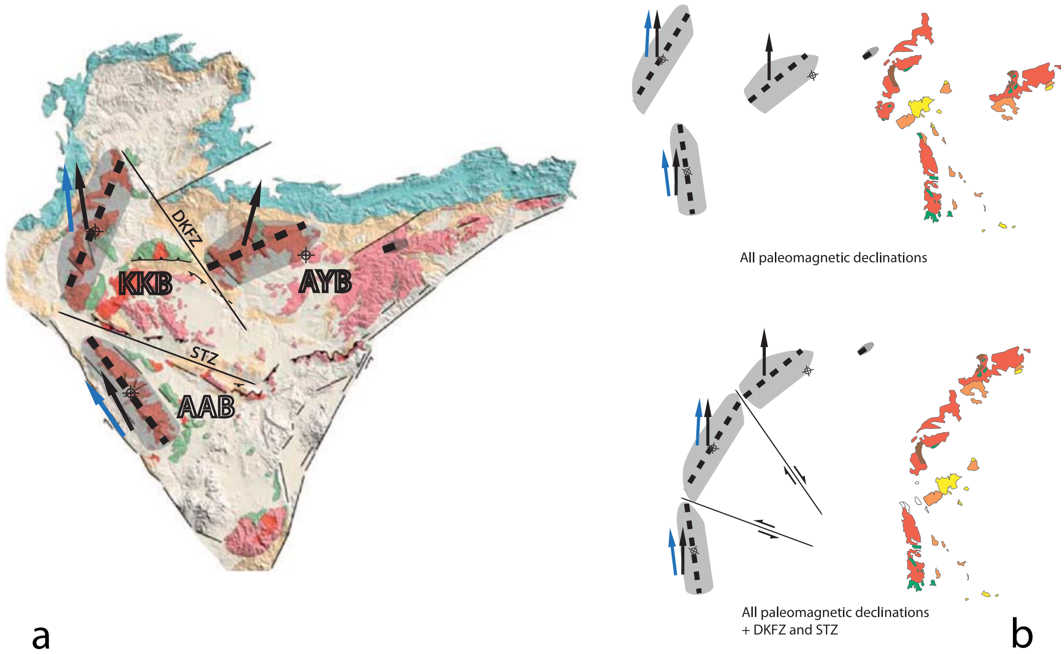

Figure 1.1. (a) The present framework of the CACC and main blocks (grey) with regard to the orientation of magmatic suites. Black arrows refer to mean declination of each block (KKB: Kırşehir-Kırıkkale, AYB: Akdağ-Yozgat, AAB: Ağaçören-Avanos). (b) The restoration of CACC by back-rotation based on the paleomagnetic data and balance among these blocks along the fault zones, STZ and DKFZ (Lefebvre *et al.*, 2013).

1.2 Location of Study Area

The Delice-Kozaklı Fault Zone extends from the central part of the Çankırı Basin to central eastern margin of the Kırşehir Block. It is covered by upper Miocene and younger deposits in its NW and SE parts. The best exposure of the fault zone is observed around the central and northeastern part of the Çiçekdağ Basin and for this reason this area formed subject of this thesis.

Geographically the study area is located NW of Yerköy (Yozgat Province) and a few km east of Mahmutlu Village of Çiçekdağı county (Kırşehir Province) (Figure 1.2).

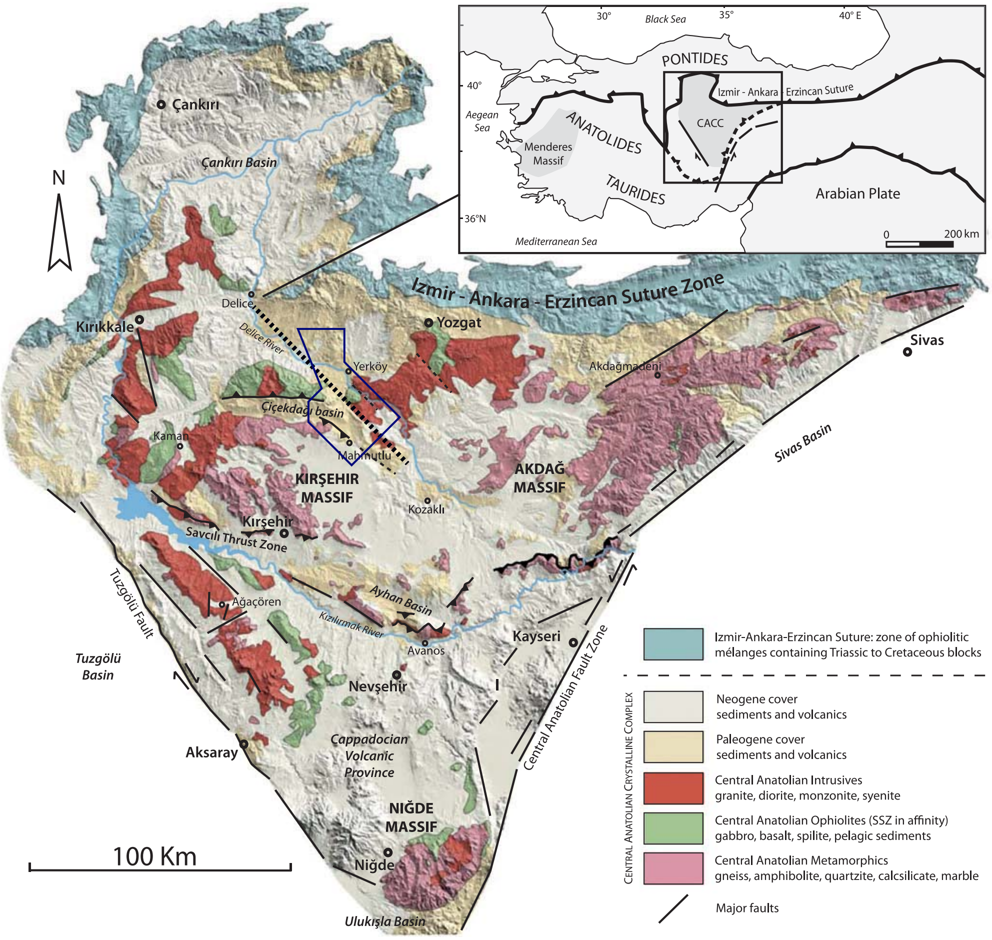

Figure 1.2. Geological map of the Central Anatolian Crystalline Complex (CACC) including the location of the study area (marked with blue line). The dashed black line is the theoretical fault. The inset map shows major tectonic subdivision of Turkey (from Lefebvre *et al.*, 2013).

1.3 Methodology

The study was performed in two stages that involve field and office works. The field studies include geological mapping, careful examination of lithological contacts, observation and measurement of geological structures and collection of fault slip data for fault kinematics. The office work includes analysis and synthesis of collected data.

1.4 Regional Tectonic Setting

Central Anatolian Crystalline Complex (CACC; Göncüoğlu *et al.*, 1991) is one of the main tectonic elements of the Turkish segment of the Alpine-Himalayan Orogenic Belt. It is sandwiched between Pontides with Laurasian affinity in the north and Taurides with Gondwana affinity in the south.

Its tectonic setting is one of the most debated tectonic blocks in Turkey. This is partly due to a fact that it undergone pervasive high-grade metamorphism during the late Cretaceous that wiped out most of the geological information about its Paleozoic and Mesozoic evolution. It collided with the Pontides along the İzmir-Ankara-Erzincan Suture Zone by the end of Cretaceous; collision and northwards convergence of the block lasted until early Miocene (Kaymakcı *et al.*, 2003, 2009; Lefebvre *et al.*, 2013; Meijers *et al.*, 2010).

In the south, it was separated from the Taurides by the Intra-Tauride Ocean which was closed by the end of Cretaceous to early Paleogene. Some researchers (e.g. Göncüoğlu *et al.*, 1991), however, argued that Intra-Tauride ocean has never been existed and that Kırşehir Block was a promontory of Taurides, which was subjected to metamorphism where degree of metamorphism in the Taurides decreases from north to south (Özgül, 1976, 1984).

Kırşehir Block comprises there metamorphic massifs. From west to east, these include Kırşehir Massif (Seymen, 1981), Akdağ Massif (Dökmeci, 1980) and Niğde Massif (Whitney & Dilek, 1997). These massifs are subjected to high-temperature medium to low pressure (HT/L-MP) metamorphism. Climax of regional metamorphism occurred at conditions up to ~8 kbar / 700°C, with local overprints at even higher temperatures (800°C) but lower pressures (3–4 kbar) around granitoid intrusions. The regional metamorphic mineral parageneses occur in a regionally pervasive, flat-lying and mildly undulating foliation that roughly follows the topography (Lefebvre, 2011; Seymen, 1982; Hinsbergen *et al.*, 2015). Exhumation of the metamorphic massifs occurred during 75–60 Ma interval (Boztuğ and Jonckheere, 2007; Gautier *et al.*, 2008; Isik, 2009; Lefebvre *et al.*, 2011). The fission-track ages from Turonian–Campanian granitoids are attributed to two different and fast stages of exhumation: the first in Early–Middle Paleocene (62–57 Ma); the second (28–32 Ma) during the Oligocene (Boztuğ & Jocnkheere, 2007). These granitoids are unconformably overlain by upper Paleocene to Lower–Middle Eocene Baraklı Formation and Miocene Kızılırmak Formation; these units are interpreted as related to the exhumation process. The first stage of exhumation was considered to relate to the collision between the CACC and Eurasia, while the second to amalgamation of CACC-Tauride-Anatolide and Arabian Plate. Based on the pattern of metamorphism, Whitney *et al.* (2001) recommended that the CACC can be separated into four blocks; Kırşehir, Akdağ, Niğde and Aksaray. The first two blocks exporiences regional Barrovian metamorphism, followed by the unroofing, folding, thrusting and intrusion during collision between the CACC and the Pontides. Their slow exhumation was associated with the erosion until the Eocene. Apatite fission track ages suggest that these massifs and Barandağ pluton (Kırşehir Block) were exhumed at ca. 47 Ma and 40 Ma in the southwestern and northeastern parts. Exhumation of Ortaköy granite occurred at 35 Ma and kyanite schist in Akdağ block at 32 Ma. (Fayon *et al.*, 2001; Whitney *et al.*, 2001). Aksaray block experienced different metamorphism as a result of widespread magmatism. As for Niğde block was subjected to a distinct type of metamorphism compared to the other blocks even though it shares almost the same lithology with the Kırşehir and Akdağ blocks. It is important to note that while three blocks were already well exhumed, the Niğde Block did not reach the surface. Whitney and Dilek (1997) ascribed it to the collision along the southern contact between the Tauride-Anatolides and the CACC, creating also a wrench zone. The discrepancy, moreover, in the positions of blocks is linked to tectonic regimes along the north and south margins. Umhoefer *et al.* (2007) proposed a model of yo-yo tectonics to exlain exhumation of the Niğde Massif. They proposed two cycles of burial and exhumation along with the existence of a wrench fault zone, i.e., CAFZ. The first cycle finished by the end of the Eocene; the second in the middle Miocene (17–9 Ma). In addition to core-complex formation and exhumation processes in the CACC, migmatization and migmatite dome formation are also considered as important processes because they have fundamental effects on the regional metamorphism and exhumation. Kırşehir and Akdağ Massifs represent dome-shaped antiforms with axes trending in NNE–SSW direction (Lefebvre, 2011). Niğde Massif incorporates a migmatic dome and a detachment fault and is interprted as a typical example of a core complex. Two structural units separated by a detachment fault exposed in the Niğde Massif: the hanging-wall rocks (lower unit) are composed of relatively low-grade metamorphosed rocks whereas upper plate, higher grade metamorphic rocks (upper unit) (Gautier *et al.*, 2008). The lower unit is so critical such that while its upper levels indicate top-to-NE/ENE shearing, its lower levels, top-to-SSW. The former is attributed to the detachment fault; the latter to migmatization during between 85–76 Ma interval. Gautier *et al.* (2008) hypothesized two scenarios to explain top-to-SSW shearing:

either local inward flow, or regional channel flow mechanisms. They favor the second scenario with regard to the presence of non-coaxial deformation and the geometric relationship between lineations and regional extension. The similar inference was made by Lefebvre (2011) using structural and paleomagnetic data. Whitney *et al.* (2007) proposed a transpressional to transtensional model associated with metamorphism within the wrench zone, thereby showing the vertical and lateral crustal motion.

The three massifs of the Kırşehir Block are tectonically overlain by ophiolites and related epi-ophiolitic deposits, obducted onto the KB. The emplacement of the ophiolitic rocks is responsible from the deep burial and metamorphism. The northward subduction of the northern branch of Neothetys, which was opened in Triassic (Şengör and Yılmaz, 1981), initiated during Cenomanian–Turonian (Görür *et al*., 1984). Ophiolite emplacement on the passive margin of the Gondwana is attributed to the collision CACC and the Tauride-Anatolide Platform (Okay *et al.* 1996). The obduction of ophiolites took place after the major regional metamorphism of the CACC since evidence for a retrograde dynamo-metamorphism are available along the tectonic contact between central Anatolian ophiolites (CAO) and central Anatolian metamorphics (CAM) (Yalınız & Göncüoğlu, 1998). More recently, Lefebvre (2011) stated that the ophiolites were emplaced onto the CACC before the peak regional metamorphism that later influenced both CAM and CAO. Okay *et al.* (1996) claimed, based on $^{40}Ar/^{39}Ar$ dating in metamorphic soles that the decollement of oceanic crust occurred in Aptian, at ca. 118 Ma.

There are several different views about the age of ophiolite emplacement; the claims are: (i) late Createcous (Görür *et al.,* 1984); (ii) late Campanian–Maastrichtian (Göncüoğlu & Türeli, 1994); (iii) 93–91 Ma based on $^{40}Ar/^{39}Ar$ age (amphibole) (Dilek *et al.,* 1994) – the ages are obtained from metamorphic soles; (iv) post Early Santonian–pre-Late Maastrichtian (Yalınız & Göncüoğlu, 1998); (v) 95–90 Ma (Lefebvre, 2011); (vi) post-Turonian–Santonian (Erdoğan *et al.*, 1996) or (vii) Late Cretaceous (Advokaat *et al.*, 2014). Nonetheless, Şengör & Yılmaz (1981) suggested that the obduction should have ended sometime before the Maastrichtian. Lefebvre (2011), on the other hand, claimed that the obduction was associated with metamorphism and magmatism during late Cretaceous. Similarly, Işık *et al.* (2008) attested, based on $^{40}Ar/^{39}Ar$ data, that the ophiolite emplacement, metamorphism, the cooling of the intrusives and ductile shearing of the intrusions took place at the same time; Late Cretaceous. The common view about the origin of ophiolites is that they were derived from İzmir-Ankara-Erzincan Suture Zone (IAESZ) and then translated southward above the metamorphics during the course of collision between the Pontides and the CACC.

These metamorphic and ophiolitic rocks are intruded by various granitic and syenitic plutons during ~85–64 Ma (Şengör & Yılmaz, 1981; Özgül, 1984; Whitney *et al.*, 2001, 2003, 2007; Whitney & Hamilton, 2004). The presence of marble fragments within the intrusives in the Kırşehir Massif and the contact metamorphic aureoles around the intrusions in Akdağ Massif marbles (Erkan 1980) indicate that the regional metamorphic event(s) was followed by an intense magmatic activity. Similarly, xenotliths of crenulated garnet-silliminate-biotite schist can be also exemplified from the observations of Whitney *et al.* (2001). More, the monzogranites and granitoids intruding both CAM and CAO (Göncüoğlu & Türeli, 1994) can be used as important evidence in determining the timing of magmatism in the CACC. The radiometric age data on these magmatic rocks will be summarized in the following paragraphs.

The plutonic rocks intruding the metamorphic basement and ophiolitic rocks are substantially separated in two major groups as granitoids and syenitoids (Kadıoğlu *et al*. 2003). The former is metaluminous to peraluminous, calc-alkaline syn-collisional volcanic arc granitoids (Göncüoğlu & Türeli, 1994; Kadıoğlu *et al.*, 2003 *references herein*). Görür *et al*. (1984) maintained that arc magmatism continued from late Maastrichtian to the end of Eocene. Other workers, however, advocated these granitoids as syn-collisional to post-collisional intrusions. The latter are interpreted as alkaline with silica-undersaturated and silica-saturated types, indicating within-plate tectonic setting (Bayhan 1988; Erler and Bayhan 1995; Alpaslan and Boztuğ, 1997; Boztuğ *et al*., 1997). There are also claims that these alkaline granitoids are post-collisional and extensional intrusions (Akıman *et al.*, 1993; Erler & Bayhan, 1995; Boztuğ *et al*., 1997).

Şengör & Yılmaz (1981) pointed out that early Paleocene–Eocene the calc-alkaline arc magmatism started with the crustal thickening and metamorphism due to the ophiolite emplacement to the south. Andean-type arc type Paleocene–Early Eocene granitoids are attributed to the eastward subduction of the Inner Tauride Ocean (Görür *et al.*, 1984). Göncüoğlu and Türeli (1994) were opposed, based on the geochemical and Nd/Sr isotope data, to these opinions regarding arc magmatism. They pointed additionally that the collision during Early Upper Cretaceous led to the partial melting of lower crust, thereby resulting in post-collisional granitic magmatism with a probable contribution of S-type granites. That interpretation triggered discussions about the presence of subduction of Intra-Tauride Ocean in eastern part of the CACC. The granitic rocks are also attributed to extensional regime predating the collision between the CACC and oceanic islands during Cretaceous (Boztuğ *et al.*, 2007). Kadıoğlu *et al.* (2003) claimed that the Andean-type subduction was the cause of granitic magmatism in Ağaçören Intrusives Domain.

Moreover, Boztuğ *et al.* (2009) proposed a geodynamic model that considers oceanic island arc and the CACC collision. According to this model, the collision took place after a post-collisional extension stage between Cenomanian-Turonian and Campanian, and then, the Eurasia-CACC collision occurred in the Campanian-Maastrichtian. The last event has resulted in fast exhumation and cooling of Central Anatolian granites until Early/Middle Palaeocene.

The reported ages of these intrusions within the CACC can be listed as follows: (i) Rb-Sr whole rock isochron age of 95±11 Ma; K-Ar ages of muscovite and biotite are 78.5±1.2 Ma and 74.5±1 Ma & 77.9±1.2, respectively, (Göncüoğlu, 1986); U/Pb ages of monazite and zircon are 13.7-20 Ma (Whitney & Dilek, 1997) and 92−85 Ma, respectively, as well as $^{40}Ar/^{39}Ar$ age of 79.4 Ma from Üçkapılı granite in Niğde Massif (Whitney *et al.*, 2003); (ii) Rb-Sr whole-rock isochron age of 70.7±1.1 Ma and of 85.1±3.6 to 70.5±3.4 Ma from the Bayındır syenite in the Kaman-Kırşehir (Gündoğdu *et al.*, 1988; Kuruç, 1990); (iii) Rb-Sr whole-rock isochron age of 110±14 Ma (Güleç 1994) and $^{40}Ar/^{39}Ar$ age of 77.6±0.3 Ma (biotite) and 78.6±0.3 (amphibole) for Ağaçören granitoids; (iv) Rb-Sr whole-rock isochron age of 110±5 Ma for the Murmana pluton (Zeck & Ünlü, 1998); (v) K-Ar age (hornblende) of granite is 79.5±1.7 Ma for Behrekdağ pluton (İlbeyli *et al.*, 2004); (vi) U/Pb age of 74.1±0.7 Ma and 74.0±2.8 Ma for Çamsarı and Barandağ granitoids (Köksal *et al.*, 2004); (vii) K-Ar age (biotite) of quartz monzonite is 66.6±1.2 Ma for Cefalıkdağ pluton (İlbeyli *et al.*, 2004); (viii) U/Pb age of titanite is 77.2±0.4 Ma from granodioritic pluton and, besides, $^{40}Ar/^{39}Ar$ age of 68.8±0.9 Ma (biotite) and of 67.0±1.2 Ma (K-feldspar) from garnet-sillimanite schists in Hırkadağ (Lefebvre, 2011); (ix) K-Ar age of quartz monzonite is 67.1±1.3 Ma & 70.1±1.5 Ma (K-feldspar) and 81.5±1.9 Ma (Amphibole) for Terlemez pluton (Yalınız *et al.*, 1999); (x) U/Pb (zircon) dating points the age of 74.4±0.6 Ma for Satansarı monzonite stock (Köksal *et al.*, 2013); (xi) the age of Ekecikdağ Granitoid is interpreted as nearly late Cretaceous (Göncüoğlu & Türeli, 1994). The age range of the intrusions is predominantly between 95 and 75 Ma (Lefebvre, 2011; Advokaat *et al.*, 2014).

Kurt *et al.* (2008) reported evidence for a magmatic activity in the Ulukışla Basin. Initial intrusives are late Cretaceous in age and represented by post-collisional, extensional alkaline rocks. Moreover, calc-alkaline diorite and shoshonitic monzogabbro and trachytes cutting alkaline rocks were described and ascribed to Middle Eocene compressional tectonics, thereby inferring to the demise of extensional Ulukışla Basin.

The orientation of Tuz Gölü Basin's geometry changed from NW−SE to E−W trend in the Paleocene (Görür *et al.*, 1984), representing the shifting of tectonic regime. A regional subsidence taking place between Late Miocene and early Pliocene was followed by compressional phase proceeding soon in the latest Miocene−Pliocene. After that time, an extensional regime occurred as a following phase (Fernández-Blanco *et al.*, 2013). Özsayın *et al.* (2013) implied that NNW−SSE to NE−SW compression ended around 6.81±0.24 Ma in accordance with $^{40}Ar/^{39}Ar$ ages of a key ignimbrite layer. After that time, N−S to NE−SW extension affected the Tuz Gölü basin during the Pliocene−Quaternary periods.

As to Sivas Basin, Poisson *et al.* (1996) is the first to assert that no oceanic crust as a basement. This is in favour of the claim that no Inner Tauride is available between the CACC and the Tauride-Anatolide Platform. They mapped two types of thrust faults as S-vergent and N-vergent. The S-vergent ones is attributed to the obduction of ophiolites in the late Cretaceous−Paleogene. On the other hand, the N-vergent thrusts are related to the regional compression owing to the convergence of Eurasian and Arabian plates. The latter might be interpreted as a back-thrust. For that reason, these faults are discussed to decide if they formed distinctly, or coevally. Dirik *et al.* (1999) demanded two models regarding the evolution of Sivas Basin. One of them is related to the closure of the Inner Tauride ocean that resulted in the formation of an accretionary prism along the suture zone; the other has resulted from a tensional-transtensional regime within the Tauride-Anatolide Platform. NE–SW-trending anticlines and synclines arose from late Eocene compression as well as the closure of Sivas and Central Kızılırmak basins. Late Eocene–Oligocene period in that basin correspond to the last collision between the CACC and the Pontides. Yılmaz & Yılmaz (2006) added that the basin was encountered with compression before the Eocene, which can be observed in the unconformity between Eocene clastic and Maastrichtian–Paleocene carbonates. Structures related to the late Eocene regional compressive regime can be traced on the nappes reactivated; this regime continued until middle Miocene. Transtensional deformation happened in Late Miocene. Yılmaz & Yılmaz (2006) pointed out that the last compressional regime is associated with the Neotectonic period commenced by late Pliocene–Quaternary like; this was latter supported by Önal *et al.* (2008) who suggested a N–S compressional regime.

Çankırı Basin, located in the northern part of the CACC, faced with two main successive events corresponding to the transition from forearc to foreland basin evolution. The late Cretaceous subduction led to pile up a forearc sequence within the basin. This forearc basin evolved into a foreland basin because the CACC indented into the Pontides by the late Paleocene (Kaymakcı *et al.*, 2009) That development manifests itself as a chains of piggy-back basins migrating southwards along the thrust faults, thereby influencing regions further south, e.g., the Çiçekdağ Basin. The interaction between the Çankırı and Çiçekdağ basins was proved by using the structural and paleocurrent data along with the magnetostratigraphic approach (Gülyüz *et al.*, 2013).

Lefebvre *et al.* (2013) argued that there is a very distinct arrangement of granitoids in all these massifs where granites are located at the outer parts. Monzonites and syenites are located at the very inner parts of the Kırşehir Block. Using this zonation Lefebvre *et al.* (2013) with the aid of paleomagnetic data reconstructed and re-aligned these metamorphic massifs: Kırşehir Block was a NNE–SSW-trending belt that was dissected into three pieces; they are translated and rotated as the Kırşehir Block collided the Pontides and this resulted in the present triangular geometry of the Block (Figure 1.1).

The study area is located at one of the transfer faults, namely Delice-Kozaklı fault zone along which the north-eastern block, Akdağ-Yozgat block, translated and rotated clockwise.

The study area comprises mainly Central Anatolian Ophiolites and central Anatolian Granitoids as the basement and Late Paleocene to Recent basin infills of the Çankırı and Çiçekdağ basins.

1.5 Previous Works

There are two groups of early studies. One is about magmatism, metamorphism, exhumation, deformation and structural setting of the CACC; the other is concerned with neotectonic structures and recent deformation/activity in the CACC region. A summary of these studies will be given below in chronologic order:

Dirik and Göncüoğlu (1996) worked on the main neotectonic structures bounding and shaping the CACC; namely Tuzgölü Fault Zone, Ecemiş Fault Zone and Yozgat-Akdağmağdeni-Boğazlıyan fault system. The structural characteristics, influences, and geologic products such as Plio–Quaternary depressions and cinder cones are examined and mapped. Some active faults are shown in their structural map without stating any fault-related features (Figure 1.3).

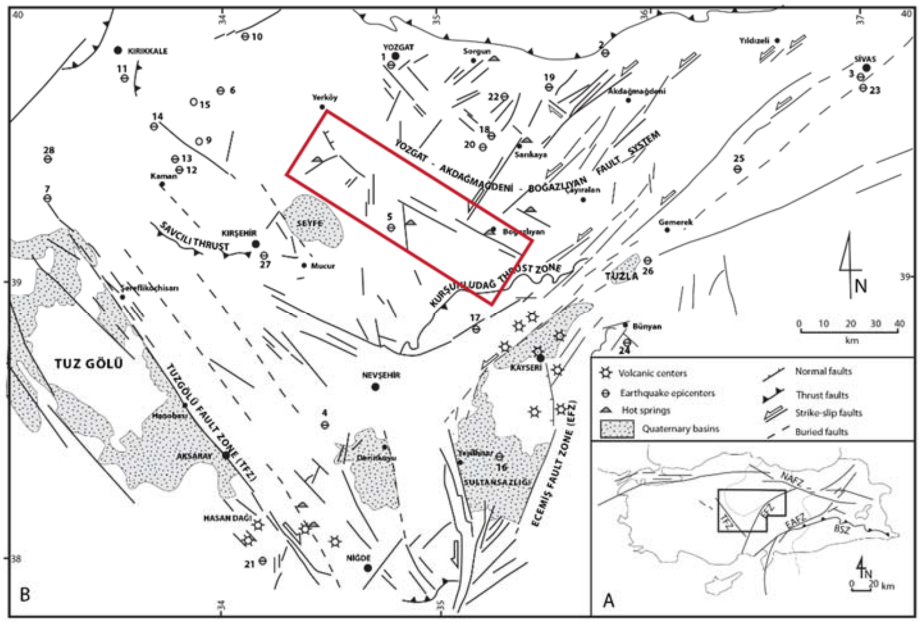

Figure 1.3. (a) The general neotectonic tectonic setting of the CACC and its proximity (Dirik & Göncüoğlu, 1996). TFZ, Tuzöglü Fault Zone; EFZ, Ecemiş Fault Zone; EAFZ, East Anatolian Fault Zone; BSZ, Bitlis Suture Zone; M, Mersin; R, Refahiye. (b) The structural map of the CACC pertaining to neotectonic period. The red rectangular shows the geographic position of the study area

Erler and Göncüoğlu (1996) classified the Yozgat Batholith into ~~the~~ subunits based on the rare earth, major- and trace-element analyses. They also illustrated faults trending similar to the proposed fault, DKFZ. Some may extend into the study area (Figure 1.4) but they did not comment on the type of the fault.

Boztuğ (1998) studied geological setting, mineralogical-chemical characteristics, geodynamics and petrogenesis of the alkaline plutons in the CACC. He mapped a fault having the same orientation as the DKFZ (Figure 1.5), but the study does not supply any observations about the structural feature of the fault.

Koçyiğit and Erol (2001) dealt with the structural characteristics of Central Anatolian Fault Zone by observing its segments. The relationships between CAFZ and Erciyes pull-apart basin, the fault motion of CAFZ and their effect on volcanic activity and evolution of subbasins of EPB. They mapped a dextral strike-slip fault with the same trend, termed as Delice Fault (Figure 1.6). However, they do not provide any structural, seismic, or geomorphologic data to prove the presence of the DF.

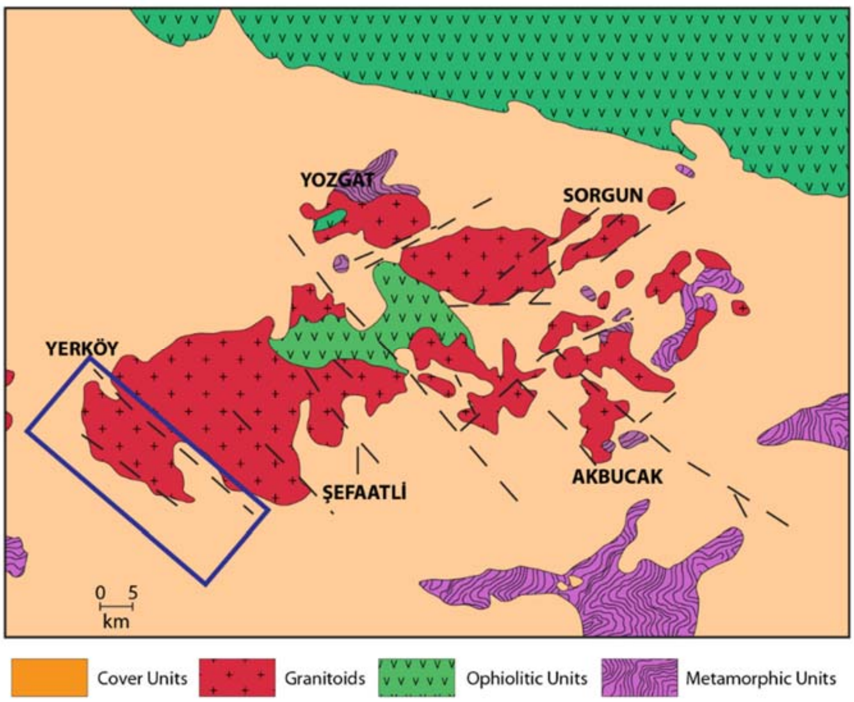

Figure 1.4. Geological map of the Yozgat Batholith (Erler & Göncüoğlu, 1996). The blue rectangular shows the geographic position of the study area.

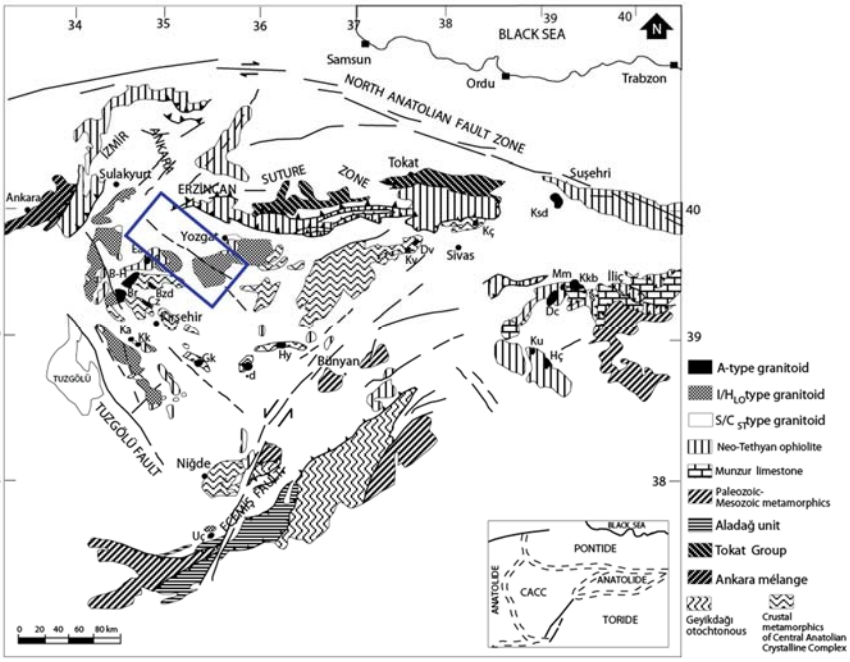

Figure 1.5. Geological map showing the metamorphic and plutonic rocks in the CACC (Boztuğ, 1998). B-H, Bayındır-Hamit; Ea, Eğrialan; Br, Baranadağ; Bzd, Buzlukdağ; Çz, Çayağzı; Ka, Kuruağıl; Kk, Kesikköprü; Gk, Gümüşkent; Uç, Uçurumtepe; Id, Idişdağ; Hy, Hayriye; Kv, Kavik; Dv, Davulalan; Kç, Karaçayır; Ksd, Kösedağ; Ku, Kuluncak; Hç, Hasançelebi; Dc, Dumluca; Mm, Murmana; Kkb, Karakeban. The blue rectangular shows the geographic position of the study area

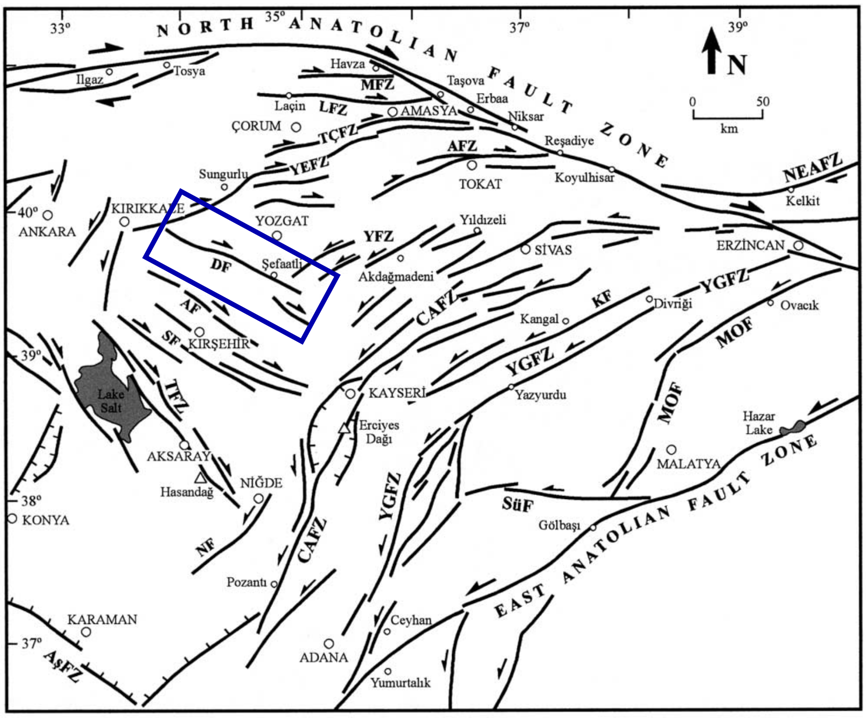

Figure 1.6. The structural settings of Central and Eastern Anatolia which is governed by the neotectonics of Anatolian platelet (Koçyiğit & Erol, 2001). The blue rectangular shows the geographic position of the study area.

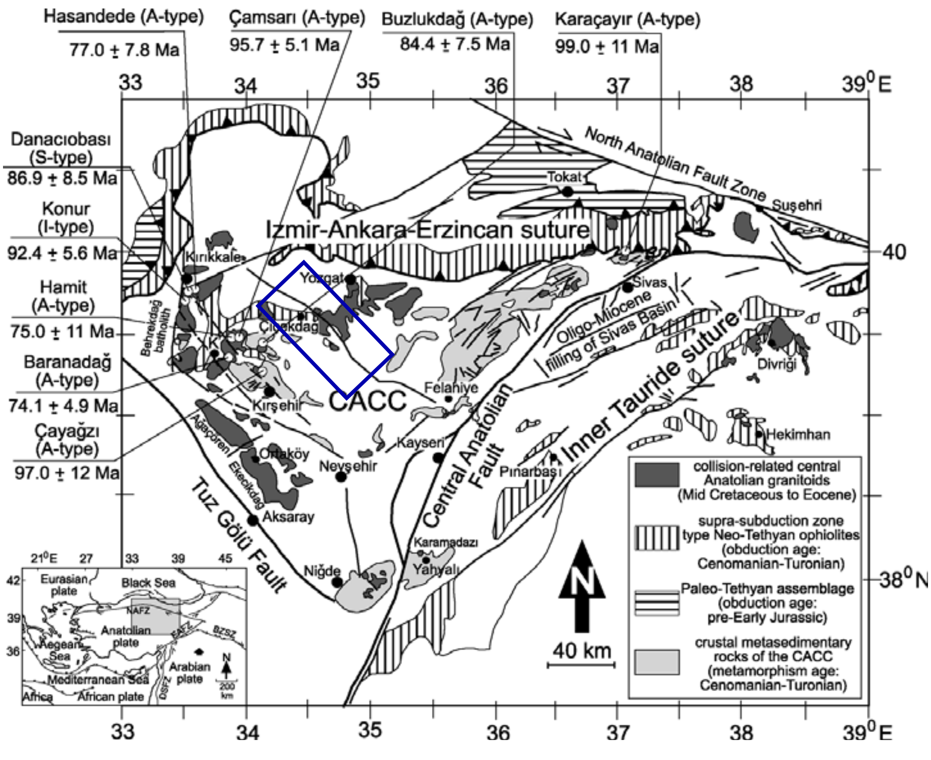

Figure 1.7. Simplified geological map indicating the basement rocks and the main structures of the CACC (Boztuğ *et al.*, 2007). The inset at the bottom left corner depicts roughly the regional tectonic settings. The blue rectangular shows the geographic position of the study area

Boztuğ *et al.* (2007) studied the emplacement ages of nine distinct granitoids units of the CACC based on $^{207}Pb/^{206}Pb$ single-zircon evaporation method. The similar fault is indicated as in the geologic map of Boztuğ (1998) (Figure 1.7).

Boztuğ *et al.* (2009) was concerned with the intrusion-cooling-exhumation of the Karaçayır syenite by relating to the evolution of the İzmir-Ankara-Erzincan (İAE) ocean. They represented the same fault as Boztuğ (1998) and Boztuğ *et al.* (2007) did (Figure 1.8). Similarly, no related observation, or measurement is available in their paper.

Gülyüz *et al.* (2013) documented the results of a magnetostratigraphic work and Ar^{40}/Ar^{39} ages from the Çiçekdağ Basin. They also contended that folding of the basin fill is related to southward movement of Çankırı Basin due to the convergence of the Pontides and the CACC. These workers mapped a concealed reverse fault which has a dextral strike-slip component in a part.

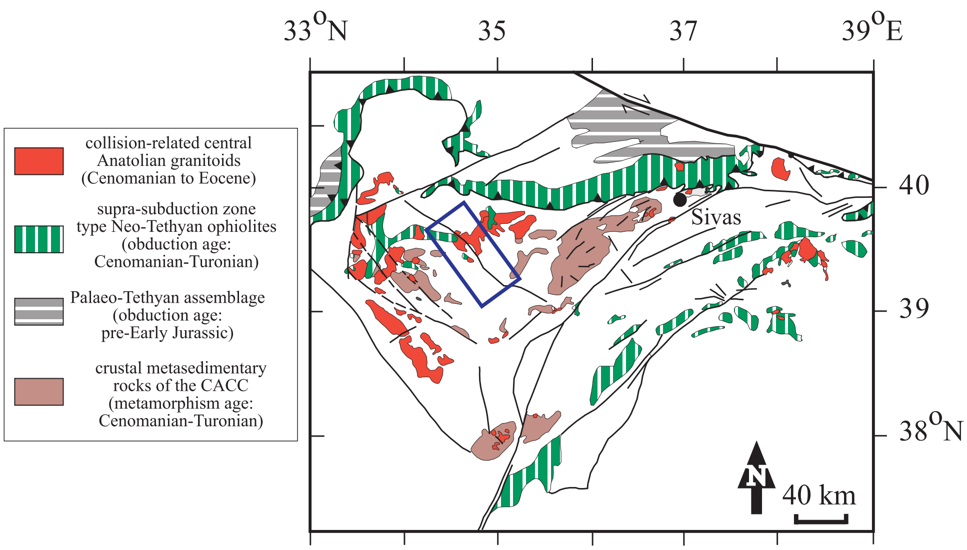

Figure 1.8. Geological map of the basement rocks in the CACC (Boztuğ *et al.*, 2009). The blue rectangular shows the geographic position of the study area.

Advokaat *et al.* (2014) studied in the Ayhan-Büyükkışla basin of the Upper Cretaceous to post-middle Eocene to determine the tectonic evolution of basin. They contended for a thrust fault and termed it as Delice-Kozaklı thrust zone (Figure 1.9) without presenting any structural data to support their assertion.

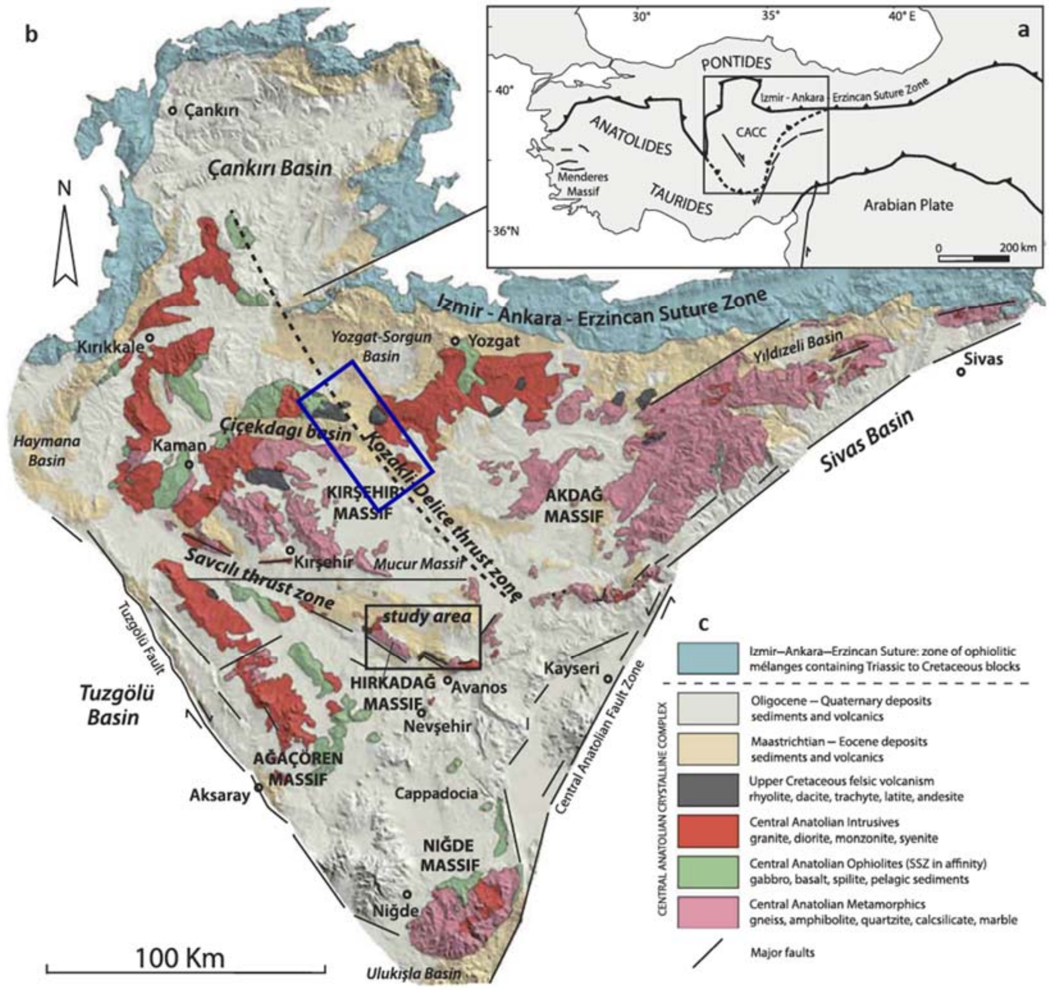

Figure 1.9. The simplified geological map of the CACC (Advokaat *et al.*, 2014). The blue rectangular shows the geographic position of the study area.

Most of the previous workers have mapped the DKFZ to some extent, but they did not comment and/or present structural data about nature and type of these faults. For this reason, the present work aims to present available structural data that may be helpful to fill this gap in the literature.

CHAPTER 2

STRATIGRAPHY

3.1 Introduction

The rock units exposed in and around the study area are classified, depending on their lithologic association(s) and stratigraphic relationships, into three groups: basement rocks, basin infill and cover units (Figure 2.1). Metamorphic, ophiolitic, volcanic and intrusive rocks constitute the basement. Basin infill corresponds to Yoncalı, İncik, Kocaçay, Bayat and Güvendik formations that unconformably overlie the basement whereas the Neogene units cover rocks overlie both the basement and the basinfill unconformably. The alluvium is the youngest unit in the region.

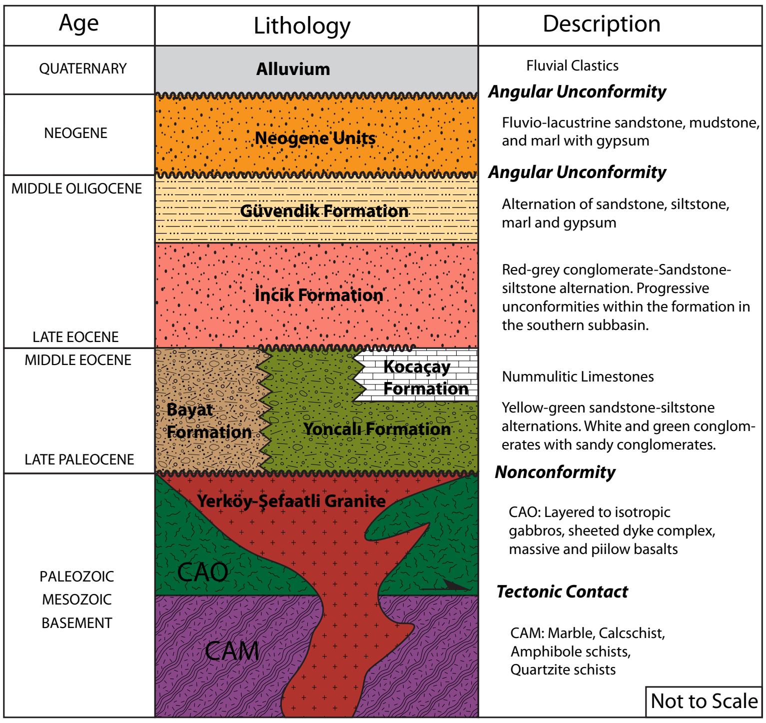

Figure 2.1. Generalized columnar section of the study area (Gülyüz, 2009; *Gülyüz et al.*, 2013)

Characteristics of various rock units, their boundary relationships and structural elements deforming them are studied in three locations (Figures 2.2–2.5).

The detailed description of rock units will be described in the following sections whereas structures form the main subject of Chapter 3.

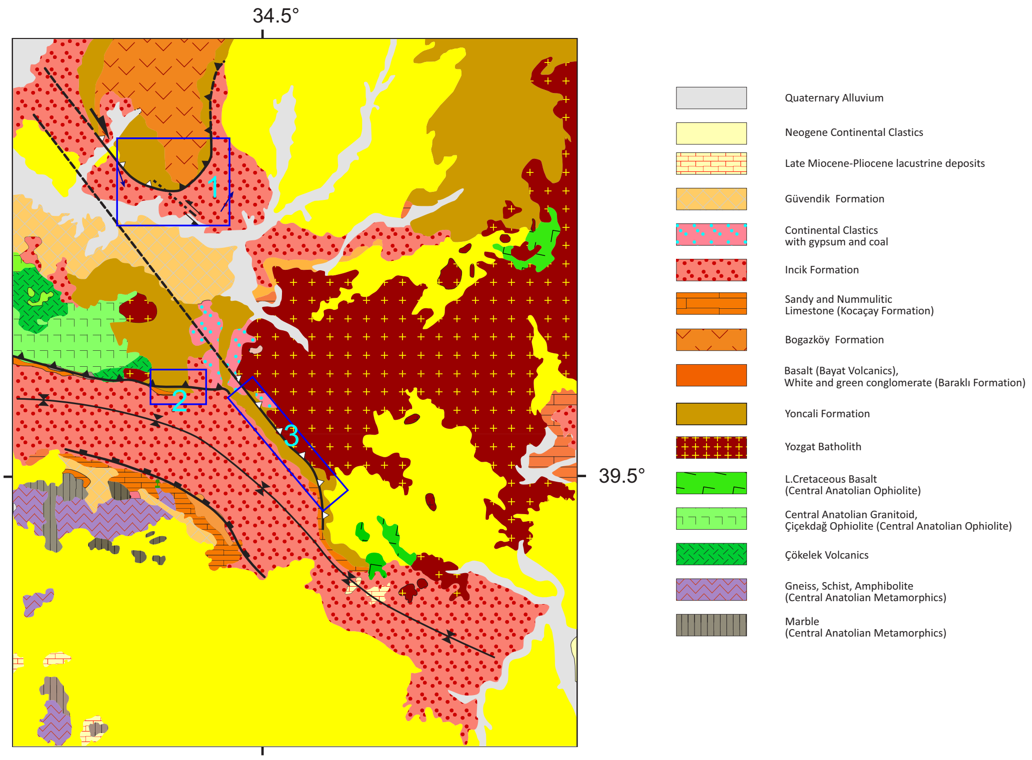

Figure 2.2. Geological map of the study area (modified from *Gülyüz et al.* 2013)

3.2 Basement Units

3.2.1 Central Anatolian Metamorphics

Metamorphic rocks are named Gümüşler Formation and exposed near Bahçepınar Village at the southern margin of Çiçekdağı southern subbasin. This formation is composed of gneiss, schist, marble, amphibole, quartzite, calcschist (Dönmez *et al.*, 2005). Kara *et al.* (1991) differentiated two units as Bozcaldağ Formation made up of marbles and Kalkanlıdağ Formation, gneiss, schist, quartzite and amphibolite.

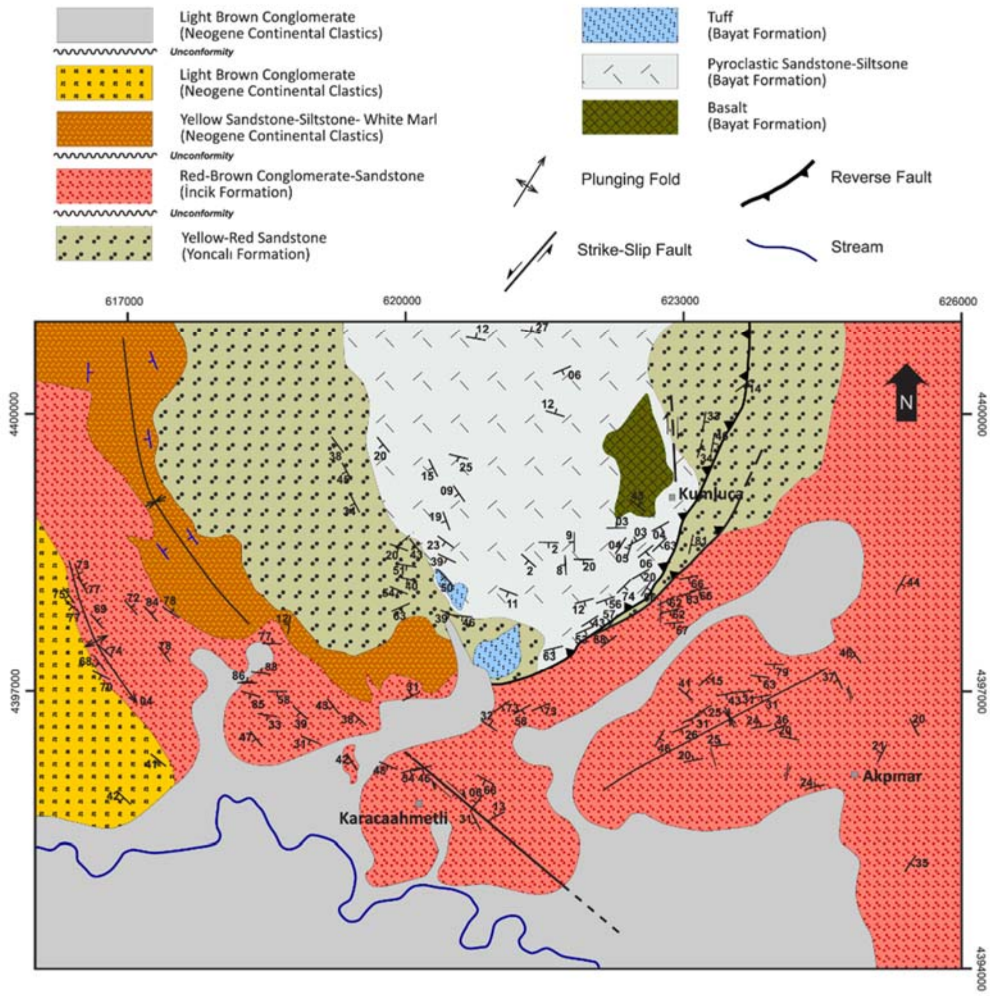

Figure 2.3 Geological map of location-1.

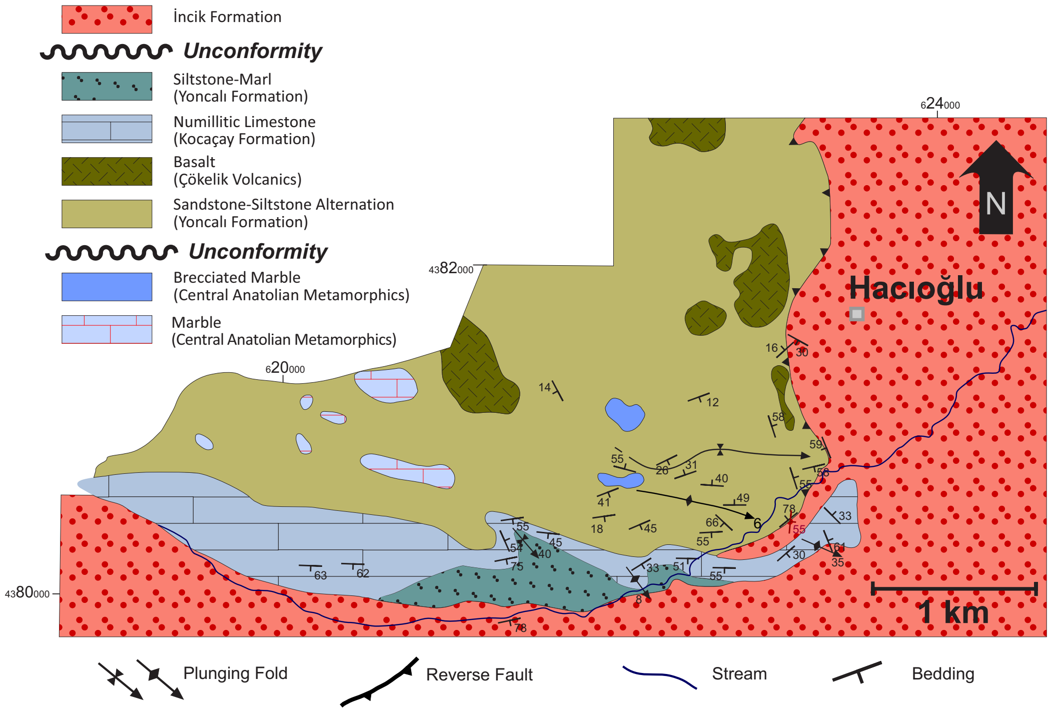

Figure 2.4 Geological map of location-2.

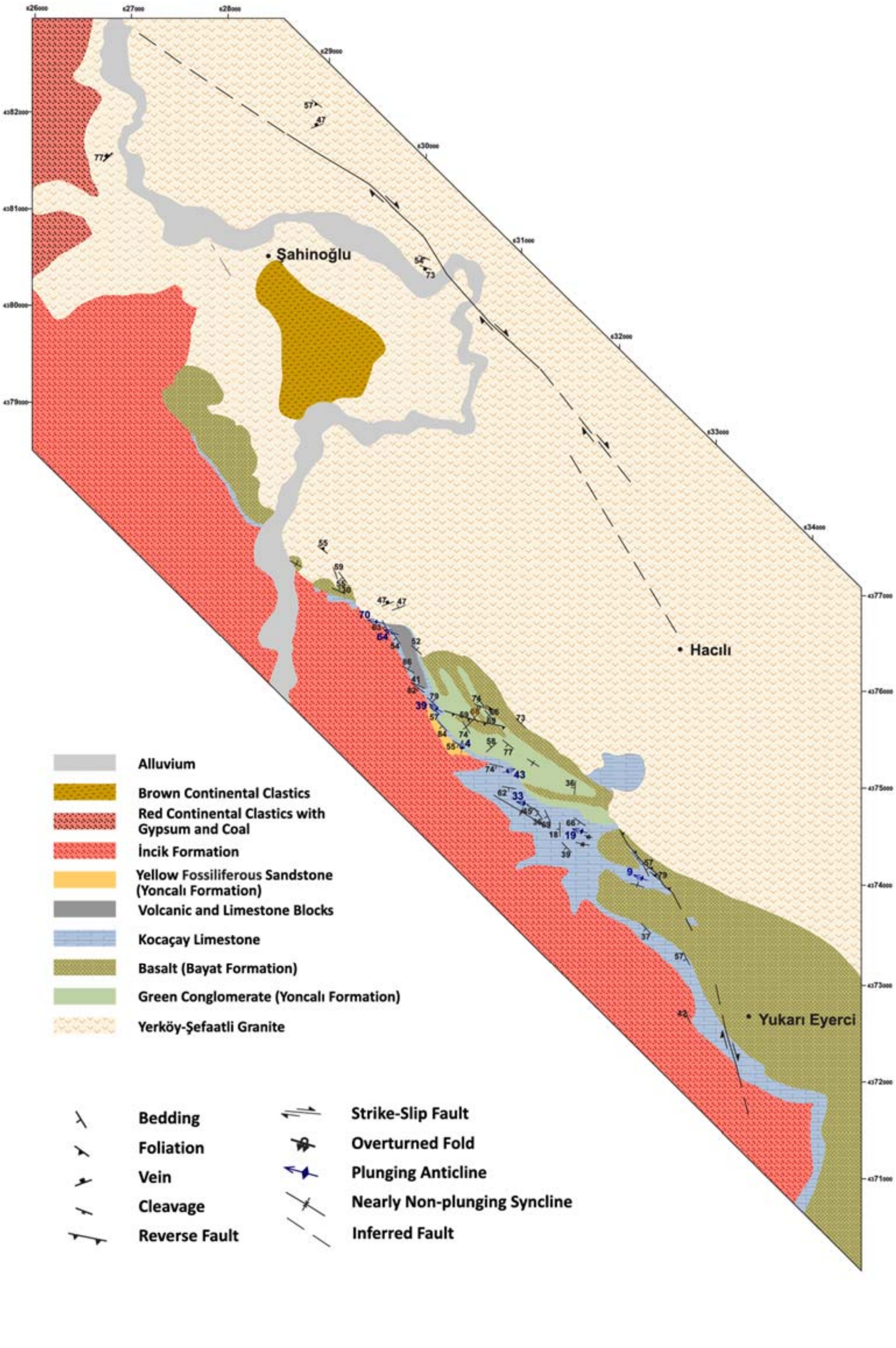

Figure 2.5 Geological map of location-3.

Banding is abundant in the range of thickness from cm to m and parallel to subparallel with respect to the bedding of sedimentary protoliths. Metasediments are commonly, quartzite, quartz schist, quartz-mica schist and mica schists, thereby suggesting a sandstone-siltstone protolith. The amphibolite and amphibole-schists are probably derived from intermediate volcanic and volcanoclastic rocks whereas marbles and calc-silicate, limestone and clayey limestone. Mineral paragenesises Mineral paragenesises as well as micro- and macro-structures are consistent with polyphase low pressure-high temperature metamorphism (reaching up granulite facies) and associated deformation (Göncüoğlu *et al.*, 1994).

3.2.2 Central Anatolian Ophiolites (CAO)

The Central Anatolian Ophiolites are a discrete and partially preserved member of the Central Anatolian Crystalline Complex. Those broke off and were transported southward from the İzmir-Ankara-Erzincan Suture Zone as allochthonous bodies along the CAM in the early middle Turonian - early Santonian (Yalınız *et al.*, 2000b). During obduction of these ophiolites, the CAM appeared as the passive northern margin of the Tauride-Anatolide Platform along the northern branch of the Neothethyan Ocean. Major rock types include: (i) metamorphic (i) Metamorphic and cumulate ultramafics, (ii) layered, cumulate and isotropic gabbros, (iii) plagiogranites, (iv) dolerite dyke complex, (v) basaltic volcanics, and (vi) epi-ophiolitic sedimentary cover constitute the CAO (Yalınız and Göncüoğlu, 1998).

A part of the CAO, termed as the Çiçekdağ Ophiolite (CO), is available in the study area and located around Çiçekdağ. The CO comprises (i) layered gabbro; (ii) isotropic gabbro; (iii) plagiogranite; (iv) dolerite dyke complex; (v) basaltic volcanic sequence and (vi) a Turonian-Santonian epi-ophiolitic sedimentary cover from bottom to top. These workers pointed out that the CO is a remnant which developed in a newly created oceanic lithospheric part (Yalınız *et al.*, 2000a). Granitoids cut all units of the CO and are covered by Eocene sedimentary units.

3.2.3 Extrusive Rocks

3.2.3.1 Çökelik Volcanics

Volcanic rocks are mainly submarine lavas with abundantly pillow structures and consist of spillite, diabase, and andesitic basalts. They occur as either isolated blocks or are intercalated with massive limestones (Ketin, 1955). The rock association of dark-green to black diabases, mafic tuffs, pillow lavas and microgabbro is named first as Çökelik volcanics by Erdoğan *et al.* (1996). Yalınız *et al.* (2000b) followed this description as well. Most or a part of this succession crops out in SE and NW of Yerköy (Erdoğan *et al.*, 1996; Yılmaz & Boztuğ, 1998). In this study, the basalts of Çökelik volcanics are exposed around Hacıoğlu Village unconformably above the Yoncalı Formation (Figure 2.6).

According to Yalınız *et al.* (2000b), the isotropic and subordinate layered gabbros are common around Çiçekdağ along with the rarity of sheeted dyke complex but there are no ultramafic rocks in this region (Göncüoğlu *et al.*, 1991). These rocks are considered as part of the Central Anatolian Ophiolites (CAO) and interpreted as (i) dispersed allochthonous bodies or blocks within the CACC (Yalınız *et al.*, 2000b), or (ii) slivers thrusted onto CACC (Yalınız&Göncüoğlu, 1998; Yalınız *et al.*, 2000a). In these models, the ophiolitic rocks are derived from İzmir-Ankara branch of Neotethys.

Yalınız and Göncüoğlu (1998) assert that the basaltic volcanics are well-exposed around Alayhanı, Devedamı, Sarıkaman, south of Yozgat and Çiçekdağı (Figure 2.2).

3.2.4 Central Anatolian Granitoids (CAG)

Granitoids of the CACC constitutes the prominent rock unit in the region and are abundant in northwestern, southeastern and northern part of the complex. They occur as variably sized plutons and intrude the ophiolitic and metamorphic rocks of the complex. Their compositions range from monzodiorite to monzonite (Erler & Göncüoğlu, 1996; Aydın *et al.*, 1998; Düzgören-Aydın *et al.*, 2001; İlbeyli *et al.*, 2004; İlbeyli, 2005; Işık *et al.*, 2008).

The granitoids of the CACC are also classified into six different lithologies (Erler & Göncüoğlu 1996): (i) two-mica leucogranites; (ii) biotite-hornblende granites; (iii) alkali-feldspar megacryst granites; (iv) granodiorites; (v) tonalites; and (vi) aplitic dikes. According to Tatar and Boztuğ (1998) the granitoids are monzonitic association composed of monzodiorite/monzogabbro, quartz monzodiorite, quartz monzonite and monzogranites.

In the study area, part of the Yozgat Batholith is exposed; this unit is largest pluton of Central Anatolian granitoids. It is grouped, based on contact relationships, structural and mineralogical-textural characteristics, into eight subunits (Erler & Göncüoğlu 1996): from west to east, these are Yerköy-Şefeatli, Yozgat, Kerkenez, Karlıtepe, Gelingüllü, Sivritepe, Ocaklı, and Mugallı subunits. The granitoids are also described as: (i) calc-alkaline, cafemic, I-type (Tatar and Boztuğ 1998), (ii) I-type (Köksal & Göncüoğlu 2008); (iii) as metaluminous and H-type (hybrid type) (Köksal *et al.*, 2004). Yerköy-Şefaatli granitoid is exposed within the study area. It is a subalkaline-calcalkaline, metaluminous monzogranite. It is typically pinkish in colour and is composed of coarse-grained K-feldspar, plagioclase, quartz, and biotite (Figure 2.6).

Figure 2.6. Field view of the Yerköy-Şefaatli granite.

3.3 Basin Infill

The basin infill corresponds to the rock units of the Çiçekdağ Basin; it is composed of five formations, namely Yoncalı, İncik, Bayat, Kocaçay, and Güvendik formations. The descriptions of these units will be given below.

3.3.1 Yoncalı Formation

The Yoncalı Formation was named first by Birgili *et al.* (1974). It is composed of white calcerous sandstone, white, green, and reddish calcerous matrix- and grain-supported conglomerates, and white and grey silty, or, sandy, or pebbly limestones. It is exposed along the eastern margin of southern subbasin of the Çiçekdağ Basin. Different lithologies of the formation show both vertical and lateral facies changes. The limestones are rich in nummulites in the lower and middle parts whereas bivalves occur in the upper parts. The conglomerates are polygenetic, poorly sorted and composed of angular, subrounded and rounded pebble-sized fragments derived from granite, basalt, limestone within a sandy-silty matrix. Depending on relative abundance of fragments and matrix, different types are present; that is, grain- and matrix-supported rocks. The colour of the conglomerates may also differ from place to place. Fragments in the sandstones and conglomerates are also cemented by calcite. The fragments are mostly derived from basalts but locally limestone fragments are also observed. According to Gülyüz *et al.* (2013), the age of these conglomerates are Late Eocene in the Çiçekdağ Basin. The conglomerates are also known as Yeşilöz Formation (Middle-Upper Paleocene; Göncüoğlu *et al.* 1993). The age of the lower part of the nummulitic limestones is Early Eocene, middle part, Lutetian (Ketin, 1955; Gülyüz *et al.*, 2013; Gökten *et al.*, 2013), upper parts, latest Eocene-Early Oligocene (Gökten *et al.*, 2013).

Figure 2.7. Field views of (a) white and (b) green conglomerates of the Yoncalı Formation.

The formation incorporates also a flysch facies and is mainly represented by yellowish green sandstone-siltstone alternation with shale and marl; it is exposed around Hacıoğlu, Karacaahmetli and Kumluca villages (Figures 2.3 & 2.4). The grains of sandstone and siltstone are rounded and subrounded. The thickness of beds changes in the range from 5-20 cm. According to Erdoğan *et al.* (1996), the sandstone and shales were deposited in a shallow marine environment. Fossiliferous limestone horizons crop out abundantly around Yozgat and Yerköy. Yellow, sandy, fossilifereous limestone horizon within a thick sandstone sequence is characteristic. The alternations of sandstone-siltstone, which are well cemented by calcite in yellow and red matrix, are mapped above tuff, tuffaceous clastics and volcanics of the Bayat Formation and beneath Yoncalı Formation conformably in this study (Figure 2.3). Even, Kaymakçı *et al.* (2009) suggested that Yoncalı Formation exhibits vertical and lateral gradations to the late Paleocene to middle Eocene Bayat Formations and early to middle Eocene Kocaçay Formation.

3.3.2 İncik Formation

İncik Formation comprises alternation of red and grey conglomerate, sandstone and siltstone (Figure 2.8). Lamination, graded, trough and cross-bedding are common syn-sedimentary structures. . Furthermore, progressive unconformity took place by piling up of İncik Formation within the southern subbasin. The conglomerates of İncik Formation are made up of angular and subrounded basalt, tuff, sandstone limestone, chert, granitic pebbles associated within a red and grey silt matrix and/or calcitic cement. In some places, fossils are also observed as fragments/grains in the conglomerates, pointing the age of these levels as post-Eocene. For that reason, the age of the formation, late Eocene-middle Oligocene, claimed by (Kaymakcı *et al.*, 2009) is preferred. The recent study observed that İncik Formation overlies the Kocaçay Formation conformably. This formation was named by Birgili *et al.* (1974).

Figure 2.8. A general view to the İncik Formation

3.3.3 Bayat Formation

Ayan (1969) was the first to term the units as Bayat Formation. Tuff, volcano-sedimentary rocks, marl, conglomerate and volcanic rocks constitute the Bayat Formation. The formation is mapped around Kumluca Village and former location of Karacaahmetli Village. The volcanoclastic rocks are composed of thin-bedded brown and grey sandstone and siltstone with a tuffic matrix (Figure 2.9). The formation is overlain conformably by the Yoncalı Formation. Its volcanic rocks are also composed of dark-green and amygloidal basalts and crops out near Şahinoğlu and Hacılı villages unconformably above the Yerköy-Şefaatli granitoid. Near Karacaahmetli and Kumluca villages, these basalts lay beneath volcanoclastic rocks and yellow-red sanstone-siltsone alternation of Yoncalı Formation. It is important to note here that the conglomerates of Yoncalı Formation mainly consist of fragments derived from the Bayat basalts.

The age of the formation is paleontologically assigned as late Paleocene-middle Eocene (Kaymakcı *et al.*, 2009).

Figure 2.9. Tuffaceous sandstone-siltstone alternation of the Bayat Formation.

3.3.4 Kocaçay Formation

The Kocaçay Formation includes in some places silty-, sandy- limestones intercalated with conglomerates; in some nummulite-rich limestones along with marl. The conglomerates are light brownish and white colored and also their grains are derived from altered and unaltered basalts, rhyolites, andesites and granites within silty matrix cemented by calcite. They are commonly grain supported conglomerates whose grains are subrounded and rounded in the size of 2 to 10 cm. That formation overlies on Yoncalı Formation conformably. In some places, it is interdigitated with; but in some places, is underlain by İncik Formation. Kocaçay Formation is dated by fossils as Early-Middle Eocene (Kaymakcı *et al.* 2009). This formation was named first by Birgili *et al.* (1974).

3.3.5 Güvendik Formation

The Güvendik Formation is composed dominantly of gypsum beds associated with white siltsone and shale (Figure 2.10). It is named first by Kaymakcı (2000). The formation may be correlated with Sekili evaporite members of Dönmez *et al.* (2005), which includes gypsum, anhydrite, mudstone and sandstone. Güvendik Formation covers basin infill and basement units with a low-angle unconformity. Neogene units and alluvium overlies Güvendik Formation unconformably. The observed rodents point the age of Güvendik Formation is Oligocene (Kaymakcı, 2000).

Figure 2.10. Thin bedded gypsum and well consolidated siltstone sequence of the Bozkır Formation.

3.3.6 Neogene Continental Clastics

This unit is mostly composed of subrounded and rounded carbonitic pebbles that come from the sandy-, silty-, and nummulitic limestones within brown sandy matrix. Channel-fill sequences which consist of angular basaltic pebble and cobbles are seen from place to place. It overlies İncik Formation unconformably. Dönmez *et al.* (2005) mapped these clastics as İç Anadolu Group with an age of late Miocene-Pliocene (MTA İ32 sheet, scale: 1/100000). The contact between these clastic rocks and İncik and Güvenik formations cannot be observed in the field. The study tends to refer to the map of Dönmez *et al.* (2005) since the contact relationship is clearly represented. They proposed that Güvendik and İncik Formations underly these clastics unconformably.

3.3.7 Quaternary Units

Quaternary alluvials are represented by the river channel and floodplain sediments of Delice River, which is the largest fluvial agent in the region. They are unconformable above all older units.

CHAPTER 3

STRUCTURES

3.1 Introduction

Geologic structures commonly observed in the study area are examined to reveal regional deformation mechanism and kinematics; they are divided into two common groups: primary and secondary structures. While the former consists of bedding and unconformities, the latter of folds, faults, and joints.

3.2 Primary Structures

3.2.1 Bed

Bedding is the most prominent structure of the lower to upper Eocene sediments of the basin infill. Graded and cross-bedding are common. Graded bedding is characteristic in red-grey conglomerate-sandstone alternation of the İncik Formation, and in white and green conglomerates of the Yoncalı Formation. Cross-bedding (i.e. current bedding, false bedding, oblique bedding and inclined bedding; cf. Hills, 1965) is common within red conglomerate-sandstone alternation of the İncik Formation. Moreover, lamination exists in red and grey sandstones of the Eocene formations in the basin infill (Çiçekdağ Basin), particularly those exposed within the major syncline of the basin. Lamination is also observed around the boundary between white silty-, sandy-, nummulitic limestones and white conglomerate and red-grey conglomerate-sandstone alternation (Figure 3.1).

Figure 3.1. Views from different types of bedding observed in the study area. (a) Planar cross-bedding, (b) trough cross-bedding, (c) lamination with intercalated tabular (planar) cross-bedding, and (d) graded bedding. Arrow (~ 20 cm) in (d) shows finning upward direction.

3.2.2 Unconformities

Three types of unconformities are present within the rock units of the study area. The nonconformity occurs between the green conglomerates of the Yoncalı Formation above and basalts of the Bayat Formation below as well as between the basalts and the Yerköy-Şefaatli granite. It is well observable at the eastern part of southern sub-basin. Further, the angular unconformities occur where Neogene units lie above the Güvendik Formation and in areas where alluvium is exposed.

Figure 3.2. (a) A view from the intraformational progressive unconformities within the İncik Formation of the southern subbasin. (b) Black lines show orientation of bedding as growth strata.

Progressive unconformities are well expressed within the growth strata of the İncik Formation in the southern subbasin (Figure 3.2). There a syncline deforms the formation. The thickness of the growth strata increases from basin margin to the center (Figure 3.3); similarly dip amount decreases up to horizontal towards the core of the syncline.

Figure 3.3. An example of growth strata in the İncik Formation of the Çiçekdağ subbasin; yellow dashed lines correspond to progressive unconformities.

3.3 Secondary Structures

These structures are common in all of the rock units exposed in the study area. They occur as three distinct structures: joints, faults, and folds. Since all is tectonic-stress related structures, they are used in kinematic and dynamic analyses.

3.3.1 Folds

A syncline of a reverse fault (***a3***) in the northeast part of Akpınar village, in the İncik Formation and an anticline, ***a1***, near Arifoğlu Village can be counted as the major folds in the study area (Figure 3.4–3.8). Folds are easy to recognize when they deform (i) white silty-, sandy-, nummulitic- limestone of the Kocaçay Formation along the contact between İncik Formation and the Yerköy-Şefaatli granite or (ii) yellow-green sandstone-siltsone alternation of the Yoncalı Formation and Kocaçay Formation in western side of Hacıoğlu Village.

Figure 3.4. A view from one of asymmetric anticlines in the study area-3.

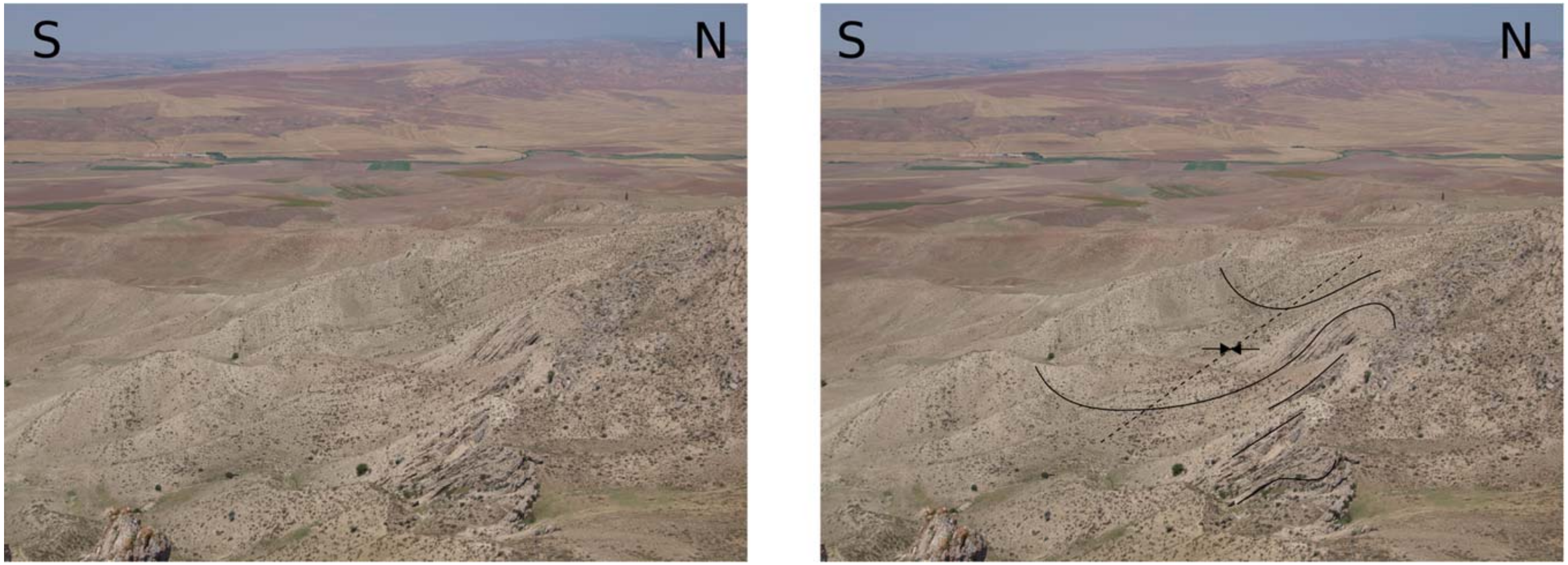

Figure 3.5. A view from the NW–SE-trending syncline deforming the Kocaçay Formation.

Figure 3.6. A view from an overturned syncline, deforming the silty limestones of the Kocaçay Formation near Aşağıeğerci Village. Traces of bedding planes in between basalts are shown as black lines.

Figure 3.7. Superposed recumbent folds deforming the Kocaçay Formation in the Keçikalesi Hill near Aşağı Eyerci Village.

Figure 3.8. Folds within Güvendik Formation with axes trending nearly 300°N. Yellow dashed line refers to a probable fault with unknown characteristics between the synclines.

3.3.2 Joints

Joints are well-observed copiously in the granitic rocks, nonetheless, they also occur in upper horizons of the İncik Formation in the limbs of the major syncline within the southern sub-basin (Figure 3.9). Towards the core of the syncline, younger growth strata do not have any joints.

Figure 3.9. A view from a systematic joint set within (a) red-grey conglomerate-sandstone alternation of the İncik Formation and (b) Yerköy-Şefaatli granite.

The joint planes observed within the Yerköy-Şefaatli granite are not smooth surfaces but ornamented by typical plumose structures (Figure 3.10). These are in fact shear joints where hackle plumes form along the direction of σ_1 (cf. Twiss & Moores, 2007). Such joint surfaces ornamented with plumose structure are important to determine direction of maximum principal stress and also, number of rupture episodes and propagation velocity via rib marks. Therefore, the minimum (σ_3) and maximum (σ_1) principal stress direction can be assigned using the orientation of joint surface and the propagation direction, respectively. Simón *et al.* (2006) pointed out that these structures can give essential information credibly regarding local stress state and stress redistribution due to local stress changes. They also claim that plumose structures cannot indicate the remote paleostress directions. It can be suggested that they provide the record of local stress. The morphology of plumose structures, rib marks and fringe cracks are, however, not explicit and well-preserved in the field since other joints cut and removed them; hence, the stress field cannot be determined concretely.

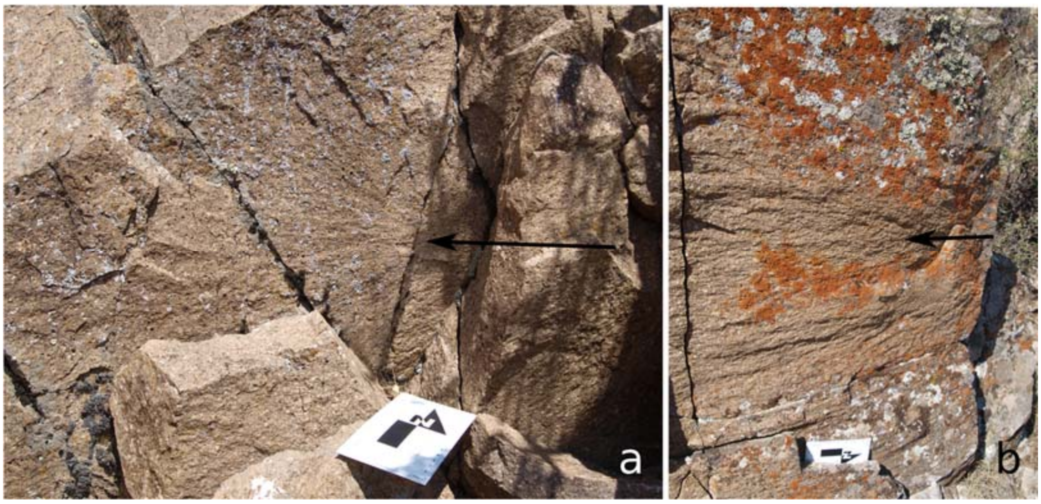

Figure 3.10. Plumose structures along joint surfaces in the Yerköy-Şefaatli granite. Arrows show the propagation direction. Curvilinear lines are rib marks on the main joint face.

Figure 3.11. Fields from (a) quartz vein in sandstone of Bayat Formation and (b) planar aplitic dykes in the Yerköy-Şefaatli granite.

3.3.3 Faults

Faults are the most conspicuous structures in the study area. Some are syn-sedimentary structures deforming basin infill, while others are secondary features cutting across the whole stratigraphy. Faults in the İncik Formation are generally observed as narrow zones without any meso-scale damage zones (Figure 3.12), thereby related subordinate structures, such as minor faults (i.e. R, or R' shear structures) cleavages, or tension gashes are sparse. Offset, morphology of slickensides, geometry of fault-zone structures, indirect geometric observation of primary structures like bedding are tools used for fault analysis during this study. Tilted and folded white silty-sandy limestones of the Kocaçay Formation incorporates faults commonly with a ‘step-like’ morphology; such structures are also common in the granite and green and white conglomerates of the Yoncalı Formation.

Figure 3.12. Field views from (a) a steep fault with a reverse component (offset: ~ 5 m) observed in the İncik Formation around Haticepınar mevkii; (b) a fault in the the İncik Formation. Narrow zone marked by red arrows shows the narrow deformation zone while the compass lies on the fault plane.

Faults in the İncik Formation could be characterized by white scaly slickensides (Figure 3.14) and they are commonly observed near Akpınar, Kumluca, and around Karacaahmetli villages. Most of the slickensides lack of evidence for a clear sense of shear. The fault-movement-related structures, such as slickenside and fault lens, however, assist to determine the sense of shear. To exemplify, Figure 3.13 shows the localized and distributed strain; that is, faulting plane and slip planes enveloping fault lenses, respectively.

Figure 3.13. (a) View from a narrow fault core, characterized by lense-shaped deformation; (b) orientation of fault lenses indicate top to the right-sense of shearing.

The orientation of fault lenses with respect to that of fault plane can be used to determine movement sense along a fault zone. These fault-zone structures are linked to the formation and growth of deformation bands closely. These structures have lense or lozenge shape; for this reason, terms like ‘fault lens’ or ‘deformation band lozenge’ are used, based on the geometry, scale, and bounding structures, to describe these structures. In this case, the critical point is the presence of slip surfaces bounding these rhomboidal elements (Awdal *et al.*, 2014). Those subparallel to fault zone are called as fault lenses.

Slickensides are examined depending on their morphology and fractures formed during faulting. Figure 3.16 can be exemplified for that slickenlines can form along with deposition of fault gouge during fault movement. In the Figure 3.14b, the presence of groove mark is used to determine the sense of movement on the fault plane; these structures are also known as tool marks (Hancock, 1985), asperity ploughing, tool tracks, or wear tracks, or wear grooves (Means, 1987).

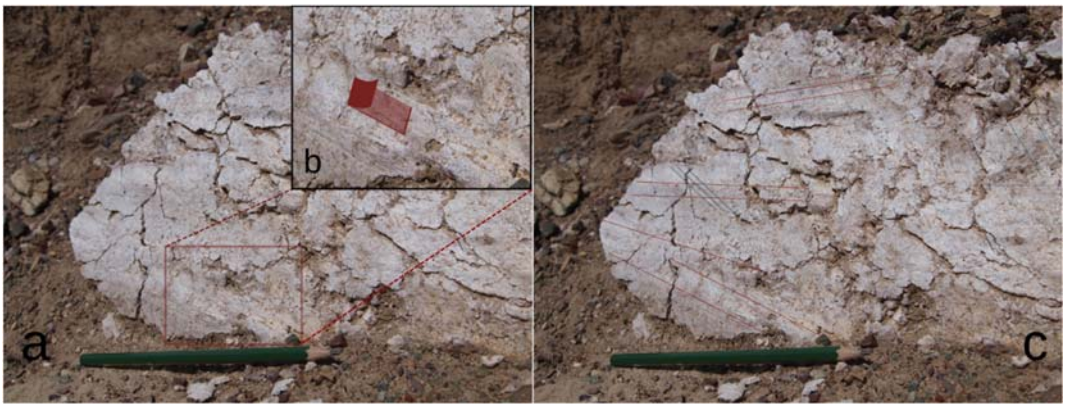

Figure 3.14. (a) A fault plane cropping out within conglomerates of İncik Formation near Akpınar Village; (b) shear sense for red (initial) and blue (following) slicken lines is determined by using a groove; (c) there are two sets of overprinting slickenlines, displayed by red and blue lines

Figure 3.16 a–c represents a fault plane where main plane and fractures due to Riedel (R) shearing are evident. The angle between M-plane and R-fractures is low and acute whereas the intersection of M-plane and R-fractures is approximately perpendicular to the slickenlines. These fractures tend to move in the same direction as the main fault. Hitherto, these second-order features are, especially RM type slickensides, categorized as group-R structures (Petit, 1987).

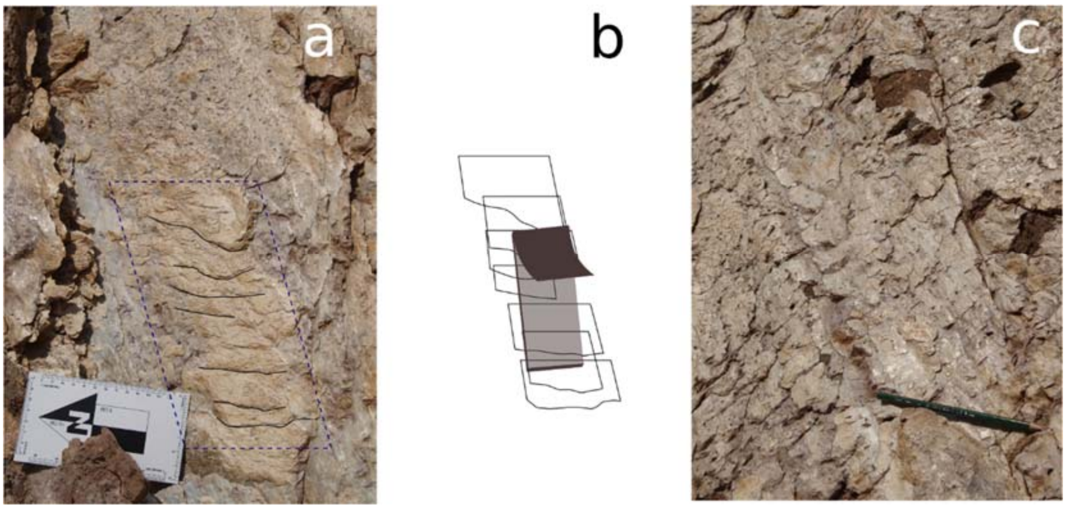

Figure 3.15. (a) A view from an R-type slickenside. The intersection of subsidiary fracture and M-plane shown by black lines refer to chatter marks; (b) schematic illustration of shear sense creating the fault plane; (c) view from a similar slickenside in another part of the same fault plane.

Other examples of step morphology along slickensides of strike-slip faults are shown in Figure 3.16. The faces of the steps indicate the motion of the opposite block. This interpretation is made in the case of none of R-criteria fractures.

Figure 3.16. Slickensides resulting from strike-slip faulting examined (a) in red-grey conglomerates of the İncik Formation with sinistral shearing; (b) in white silty limestone of the Kocaçay Formation with dextral shearing; and (c) in granite with dextral shearing. Stereonets show the results of paleostress analyses.

Fossen (2010) stated that one stage is erased by following ones throughout phenomena of faulting. Therefore, slickenlines on fault planes record the last slip increment. Some of the observed fault planes appear to be problematic. In these locations, R-type slickensides do not display common, but different and opposite shear senses. For example in Figure 3.17 a & b, slickensides show a dextral strike-slip motion. On the basis of the statement of Fossen (2010), they belong to last stage of fault.

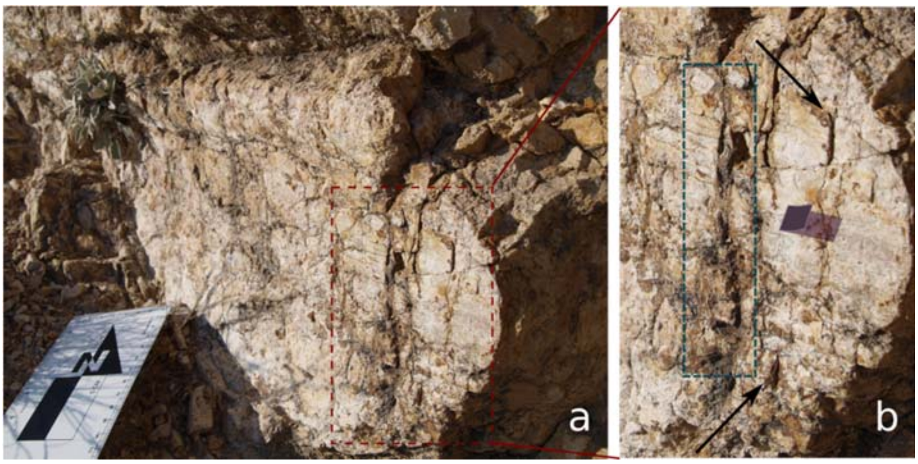

Figure 3.17. (a) A view from a fault plane deforming the Yerköy-Şefaatli granite; (b) a groove, shown by black arrows, are consistent with a right-lateral shear sense.

Other parts of the same fault plane display different structures suggesting possibility of reactivation (Figures 3.17 and 3.18). It is, nonetheless, known that overprinting striations and other kinematic indicators exhibiting different motions do not always mean polyphase deformation or that each discrepancy corresponds to a particular phase (Angelier, 1989, 1990 and 1994).

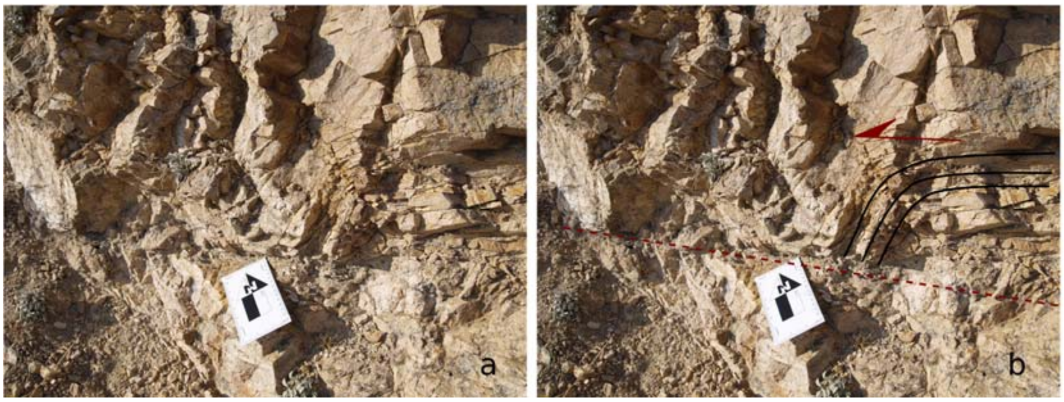

Figure 3.18. (a) Another part of fault plane illustrated in Figure 3.17, disclosing shearing of joint planes within the Yerköy-Şefaatli granite; (b) interpretation of this outcrop where a left-lateral shear sense is proposed. Black lines refer to folding of joints forming within the granite. This evidence is used to suggest the presence of another phases during faulting.

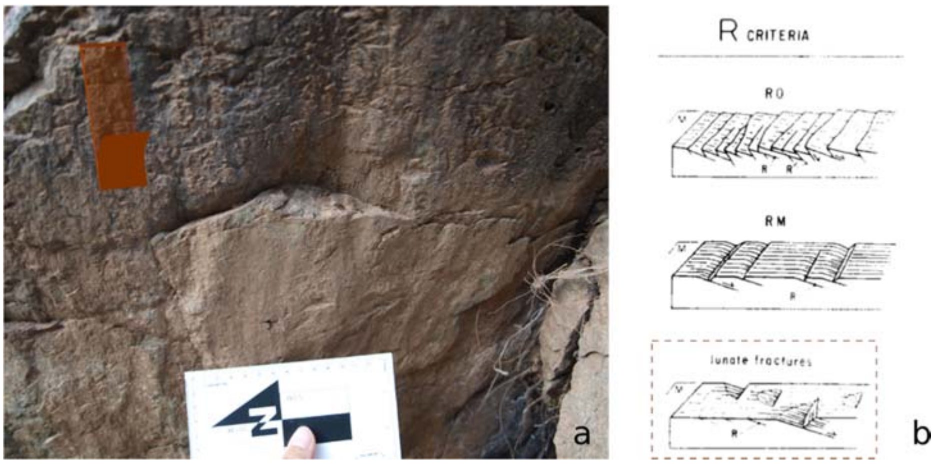

Figure 3.19. (a) A view from a fault plane deforming within the Yerköy-Şefaatli granite; (b) illustration of lunate fractures of R-type slickenside (Petit, 1987); (c) results of paleostress analysis of this fault plane.

The strike-slip fault (Figure 3.24), which is interpreted as a master fault, has no observed fault, except for one location where a weakly preserved fault plane trends in ~310˚direction. The shear senses are detected in the fault planes (see F09, F10, and F11 in Appendices), trending in nearly from 90° to 110°. Their orientations coincide with those of synthetic faults (R-shear faulting) in strain field of strike-slip fault zones. Thus, the slickensides measured on these planes can be used to refer to the shear sense of the master fault since they can share the same Riedel shear pattern between Y and R shear.

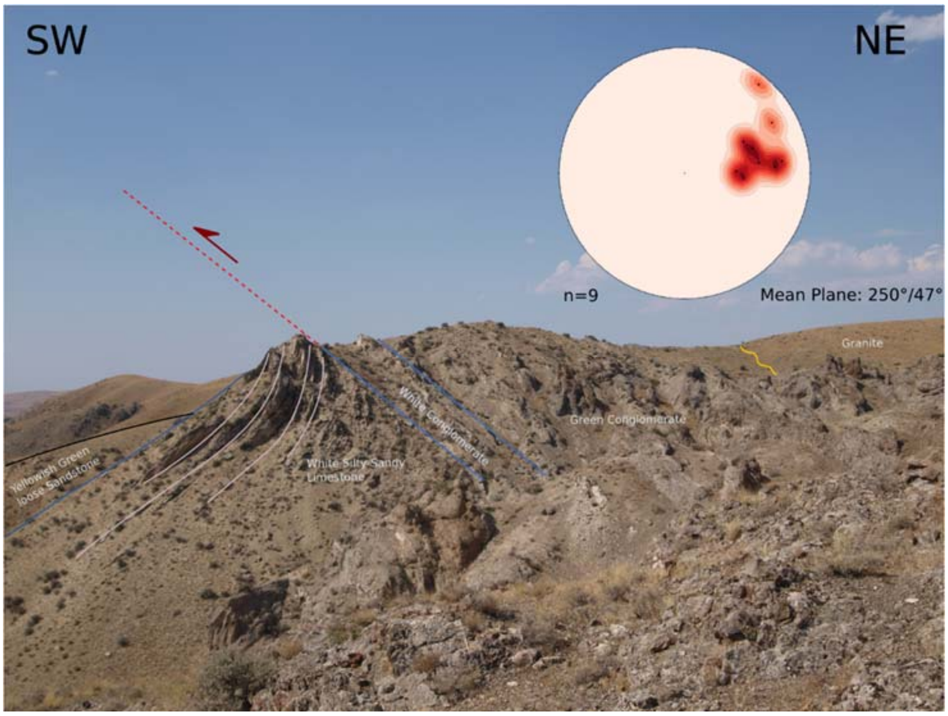

Figure 3.20. A reverse fault forming within the Yoncalı Formation. The stereonet indicates the poles to beds of a homocline in white silty/sandy limestones of the Kocaçay Formation (n: number of measurements).

Figure 3.21. (a) Normal fault cutting Kocaçay Formation; (b) close-up view of the fault plane.

3.4 Paleostress Analysis

Numerous aspects are attended to the reconstruction of orientations of principal stresses by examining the structures owing to brittle, or ductile deformation such as fault populations, joint set, tension gashes, stylolites, kink bands, dike sets, calcite e-twins, fracture markings on joint surfaces, and Riedel shears as well as earthquake focal mechanism data. In this study, the fault slip data are handled totally for the paleostress analysis.

The dynamic analysis of faulting was performed first by Anderson (1905) using the intersection of the faults (conjugate faults) and the orientation of slickenlines. This premise is based on Coulomb's (1776) failure hypothesis, the necessity of the vertical direction of a principal stress and the rupture occurrence within isotropic rocks (Célérier, 2005). Then, Wallace (1951) claimed that there is a mechanical relationship between shearing stress magnitude and orientation of fault plane, thereby controlling directly the slip direction. Bott (1959) proposed that the motion of blocks relative to each other along a fault surface results from a maximum resolved shear stress, which is related to the magnitudes and orientations of principal stress in a stress system. Those findings on the stress-shear relation formed a basis to create numerical algorithms, which improved the paleostress analysis until a more realistic results to be obtained. As cited in Angelier (1979, 1984, 1989, 1990, and 1994), the first application based on the stress-shear relationship of Wallace (1951) and Bott (1959) was made by Carey and Brunier (1974) with related assumptions, such as independency of each fault on motion and a *single common deviatoric mean stress tensor* governing the shear direction. *Wallace-Bott Criterion* proposed that if one knows the stress state, the shear stress can be decided and therefore, the slip orientation on any fault plane (Angelier, 1979, 1989); this is termed as forward modelling. The inverse modelling means the calculation of theoretical shear stress and consequently the mean stress tensor from the orientation and senses of slip in fault population. In such efforts, stress tensor should consist of minimized unknowns, which is called as *reduced stress tensor* in the literature, to avoid complexity in the numerical computations.

Three main assumptions underlying most of algorithms of paleostress analysis are (Angelier, 1979, 1984, 1994; Etchecopar *et al.*, 1981; Michael, 1984; Schimmrich, 1991):

i) The fault populations associated with their slip orientations are produced by a unique and homogenous regional stress tensor corresponding to a single tectonic event.

ii) Local effect of faulting and the interaction of fault motions are neglected.

iii) Motion on each fault is mechanically equivalent to the direction of maximum shear stress.

The approach of Žalohar & Vrabec (2007) recommends that even large angular misfits can contribute to determine optimal stress tensors for homogeneous fault subsets. The Gauss Method is interested not only in this parallelism between striations and shear stress, but also in the mechanical consistency of the paleostress inversion. On that account, it deals with the mechanical reality of the stress tensors found by obeying the Amonton's Law which states

$$\tau \geq \mu\sigma_n = \tan\emptyset_2.\sigma_n$$

where μ is the coefficient of residual friction for sliding on a pre-existing fault and σ_n is the normal stress on the fault. This relation declares that when the shear stress exceeds the frictional shear strength, which is depicted by $\mu\sigma_n$, slipping can take place along the fault associated with $\emptyset_i$, the angle of internal friction. The parameters of $\emptyset_1$ and $\emptyset_2$ refer to angle of internal friction for intact rock and the angle of residual friction on a fault which formed before, respectively. Hence, it can be predicted that the value of $\emptyset_1$ is higher than that of $\emptyset_2$ on the Mohr diagram.

Like the Gauss method, the similar efforts to prove the mechanical acceptance of paleostress inversion, unfortunately, were not sufficiently prevalent (Reches, 1987; Angelier, 1989; Reches et al., 1992; Yin and Ranalli, 1993; Fry, 2001 as cited in Žalohar & Vrabec, 2007).

Owing to those reasons, this study prefers to perform T-Tecto 3.0 rather than others for the reconstruction of principal stresses' axes, and the related stress ratio (Φ). The results are put in the geologic and structural maps of the study area (Figures 3.24, 3.26 & 3.28). The detailed ones are represented in the Appendices.

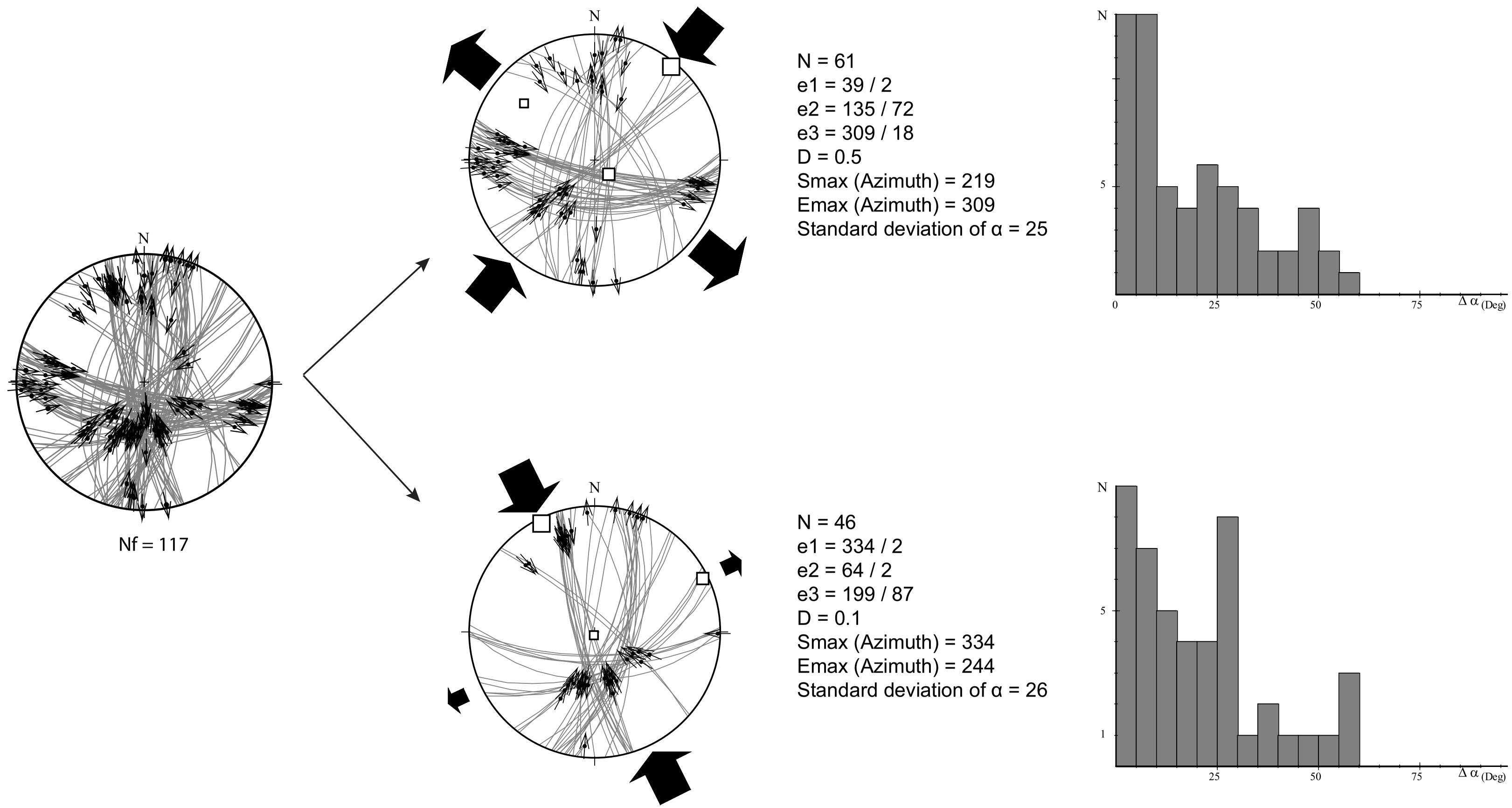

Figure 3.22. The stress tensors, and related results pertaining to study area-1. The graphs exhibit the distribution of number of compatible faults compared to misfit angles of each (N: the number of compatible faults; e_1, e_2, e_3: principal stress directions; D: ratio of principal stress; α: angular misfit)

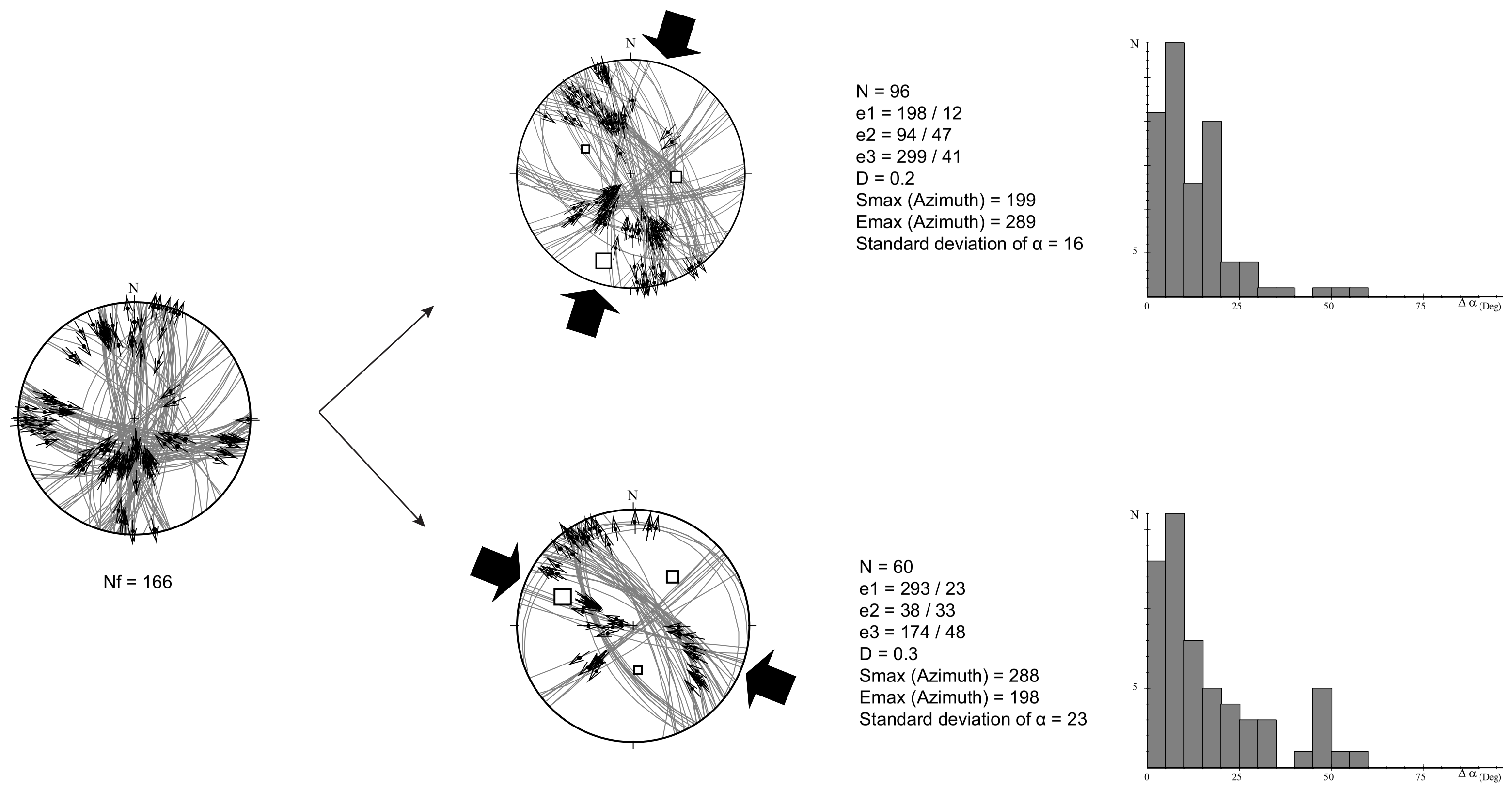

Figure 3.23. The stress tensors, and related results pertaining to study area-3. The graphs exhibit the distribution of number of compatible faults compared to misfit angles of each (Nf: the total measurements of fault planes; N: the number of compatible faults; e_1, e_2, e_3: principal stress directions; D: ratio of principal stress; α: angular misfit)

3.5 Results

The results of structural and paleostress analyses will be represented in this section. While the geometry and orientation of structures are plotted by graphical techniques such as rose diagrams and stereonets, the paleostress results are indicated directly by simple arrows referring to the compression-tension axes. All are compiled in the geologic and structural maps of study area-1, -2 and -3.

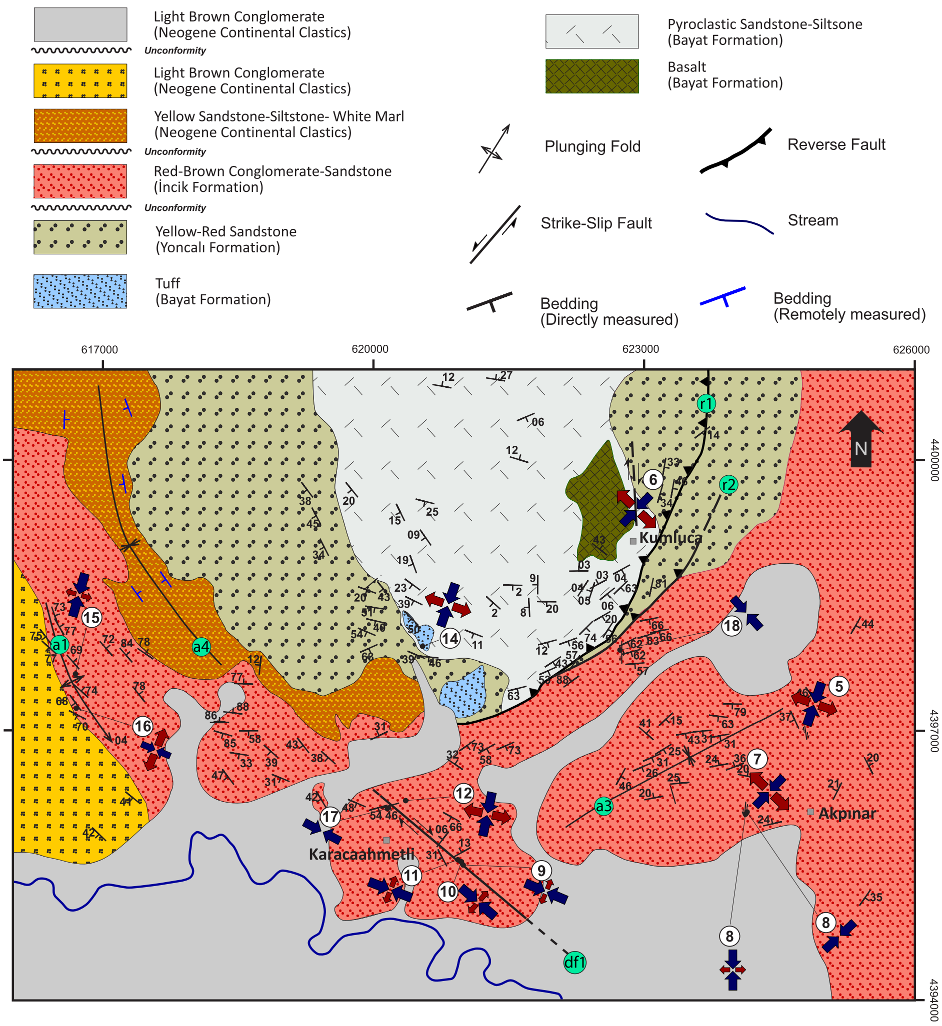

Figure 3.24. Structural map of study area-1. Blue and red arrows illustrate the results of paleostress analyses.

Major structure of the study area-1 is a reverse fault (***r1***) which cuts the İncik, Yoncalı, and Bayat Formation; it runs along the proximity to Ankara-Yozgat highway with an slightly arc geometry towards NE (Figure 3.24). No slickenside is observed along the line of the reverse fault which disappears beneath Neogene units in the further southern side. Other reverse fault (***r2***) is connected to ***r1***, which cuts off the Yoncalı Formation beneath Bayat Formation.

There is a syncline whose bearing is nearly 060º, named as ***a3*** near Akpınar village. Another type of fault is a dextral strike-slip structure (***df1***) trending in ~130º in the north of the new settlement of Karacaahmetli Village and near Ankara-Yozgat main road. Fault planes examined are sub-parallel (~110–120º) to the main fault plane (paleostress results; (9), (10) and (11)). In the eastern part of this area, around Haticepınar Mevkii, there is an anticline (***a1***) with axis trending in 160º within İncik Formation. The similar orientation can be seen as a consequence of folding of Neogene units located above İncik Formation along with angular unconformity.

The striking structures at the study area-2 are the folds deforming the sediments of the Kocaçay Formation, which is considered as a key unit (Figure 3.26). The attitudes of fold axes of three measured folds are 116º, 32º; 150º, 08º and 111º, 40º, from east to west, respectively (Figures 3.26 a & b). Further, one of these folds shown was cut by a normal fault supported by measurement (43) (Figure 3.21 a & b and Figure 3.26). Another major structure at the western part of Hacıoğlu village is a reverse fault, named as ***r3***. That faulting resulting in thrusting of Yoncalı Formation over İncik Formation, which can be seen along the line H-H’ (Figure 3.27). The tectonic contact exhibits obviously the extent of shearing to Çökelik volcanics (Figure 3.25 b). Furthermore, folded parts of Yoncalı Formation are composed of E-W trending anticline and syncline.

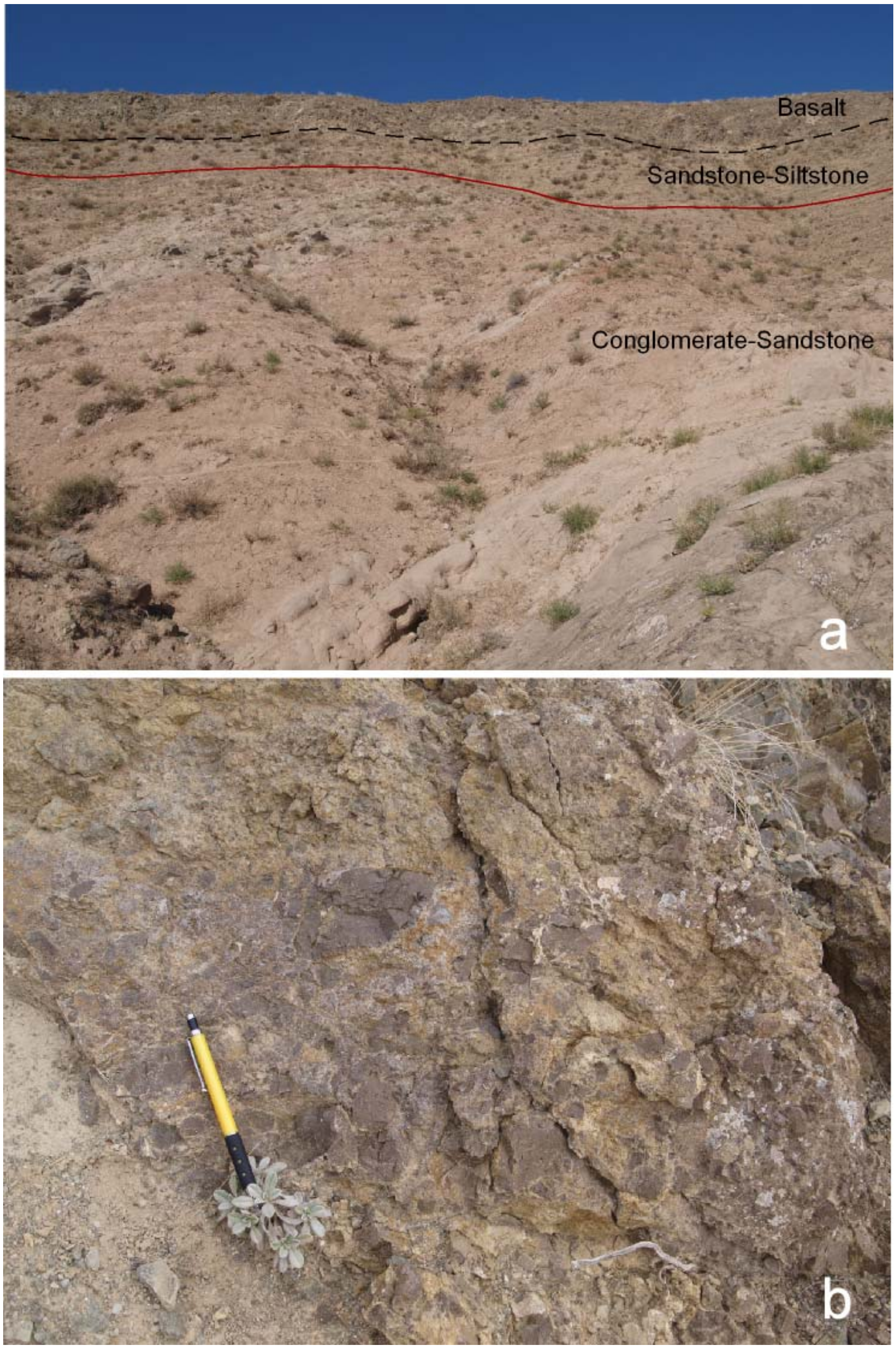

Figure 3.25. (a) Tectonic contact (solid red line) between basalt and sandstone-siltstone alternation of the Yoncalı Formation above and conglomerate-sandstone unit of the İncik Formation; (b) close-up view from sheared basalts, indicating the extend of the effect of the reverse faulting.

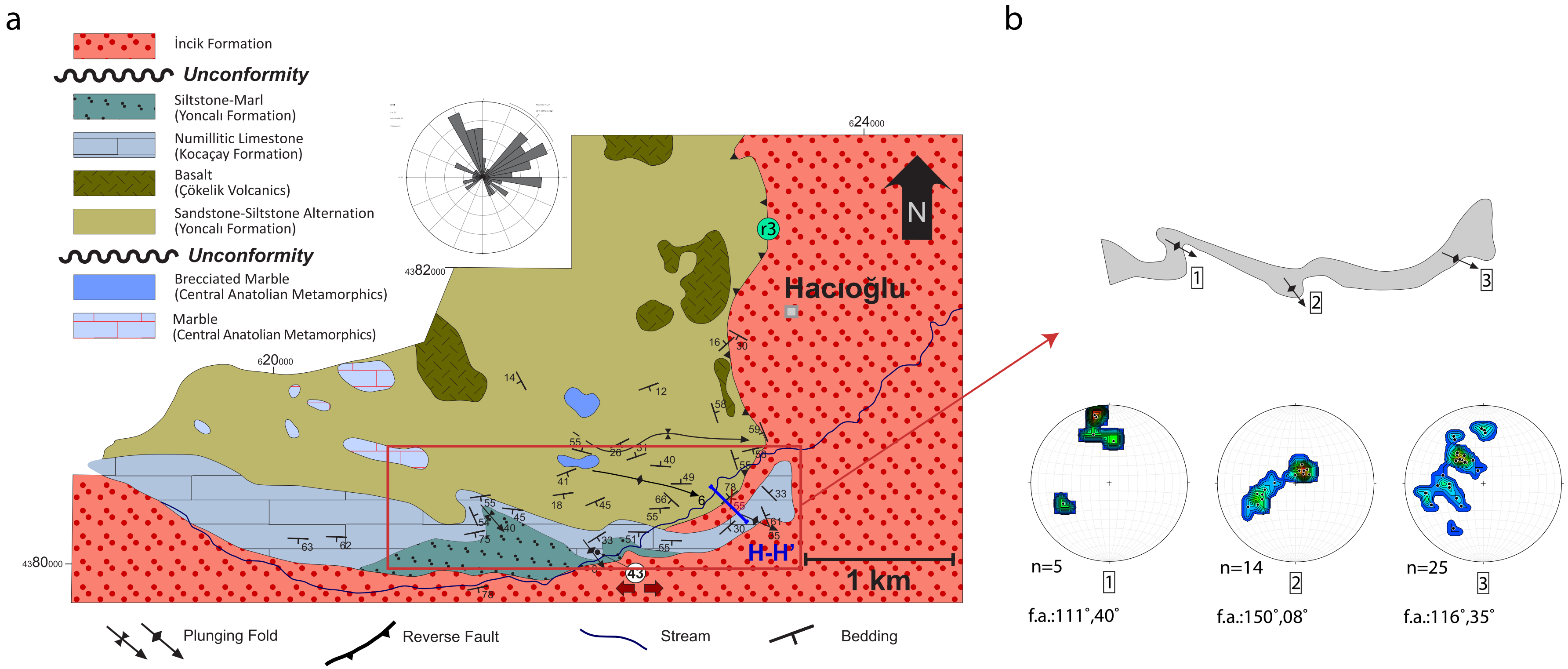

Figure 3.26. (a) The geological map of study area-2 associated with tensional stress direction having creating a normal fault. (b) The orientations of folds via plotting stereonets (f.a: foldaxis; n: the number of measurements).

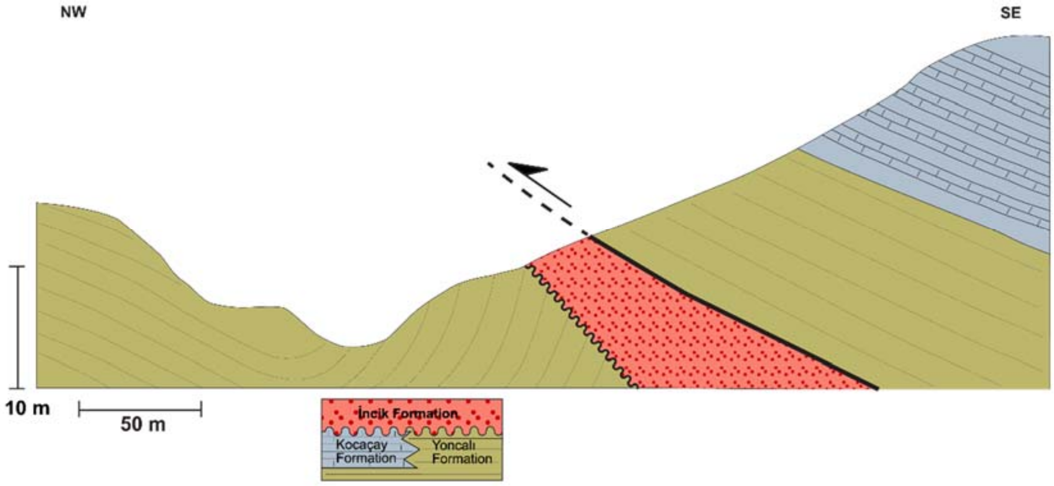

Figure 3.27 The cross-section along the line H-H' (See its location in Figure 3.26).

The major structure is a strike-slip fault (***df2***) located in the northern part of the study area -3 (Figure 3.28). The distinct movements of ***df2*** are seen in different outcrops by observing structures displaying sinistral (Figure 3.18), and dextral motion (Figure 3.17) such as slickensides and folded joints. Another structure is a reverse faults trending in ~280º (***r7***). Further reverse fault (***r5***) is available with trend of NW-SE. The general tendency of beds in Yoncalı and Kocaçay Formation is southwestward, and almost ~70º -90º. From northwest to southeast, deformation changes with respect to type and amount. Especially, between places where Yoncalı Formation does, or does not crop out, relatively large syncline (Figure 3.5) and superposed fold (Figure 3.7) exist around Keçikalesi hill. Besides, a reverse (***r5***) and strike-slip faults (***r6***) cuts the basalts of Bayat volcanics and can create a tectonic contact with the limestones of Kocaçay Formation.

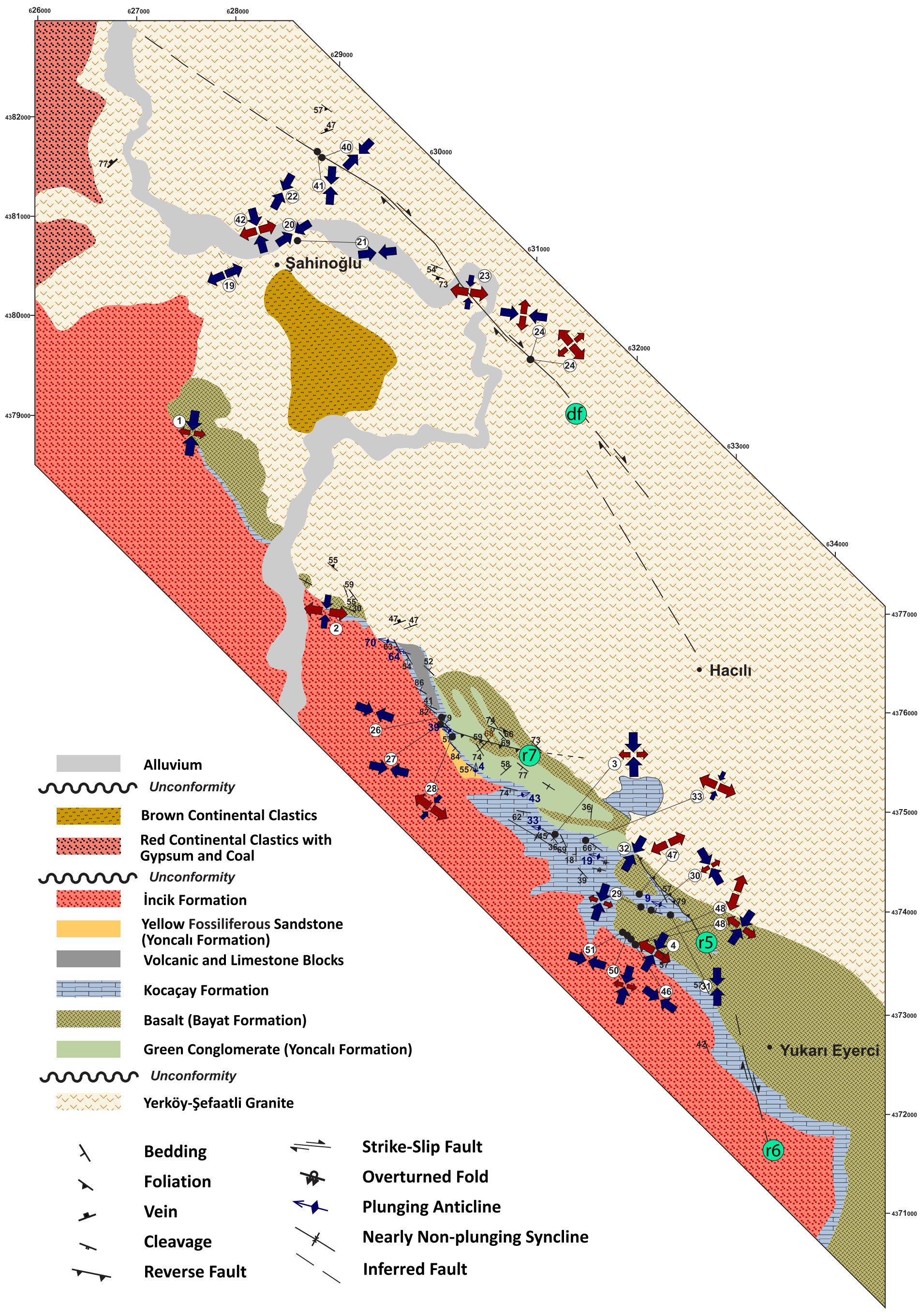

Figure 3.28. The geological map of study area-3. The results of paleostress analysis for slickenside measurements are also shown by red (compression) and blue arrows (extension).

As a result of folding the units of the Kocaçay Formation, a chain of anticline is observed along the NW-SE bearing basin margin. There are eight folds mapped; six of them show the same geometric features (Figure 3.29). Possible explanations of why two of these folds exhibit different orientations are: (i) they may be related to a different deformation stage, or (ii) the low number of measurements due to the scarce exposures of the folds.

The six folds exhibit similar geometry and the attitudes of their fold axes, from northwest to southeast, are: (i) 277º, 70º; (ii) 323º, 43º; (iii) 299º, 39º; (iv) 283º, 33º; (v) 285º, 19º and (vi) 292º, 04º (Figure 3.29).

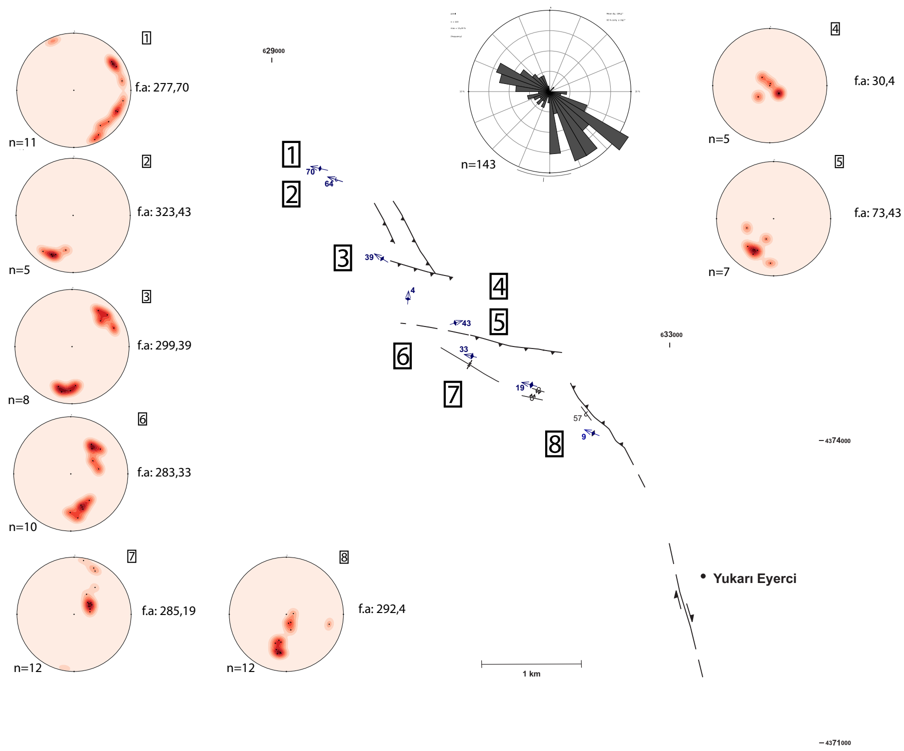

Figure 3.29. The structural map of study area-3 representing folds (blue) associated with the faults. The stereonets of folds with their numbers which are put into the exact location in the map (n: the number of measurements; f.a: fold axis). The rose diagram shows the strikes of beds measured overall.

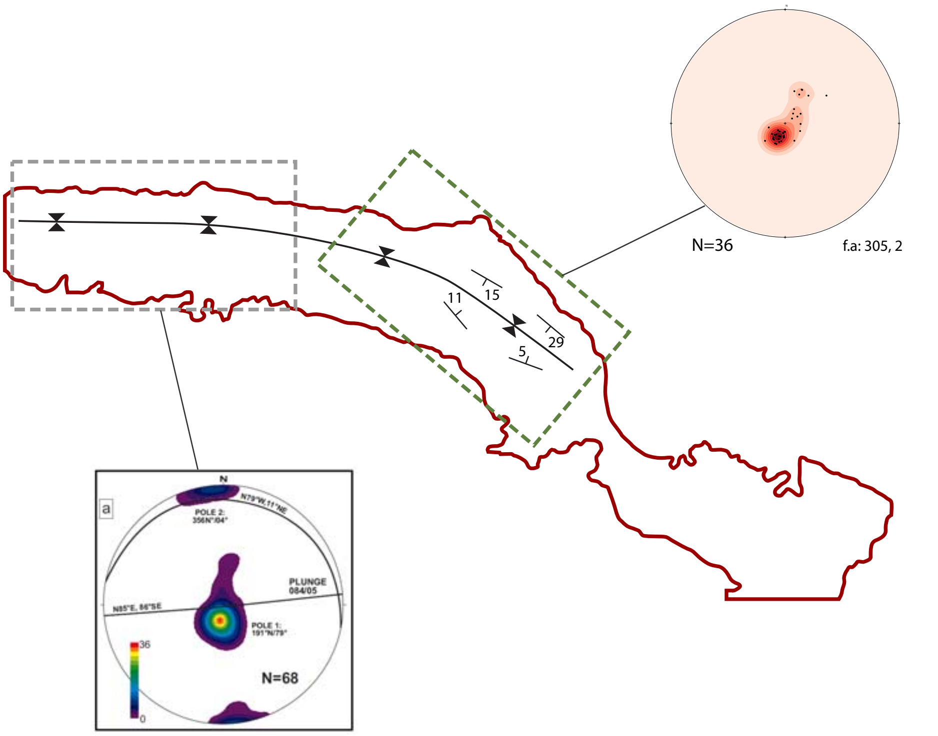

Figure 3.30. Stereonets showing the attitude of the syncline in the southern subbasin; red line outlines the basin boundary. Lower inset belongs to the measurements of Gülyüz (2009); the upper to this study (N: number of measurements; f.a : fold axis).

CHAPTER 4

DISCUSSION

The study was carried out in three localities; two of them lies within the southern sub-basin of the Çiçekdağ Basin and one in the northern sub-basin (Figure 2.2). These locations are labelled as study area-1, -2 and -3. (Figures 2.3, 2.4 & 2.5). Study area-1 and -2 are located on each side of the proposed fault zone; the study area-3 along a part of the zone. The structures in these areas are examined, based on the geometry of structures, and their spatial distributions, to determine the kinematics of the deformations. Deformation patterns of each location are correlated and then, the similarities, or differences are detected by combining all results.

In study area-1, the apparent major structure is a reverse fault, ***r1***, occuring between the Bayat and the Yoncalı formations and continues within the Yoncalı Formation. Its deformational effect and interaction with ***r2*** can be observed along the trace of ***r1***. The beds dip to the southeast and the dip amount and direction change dramatically along a NE to SW traverse within yellow sandstone-siltstone alternation of the Yoncalı Formation. The dip amount in the northeast of Kumluca Village varies between 30º and 35º and ~80º further in the south; there is an obvious increase in dip amount from NE to SW. Even, there is an observed shifting in the dip direction from southeast to northwest (Figure 2.3). This pronounced change in dip direction and amount of the bedding is associated with cut-off of the Yoncalı Formation beneath pyroclastic sandstone-siltstone alternation of the Bayat Formation; this relationship is used as an evidence of the reverse fault ***r1*** in the study area-1 (Figures 2.3 No slickenside was observed along a fault trace of ***r1***. However, the slickenside (18) might be indirectly representative since it exits in proximity of the fault and also its result, NW–SE compression direction, is compatible with the orientation and characteristic of the fault.

The fault population argues for two distinct stress regimes in the study area-1; NW−SE and NNE−SSW (or, NE-SW) compressions (Figure 3.22). The latter is related to the folding of the İncik Formation, ***a1***; the former to ***a3***.

Moreover, the paleostress analyses (9), (10) and (11) pertaining to ***df1*** represent compatible kinematic axes that may create dextral strike-slip fault. Almost NW−SE compression is detected from the fault planes of ***df1***. The kinematics of fault planes (9), (10), (11), (17) and (18) are similar to each other, and they all indicate a single phase of NW−SE compression.

As for small faults, they can help us to see deformation phases as a mimic. Most slip data imply NE−SW compression. Faults (5), (6), (7), (8), (12) and (14) can be clustered into one group to display one deformation phase (Figure 3.24). Furthermore, Fault (8) records two phases; N−S and NE−SW compression. Besides, fault planes deforming the anticline are measured at locations (15) and (16); they have different phases of deformation, separately. Fault plane (15) results from NW−SE compression; on the other hand, location (16) does NE−SW compression with dominant extensional component. The two slickensides cannot be used to decipher a geologic order of the fault plane (8).

One hand, the orientations of reverse faults, ***r1*** and ***r2***, and fold axis of the anticline, ***a3***, are almost compatible, which in turn suggest that these structures have formed under the same stress regime, NW−SE compression. On the other hand, ***a1*** and ***a4*** associated with ***sf*** correspond to structures pertaining to a distinct phase; NE−SW compression. The Neogene units are critical to separate these compressional phases in a chronologic order. The folding of the Neogene units, ***a4***, suggests that NE−SW compression postdates NW−SE compression.

As to study area-2, most of beds of the İncik and the Yoncalı formations along ***r3*** strike nearly NW−SE (Figures 3.26), suggesting a likely NE−SW compression. The faulting ***r3*** probably post-dates middle Oligocene. Since the İncik Formation covers unconformably the Yoncalı and the Kocaçay formations, the activity of ***r3*** might have began after the end of sedimentation of the İncik Formation in this area. Further, one of these folds is cut by a normal fault (Figure 3.21). The analysis of the slickenside suggests an almost E−W extension. This normal fault might have occured due to local stress disturbance because extensional structures are not seen abundantly in the study area.

As for study area-3, the prominent structure is a dextral strike-slip fault, ***df2***, in the northern part. This could be attributed to the reactivation of ***df2*** in study area-3 (Figure 3.28). The sinistral motion is followed by the dextral one. Based on the orientation of the fault, ~130−140º, which is similar to that of the proposed fault zone, the change in sense of shearing might be due to a change from NW−SE compression to NNE−SSW. This further suggests that the earliest phase is a NW−SE compression.

NW−SE-trending (~320°) structure (***r5***) is possibly a continuation of right-lateral strike-slip fault; ***r6***, (Figure 3.28). Approximately E−W-striking (280°−285°) Reverse fault (***r7***) and NW−SE-trending folds are oblique to reverse and strike-slip faults as well (Figure 4.1). The angular relationship between ***df2*** and ***r6*** coheres with the orientation of P and R shear. The main shear plane; that is, Y shear, corresponds likely to the orientation displayed in Figure 4.1. This is consistent of dextral motion under NNE−SSW compression. The oblique relationship of folds and reverse faults with ***df2*** means transpressional deformation; it is interpreted as last phase phase of deformation in the study area-3 (Figure 4.1b).

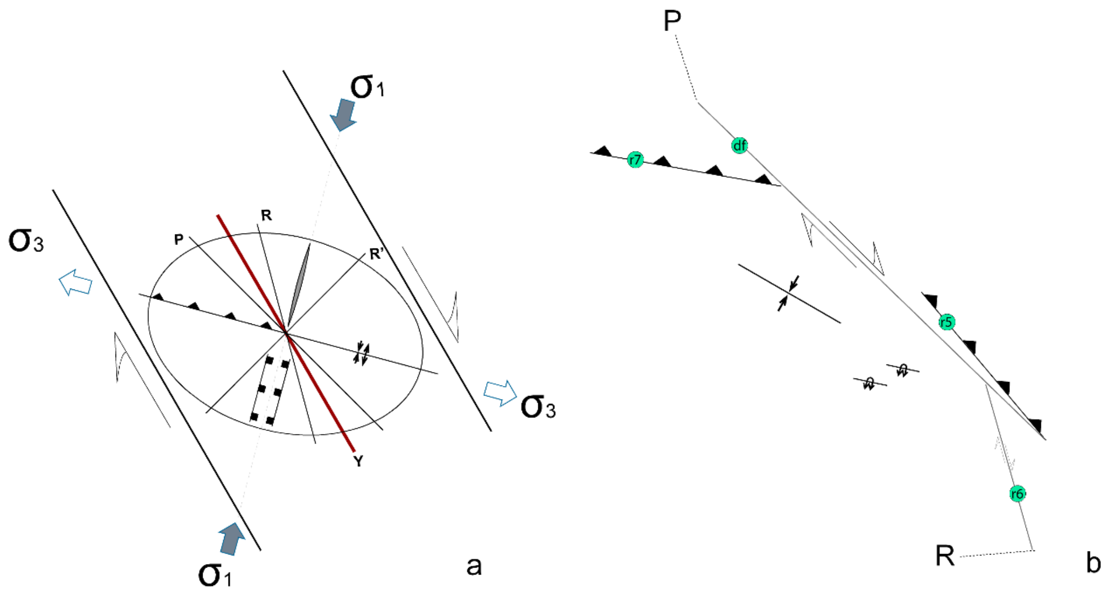

Figure 4.1. (a) Riedel pattern of deformation as a result of NNE-SSW compressional phase (b) Simplified representation regarding geometric relationship among structures of the study area-3.

The southeast-trending part of the syncline adjacent to the study area-3 displays similar geometric relationships with the bedding of other basin infill units since the general trend of their beds is approximately 300º (Figure 3.29 & 3.30). They are nearly perpendicular to the orientation of σ_1 of NNE−SSW compression.

Progressive unconformities in the study area-3 may therefore be considered to indicate convergence bringing about syncline and the fault motion along the basin margin since the sedimentation continues at the same time with faulting, thereby forming the intraformational syn-depositional unfonconformities in the İncik Formation (Kaymakcı, 2000). This supports existence of a transpressional stress regime.

The former researchers worked in the CACC designate regional deformation phases as recognized along the fault zone and in the basin. To illustrate, NW−SE compression was interpreted by studying structures deforming the Middle Miocene mollasse basin sediments of the CACC by Dirik & Göncüoğlu (1996). They also contended that the NE−SW compression proceeded up to the latest Miocene. Moreover, the deformations under this stress state could be observed in the uppermost Miocene−Pliocene basins limited by oblique-slip, or normal faults. The motion of the Savcılı Thrust Zone towards NNE after Middle Miocene (Seymen, 2000) may be congruent with that stage.

As a summary, present study claims that this region was subjected to a NW−SE compression until pre-Middle Oligocene and then to NNE−SSW compression during the Neogene period. Kinematic patterns are common in all locations of the study area. Accordingly, the study area-1, -2, and -3 are located in the same deformation zone as proposed by previous workers (Dirik & Göncüoğlu, 1996; Erler & Göncüoğlu, 1996; Boztuğ, 1998; Koçyiğit & Erol, 2001; Boztuğ *et al.*, 2007, 2009; Lefebvre, 2011; Lefebvre *et al.*, 2013; Advokaat *et al.*, 2014). It is concluded that the presence of DKFZ is supported by new stuctural data presented in the study; there is, however, no observation, or no measurement to support dextral displacement of ~90 km as suggested by Lefebvre *et al.* (2013).

CHAPTER 5

CONCLUSION

Based on the structural and stratigraphic data, the recent study suggested an order of stress regimes in the whole of the study area as below:

i. pre-Middle Oligocene NW−SE compression
ii. post-Oligocene NNE−SSW compression

It is advocated that the first deformation phase gave rise to NE-SW trending reverse faults and syncline. Folding of Neogene units are related to a subsequent deformation (after hiatus) NE−SW compression. A change in stress regime is indicated by the reactivation of the NW−SE-trending sinistral strike-slip fault as a dextral structure. The second stress state resulted in NW−SE-trending reverse faults, strike-slip faults, and anticlines as well as en-échelon folds plunging towards WNW. The obliquity of reverse faults, overturned folds and asymmetric syncline-anticline groups with each other are consistent with a transpressive stress regime. Accordingly, the characteristics of faults indicate that transpressional deformation with dextral motion took place as a last phase.

The geometric and kinematic analyses represent the coherency of deformation phases in the study area. Particularly, observing similar patterns with respect to kinematics in study area-1 and -3 points out that all belong to the same deformation zone. The structures and their mutual relationships presented in the preceding sections indicate the existence of the Delice-Kozaklı fault zone, which is recommended by Lefebvre *et al.* (2013) like the previous workers who contended a fault, or fault zone (Dirik &

Göncüoğlu, 1996; Erler & Göncüoğlu, 1996; Boztuğ, 1998; Koçyiğit & Erol, 2001; Boztuğ *et al.*, 2007 & 2009; Advokaat *et al.*, 2014).

REFERENCES

Advokaat, E.L., Van Hinsbergen, D.J.J., Kaymakcı, N., Vissers, R.L.M. & Hendriks, B.W.H. (2014) Late Cretaceous extension and Palaeogene rotation-related contraction in Central Anatolia recorded in the Ayhan-Büyükkışla basin, *International Geology Review*, 56 (15) , pp. 1813-1836.

Akıman, O, Erler, A., Göncüoğlu, M.C., Güleç, N. & Geven, A. (1993) Geochemical characteristics of granitoids along the western margin of the Central Anatolian Crystalline Complex and their tectonic implications, *Geological Journal*, 28, pp. 371-382.

Alpaslan, M. & Boztuğ, D. (1997) The co-existence of the syn-COLG and post-COLG plutons in the Yıldızeli area (W-Sivas). *Turkish Journal of Earth Sciences*, 6, 1–12.

Anderson, E.M. (1905) Facsimile reproduction of The Dynamics of Faulting, Geological Society, Special Publications, 2012, 367, pp. 231-246, London.

Angelier, J. (1979) Determination of the mean principal directions of stresses for a given fault population, *Tectonophysics*, 56, T17-T26.

Angelier, J. (1984) Tectonic Analysis of Fault Slip Data Sets, *Journal of Geophysical Research*, Vol. 89, No. B7, pp. 5835-5848.

Angelier, J. (1989) From orientation to magnitudes in paleostress determinations using fault slip data, *Journal of Structural Geology*, 11 (1/2), pp. 37-50.

Angelier (1990) Inversion of field data in fault tectonics to obtain the regional stress-III. A new rapid direct inversion method by analytical means, *Geophys. J. Int.*, 103, pp. 363-376.

Angelier, J. (1994) Fault slip analysis and paleostress reconstruction. In Paul L. Hancock (Ed.), *Continental Deformation*. Pergamon Press, Exeter, pp. 53-100.

Awdal, A., Healy, D. & Alsop, G.I. (2014) Geometrical Analysis of deformation band lozenges and their scaling relationships to fault lenses, *Journal of Structural Geology*, 66, pp. 11-23.

Aydın, N.S., Göncüoğlu, M.C. & Erler, A. (1998) Latest Cretaceous Magmatism in the Central Anatolian Crystalline Complex: Review of Field, Petrographic and Geochemical Features, *Turkish Journal of Earth Sciences*, 7, pp. 259-268.

Birgili, S., Yoldas, R. & Ünalan, G. (1974) Çankırı-Çorum Havzası'nın jeolojisi ve petrol olanakları ön raporu, TPAO, Report No. 1216 (unpublished).

Bott, M.H.P (1959) The mechanisms of oblique slip faulting, *Geol. Mag.*, 96, pp. 109-117.

Boztuğ, D. (1998) Post-Collisional Central Anatolian Alkaline Plutonism, Turkey, *Turkish Journal of Earth Sciences*, 7, pp. 145-165.

Boztuğ, D. & Jonckheere, R.C. (2007) Apatite fission-track data from central-Anatolian granitoids (Turkey) constrain Neo-Tethyan closure. *Tectonics*, 26, TC3011.

Boztuğ, D., Tichomirowa, M. & Bombach, K. (2007) ^{207}Pb-^{206}Pb single-zircon evaporation ages of some granitoid rocks reveal continent-oceanic island arc collision during the Cretaceous geodynamic evolution of the central Anatolian crust, Turkey, *Journal of Asian Earth Sciences*, 31, pp. 71-86.

Boztuğ, D., Jonckheere, R.C., Heizler, M., Ratschbacher, L., Harlavan, Y. & Tichomirova (2009) Timing of Post-Obduction Granitoids from Intrusion through Cooling to Exhumation in Central Anatolia, Turkey, *Tectonophysics*, 473, pp. 223-233.

Cardozo, N. & Allmendinger, R.W. (2013) Spherical projections with OSXStereonet: *Computer & Geosciences*, 51 (51), pp.193-205.

Célérier, B. (2005) Celebrating Anderson's faulting centenary, Geophysical Research Abstracts, Vol.7, 06903, EGU 2005, Vienna, Austria.

Davis, G.H. & Reynolds, S.J. (1996) Structural Geology of Rocks and Regions, the United State of America, John Wiley & Sons, Inc.

Davis, G.H., Bump, A.P., García & Ahlgren, S.G. (2000) Conjugate Riedel deformation band shear zones, *Journal of Structural Geology*, 22, pp. 169-190.

Delvaux, D. & Sperner, B. (2003) New Aspects of Tectonic Stress Inversion with Reference to the TENSOR Program, In Nieuwland, D.A. (Ed) New Insights into Structural Interpretation and Modelling, Geological Society, London, Special Publications, 212, pp. 75-100.

Dirik, K. & Göncüoğlu, M.C.(1996) Neotectonic Characteristics of Central Anatolia, *International Geology Review*, 38, pp. 807-817.

Dirik, K., Göncüoğlu, M.C. & Kozlu, H. (1999) Stratigraphy and pre-Miocene tectonic evolution of the southwestern part of the Sivas Basin, Central Anatolia, Turkey, *Geological Journal*, 34, pp. 303-319.

Doblas, M. (1998) Slickenside kinematic indicators, *Tectonophysics*, 295, pp. 187-197.

Dökmeci, L. 1980. Akdagmadeni yöresinin jeolojisi. M.T.A. Raporu No. 6953, 37p.

Dönmez, M., Akçay, A.E., Kara, H., Yergök, A.F., Esentürk, K. & Bilgin, Z.R. (2005) Geological Map of the Kırşehir – I32 Quadrangle, General Directorate of Minearl Research and Exploration, Ankara/Turkey.

Dresen, G. (1991) Stress distribution and the orientation of Riedel shears, *Tectonophysics*, 188, pp. 239-247.

Düzgören-Aydın, N.S., Malpas, J., Göncüoğlu, M.C. & Erler, A. (2001) A Review of the Nature of Magmatism in Central Anatolia during the Mesozoic Post_Collisional Period, *International Geology Review*, 43, pp. 695-710.

Erdogan, E., Akay, E., Ugur, M.S., 1996. Geology of the Yozgat region and evolution of the collisional Çankırı basin, *International Geology Review,* 38, 788–806.

Erler, A. & Göncüoğlu, M.C. (1996) Geologic and Tectonic Setting of the Yozgat Batholith, Northern Central Anatolian Crystalline Complex, Turkey, *International Geology Review*, 38, pp. 714-726.

Etchecopar, A., Vasseur, G. & Daignieres, M. (1981) An inverse problem in microtectonics for the determination of stress tensors from fault striation analysis, *Journal of Structural Geology*, 3 (1), pp. 51-65.

Fernández-Blanco, D., Bertotti, G. & Çiner, T.A. (2013) Cenozoic tectonics of the Tuz Gölü Basin (Central Anatolian Plateau, Turkey), Turkish Journal of Earth Science, 22, pp. 715-738.

Fleischmann, K.H. & Nemcok, M. (1991) Paleostress inversion of fault-slip data using the shear stress solution of Means (1989), *Tectonophysics*, 196, pp. 195-202.

Fossen, H. (2007) Deformation bands in sandstone: a review, Journal *of the Geological Society, London*, 164, pp. 755-769.

Fossen, H. (2010) *Structural Geology,* the United State of America, Cambridge University Press.

Fry, N. (1999) Striated faults: Visual Appreciation of their constraint on possible paleostress tensors, *Journal of Structural Geology*, 21, pp. 7-21.

Gautier, P., Bozkurt, E., Bosse, V., Hallot,E. & Dirik, K. Coeval extensional shearing and lateral underflow during Late Cretaceous core complex development in the Nig˘de Massif, Central Anatolia, Turkey, *Tectonics*, 27, TC1003.

Göncüoğlu, M.C. (1986) Geochoronological data from the southern part (Niğde area) of the Central Anatolian Massif, *Bulletin of Mineral Research and Exploration Institute of Turkey*, 105/106, pp. 83–96.

Göncüoglu, M.C., Toprak, V., Kuscu, I., Erler, A., Olgun, E., 1991. Geology of the western part of the Central Anatolian Massif, part 1: southern section. Turkish Petroleum Corporation (TPAO) Report, 2909, pp. 1–140 (In Turkish).

Göncüoğlu, M.C., Dirik, K., Erler A. & Yalınız, K. (1994) Orta Anadolu Masifinin Doğu Bölümünün Jeolojisi Bölüm-4: Orta Anadolu Masifinin Sivas Baseni ile İlişkisi. Turkish Petroleum Corporation (TPAO) Report No. ? (Unpublished), 135 pp (in Turkish).

Göncüoğlu, M.C., Erler A. Dirik, K., Yalınız, K., Olgun, E. & Rojay, B. (1992) Orta Anadolu Masifinin Batı Bölümünün Jeolojisi Bölüm-2: Orta Kesim. Turkish Petroleum Corporation (TPAO) Report No. 3155 (Unpublished), 76 pp (in Turkish).

Göncüoğlu, M.C. & Türeli, T.K. (1994) Alpine Collisonal-Type Granitoids from Western Central Anatolian Crystalline Complex, Turkey, *Journal of Kocaeli Univseriity, Earth Science Section*, No.1, pp. 39-46.

Göncüoğlu, M.C., Dirik, K. & Kozlu, H. Pre-Alpine and Alpine Terranes in Turkey: Explanatory Notes to the Terrane Map of Turkey, *Annales Géologique de Pays Héllenique*, 37, Geol. Soc. Greece, 515-536, Athens, 1997.

Görür, N., Oktay F.Y., Seymen, İ. & Şengör, A.M.C. (1984) Paleotectonic evolution of the Tuzgölü Basin complex, Central Turkey: Sedimentary Record of a Neo-Tethyan Closure, In, J. Dixon and A. Robertson (Ed.), The Geological Evolution of the Eastern Mediterranean. Geological Society Special Publication, 17, pp. 467-482.

Grohmann, C.H. & Campanha, G.A.C. (2010) OpenStereo: Open Source, Cross-Platform Software for Structural Geology Analysis, AGU Fall Meeting 2010, San Francisco, California, USA.

Güleç, N. (1994) Rb-Sr isotope data from the Ağacoren Granitoid (East of Tuz Golu): Geochronological and genetical implications. Turkish Journal of Earth Sciences, 3, 39–43.

Gülyüz, E., Kaymakci, N., Meijers, M.J.M., van Hinsbergen, D.J.J., Lefebvre,C., Vissers, R.L.M., Hendriks, B.W.H. & Peynircioğlu, A.A. (2013) Late Eocene Evolution of the Çiçekdağı Basin (Central Turkey): Syn-sedimenraty compression during microcontinent-continent collision in Central Anatolia, *Tectonophysics*, 602, pp. 286-299.

Gündoğdu, N., Bros, R., Kuruç, A. & Bayhan, H. (1988) Rb-Sr isotope data from the Bayındır feldspatoid-bearing syenites (Kaman-Kırşehir). Twentieth Earth Sciences of Hacettepe University Symposium, Abstracts, pp. 55.

Gürer, O.F. & Aldanmaz, E. (2002) Origin of the Upper Cretaceous – Tertiary sedimentary basins within the Tauride-Anatolide platform in Turkey, *Geological Magazine*, 139, pp. 191-197.

Hancock, P.L. (1985) Brittle microtectonics: principles and practice, *Journal of Structural Geology*, 7 (3/4), pp.437-457.

Hills, E.S., (1965) *Outlines of Structural Geology* (3rd Edition), Great Britain, Butler & Tanner Ltd.

Hinsbergen, D. J. J. v., Maffione, M., Plunder, A., Kaymakcı, N., Ganerød, M., Hendriks, B. W. H., Corfu, F., Gürer, D., Gelder, G. I. N. O. d., Peters, K., McPhee, P. J., Koç, A., Brouwer, F. M., Advokaat, E. L. & Vissers, R. L. M. (Submitted). Tectonic evolution and paleogeography of the Kırşehir Block and the Central Anatolian Ophiolites, Turkey. *Tectonics*.

Huang, Q. (1988) Computer-based method to separate heterogeneous sets of fault-slip data into sub-sets. *Journal of Structural Geology*, 10 (3), pp. 297-299.

Ingersoll, R.V. (2012) Tectonics of sedimentary basins, with revised nomenclature. In: Busby, C.J. & Ingersoll, R.V. (eds) *Tectonics of Sedimentary Basins*, 2nd edn. Wiley-Balckwell, Oxford, 3-43.

Işık, V., Lo, C-H, Göncüoğlu, M.C. & Demirel,S. (2008) Ar/Ar Ages from the Yozgat Batholith: Preliminary Data on the timing of Late Cretaceous Extension in the Central Anatolian Crystalline Complex, Turkey, *Journal of Geology*, 116, p.510-526.

İlbeyli; N., Pearce, J.A., Thirwall, M.F. & Mitchell, J.G. (2004) Petrogenesis of collision-related plutonics in central Anatolia, Turkey, *Lithos*, 72, 163–182.

Kadıoğlu, Y.K., Dilek, Y., Güleç, N. & Foland, K.A. (2003) Tectonomagmatic Evolution of Bimodal Plutons in the Central Anatolian Crystalline Complex, Turkey, *The Journal of Geology*, 111, pp. 671-690.

Kara, H., Bozkurt, E.H., Dalkılıç, H., Dönmez, M., Esentürk, K., Özbenden, H., Özbek, T., Keskin, İ. & Yergök, A.F. (1991) Geological Map of the Kırşehir – G18 Quadrangle, General Directorate of Minearl Research and Exploration, Ankara/Turkey.

Kaymakcı, N. (2000) Tectono-stratigraphical evolution of the Çankırı Basin (Central Anatolia, Turkey), Mededelingen van de, Faculteit Aardwetenschappen, Utrecht University, The Netherlands, (PhD. Thesis), 139 p.

Kaymakcı, N., De Bruijn, H. White, S.H., Van Dijk, .M., Saraç, G. and Unay, E. 2001. Tectonic implications of the Neogene stratigraphy of the Çankiri basin with special reference to the Çandir locality (North-Central Anatolia, Turkey). In Güleç, E, Begun, D.R., and Geraads, D. (eds.) *Geology and Vertebrate Paleontology of the Miocene hominoid locality of Çandir*. Courier Forschungsinstitut Senckenberg. 240, 9-28.

Kaymakcı, N., Özçelik, Y., White, S.H. & Van Dijk, P.M. (2009) Tectono-stratigraphy of the Çankırı Basin: Late Cretaceous to early Miocene evolution of the Neotethyan Suture Zone in Turkey. In Van Hinsbergen, D.J.J., Edwards, M.A. & Govers, R. (eds) *Collision and Collapse at the Africa-Arabia-Eurasia Subduction Zone*, The Geological Society, London, Special Publications, 311, pp. 67-106.

Ketin, İ. (1955) Yozgat Bölgesinin Jeolojisi ve Orta Anadolu Masifinin Tektonik Durumu, *Türkiye Jeoloji Kurumu Bülteni*, 6, pp.1-28.

Ketin, İ. (1966) Tectonic units of Anatolia (Asia Minor), *Min. Res. Explor. Inst. Turkey (MTA) Bull.,* 66, pp.23-34.

Koçyiğit, A. & Erol, O. (2001) A tectonic escape structure: Erciyes pull-apart basin, Kayseri, central Anatolia, Turkey, *Geodinamica Acta*, 14: 1-3, pp. 133-145.

Köksal, S. & Göncüoğlu, M.C. (2008) Sr and Nd Isotopic Characteristics of Some S-, I- and A-type Granitoids from Central Anatolia, *Turkish Journal of Earth Sciences*, 17, pp. 111-127.

Köksal, S., Romer, R.L., Göncüoğlu, M.C. & Toksoy-Köksal, F. (2004) Timing of post-collisional H-type to A-type granitic magmatism: U-Pb titanite ages from the Alpine Central Anatolian granitoids (Turkey), *Int J Earth Sci (Geol Rundsch)*, 93, pp. 974-989.

Köksal S., Toksoy-Köksal F., Göncüoglu M.C., Möller A., Gerdes A., Frei D. (2013) 3.8 Ga zircons sampled by Neogene ignimbrite eruptions in Central Anatolia: Comment. *Geology*.

Kurt, M.A., Alpaslan, M., Göncüoğlu, M.C., & Temel, A. (2008) Geochemistry of the Late Stage Medium to High-K Calc-Alkaline and Shoshonitic Dykes in the Ulukışla Basin (Central Anatolia, Turkey): Petrogenesis and Tectonic Setting, *Geochemistry International*, 46 (11), pp.1145-1163.

Kuruç, A. (1990) Rb-Sr Geochemistry of Syenitoids from Kaman-Kırşehir Region. (MSc Thesis), Hacettepe University, Ankara [in Turkish with English abstract, unpublished].

Lefebvre, C. (2011) The Tectonics of the Central Anatolian Crystalline Complex: a Structural, Metamorphic and Paleomagnetic Study (PhD. Thesis), Utrecht Studies in Earth Sciences, Utrecht University, The Netherlands, 139 p.

Lefebvre, C., Meijers, M.J.M., Kaymakci, N., Peynircioğlu, A., Langereis, C.G. & van Hinsbergen, D.J.J. (2013) Reconstructing the geometry of central Anatolia during the Late Cretaceous: Large-scale Cenozoic rotations and deformation between the Pontides and Taurides, *Journal of Structural Geology*, 366, pp. 83-98.

Means, W.D. (1987) A newly recognized type of slickenside striation, *Journal of Structural Geology*, 9 (5/6), pp.585-590.

Meijers, M.J.M., Kaymakci, N., Van Hinsbergen, D.J.J., Langereis, C.G., Stephenson, R. & Hippolyte, J.C. (2010) Late Cretaceous to Paleocene oroclinal bending in the central Pontides (Turkey), 29 (4), pp. 1-21.

Michael, A.J. (1984) Determination of stress from slip data: Faults and Folds, *Journal of Geophysical Research*, 89 (B13), pp. 11517-11526.

Mostafa, E.M. (2005) Iterative direct inversion: An exact complementary solution for inverting fault-slip data to obtain palaeostresses, *Computers & Geosciences*, (31), pp. 1059-1070.

Nemcok, M. & Lisle, R.J. (1995) A stress inversion procedure for polyphase fault/slip data sets, *Journal of Structural Geology*, 17 (10), pp. 1445-1453.

Nieto-Samaniego, Á. F. (1999) Stress, Strain and Fault Patterns, *Journal of Structural Geology*, 21, pp. 1065-1070.

Okay, A.I., Satır, M., Maluski, H., Siyako, M., Monie, P., Metzger, R. & Akyüz, S. (1996) Paleo- and Neo-Tethyan Events in Northwestern Turkey: Geologic and Geochronologic Constraints, In Yin, A & Harrison, T.M. (Ed), *The Tectonic Evolution of Asia*, Cambridge University Press, pp. 420-441.

Okay, A.I., Altıner, D. & Kılıç, A.M. (2015) Triassic limestone, turbidites and serpentinite – the Cimmeride orogeny in the Central Pontides, *Geological Magazine*, 152 (03), pp. 460-479.

Önal, A., Boztuğ, D., Kurum, S., Harlavan, Y., Arehart, G.B. & Arslan, M. (2005)

K-Ar age determination, whole rock and oxygen isotope geochemisty of the post-collisional Bizmişen and Caltı plutons, SW Erzincan, eastern Central Anatolia, Turkey. *Geological Journal*, 40, 457–476.

Özgül, N. (1976) Toroslar′ın bazı temel jeoloji özellikleri. *Türkiye Jeol. Kur. Bült.*, 19 (1), 65–78.

Özgül, N., 1984, Stratigraphy and tectonic evolution of the Central Taurides. In: O.Tekeli and M.C. Göncüoğlu (Editors), *Geology of the Taurus Belt*, Mineral research and Exploration Ins. Turkey, Ankara, 77-90.

Özsayın, E., Çiner, A., Rojay, B., Dirik, K., Melnick, D., Fernández-Blanco, D., Bertotti, Schildgen, T.F., Garcin, Y., Strecker, M.R. & Sudo, M. (2013) Plio-Quaternary extensional tectonics of the Central Anatolian Platesu: a case study from the Tuz Gölü Basin, Turkey, *Turkish Journal of Earth Sciences* , 22, pp. 1-24.

Petit, J.P. (1987) Criteria for the sense of movement on fault surfaces in brittle rock, *Journal of Structural Geology*, 9 (5/6), pp. 597-608.

Poisson, A., Guezou, J.C., Ozturk, A., Inan, S, Temiz, H., Gürsoy, H., Kavak, K.S. & Özden, S. (1996) Tectonic Setting and Evolution of the Sivas Basin, Central Anatolia, Turkey, *International Geology Review*, 38:9, pp. 838-853.

Reches, Z. (1987) Determination of the Tectonic Stress Tensor from Slip along Faults that Obey the Coulomb Yield Condition, *Tectonics*, 6 (6), pp 849-861.

Schimmrich, S.H. (1991) Evaluation of Computational Methods of Paleostress Analysis Using Fault-Striation Data (Master Thesis), the State University of New York at Albany, the US, 422 p.

Seymen, İ. (1980) Orta Anadolu Masifinin kuzeydoğusunda (Akdağmadeni, Yozgat) etkili olan bölgesel metamorfizmanın incelenmesi, *Bulletin of the Geological Society of Turkey*, 23, pp. 213-218.

Seymen, İ. (1981) Kaman (Kırşehir) dolayısında Kırşehir Masifi'nin stratigrafisi ve metamorfizması, *Bulletin of the Geological Society of Turkey*, 24, pp. 7-21.

Seymen, I. (1982). Kaman Dolayında Kırşehir masifi'nin Jeolojisi. *ITÜ Maden Fakültesi, Doçentlik Tezi, Istanbul*, 164 p.

Shan, Y., Suen, H. & Lin, G. (2003) Separation of polyphase fault/slip data: an objective-function algorithm based on hard division, *Journal of Structural Geology*, 25, pp. 829-840.

Simón, J.L., Arlegui, L.E. & Pocoví (2006) Fringe cracks and plumose structures in layered rocks: stepping senses and their implications for palaeostress interpretation, *Journal of Structural Geology*, 28, pp. 1103-1113.

Tatar, S. & Boztuğ, D. (1998) Fractional Crystallization and Magma Mingling/Mixing Processes in the Monzonitic Association in the SW Part of the Composite Yozgat Batholith (Şefaatli–Yerköy, SW Yozgat), *Turkish Journal of Earth Sciences*, 7, pp. 215-230.

Twiss, R.J. & Unruh, and J.R. (1998) Analysis of fault slip inversions: Do they constrain stress or strain rate? Journal of Geophysical Research, 103(B6), pp. 12205-12222.

Twiss, R.J. & Moores, E.M. (2007) Structural Geology (2nd Edition), the United State of America, W. H. Freeman and Company.

Wallace, R. E. (1951) Geometry of Shearing Stress and Relation to Faulting, *The Journal of Geology*, 59 (2), pp. 118-130.

Whitney, D.L. & Dilek, Y. (1997) Core complex development in central Anatolia, Turkey, *Geology*, 25 (11), pp 1023-1026.

Whitney, D.L., Teyssier, C., Dilek, Y., Fayon, A.K. (2001) Metamorphism of the Central Anatolian Crystalline Complex, Turkey: influence of orogen-normal collision vs wrench-dominated tectonics on P-T-t paths. *Journal of Metamorphic Geology,* 19, 411–432.

Whitney, D.L., Teyssier, Heizler, M. T. (2001) Gneiss domes, metamorphic core complexes, and wrench zones: Thermal and structural evolution of the Niğde Massif, central Anatolia, *Tectonics*, 26, TC5002.

Wojtal, S. & Pershing, J. (1991) Paleostresses Associated with Faults of Large Offset, *Journal of Structural Geology*, 13(1), pp. 49-61.

Woodcock, N.H. & Schubert, C. (1994) Continental Strike-Slip Tectonics. In Paul L. Hancock (Ed.), *Continental Deformation*. Pergamon Press, Exeter, pp. 251-263.

Xu, S. & Ben-Zion, Y. (2013) Numerical and theoretical analyses of in-plane dynamic rupture on a frictional interface and off-fault yielding patterns at different scales, *Geophysical Journal International*, 193, pp. 304-320.

Yalınız, K.M. & Göncüoğlu, M.C. (1998) General geological characteristics and distribution of the Central Anatolian Ophiolites, *Yerbilimleri, Bulletin of Earth Sciences Application and Research and Center of Hacettepe University*, 20, pp. 19-30.

Yalınız, M.K., Aydın, N.S., Göncüoğlu, M.C. & Parlak, O. (1999) Terlemez quartz monzonite of central Anatolia (Aksaray-Sarıkaman): age, petrogenesis and geotectonic implications for ophiolite emplacement. *Geological Journal*, 34, 233–242.

Yalınız, K.M., Göncüoğlu, M.C. & Özkan-Altıner, S. (2000a) Formation and emplacement ages of the SSZ-type Neotethyan ophiolites in Central Anatolia, Turkey: palaeotectonic implications, *Geological Journal*, 35, pp. 53-68.

Yalınız, K.M., Floyd, P.A. & Göncüoğlu, M.C. (2000b) Geochemistry of volcanic rocks from the Çiçekdağ Ophiolite, Central Anatolia, Turkey, and their inferred tectonic setting, within the northern branch of the Neotethyan Ocean. In Bozkurt, E., Winchester, J.A. & Piper, J.D.A. (Ed.), *Tectonics and Magmatism in Turkey and the surrounding Area*. Geological Society, London, Special Publications, 173, 203-218.

Yamaji, A. (2000) The multiple inverse method: a new technique to separate stresses from heterogenous fault-slip data, *Journal of Structural Geology*, 22, pp. 441-452.

Yılmaz, S. & Boztuğ, D. (1998) Petrogenesis of the Çiçekdağ Igneous Complex, N of Kırşehir, Central Anatolia, Turkey, *Turkish Journal of Earth Science*, 7, pp. 185-199.

Žalohar, J. & Vrabec, M. (2007) Paleostress analysis of heterogeneous fault-slip data: The Gauss method, *Journal of Structural Geology*, 29, pp. 1798-1810.

Žalohar, J. & Vrabec, M. (2008) Combined kinematic and paleostress analysis of fault-slip data: The Multiple method, *Journal Structural Geology*, 30, pp. 1603-1613.

Žalohar, J. & Vrabec, M. (2010) Kinematics and dynamics of fault reactivation: The Cosserat Approach, *Journal Structural Geology*, 32, pp. 15-27.

Zeck, H.P. & Ünlü, T. (1988) Alpine ophiolite obduction before 110±5Ma ago, Taurus belt, Eastern central Turke *Tectonophysics*, 145, 55–62.

APPENDICES

APPENDIX A: DATA

#	Structure	Strike	Dip	Spatial Point
1	Lamination	120	39	put on the map
2	Lamination	137	25	put on the map
3	Bed	301	85	36628156 E 4378098 N
4	Foliation	126	37	36628156 E 4378098 N
5	Bed	109	32	3672881 E 437687 N
6	Foliation	225	37	36628756 E 4377248 N
7	Foliation	130	84	
8	Bed	152	89	36628688 E 4377248 N
9	Foliation	325	55	36628888 E 4377317 N
10	Vein	161	59	36629026 E 4377023 N
11	Bed	309 296 275	29 35 30	36629067 E 4376883 N
12	Joint	241	47	36629571 E 4376746 N
13	Joint	58	26	36629601 E 4376740 N
14	Bed	293	90	36629457 E 4376560 N
15	Bed	154	63	36629554 E 4376509 N
16	Bed	302	39	36629620 E 4376438 N
17	Fold	154 302	63 39	put on the map
18	Fold	299 297 310 294 282	67 69 71 64 52	36629633 E 4376440 N
19	Bed	151	69	36631250 E 4374565 N
20	Bed	117	74	36630707 E 4375060 N
21	Bed	187	36	36631519 E 4374823 N
22	Bed	162	46	36631252 E 4374559 N
23	Bed	132	36	36631147 E 4374559 N
24	Bed	117	45	36631099 E 4374627 N
25	Bed	130	61	36631024 E 4374659 N
26	Fold	125 130 140 170 149 252 251 235 261 271	53 48 57 41 37 48 55 47 67 57	36630982 E 4374688 N
27	Fold	302 313 274 300 341 297 290	54 56 67 61 41 52 31	36630802 E 4375023 N
28	Bed	100	62	36630708 E 4375061 N
29	Bed	130	55	36630311 E 4375279 N
30	Fold	220 103 316 221 47	17 03 23 17 16	36630311 E 4375279 N

31	Bed	130	84	36630160 E 4375478 N
32	Fold	174 241 254 257 293 291 278 283 281 286 279 286	10 13 23 13 66 45 58 60 41 54 57 39	36632344 E 4373852 N .. .. ..
33	Foliation	296	79	36632323 E 4373936 N
34	Bed	330	57	36632259 E 4374007 N
35	Bed	151	57	36632714 E 4373070 N
36	Bed	122	37	36632224 E 4373410 N
37	Lamination	152	42	P6555
38	Bed	203	10	36633890 E 4369279 N
39	Bed	171	15	36633883 E 4369460 N
40	Bed	152	58	36633606 E 4366553 N
41	Bed	132	57	36633329 E 4366798 N
42	Bed	130	58	36633555 E 4367146 N
43	Bed	174	33	36634030 E 4368027 N
44	Bed	178	32	36634025 E 4368233 N
45	Bed	35	35	36625434 E 4394968 N
46	Fold	38 59 33 32 318 005 000 334 18 19 335	39 28 20 21 14 06 16 06 50 49 26	36624928 E 4395449 N
47	Bed	227	21	36625108 E 4396148 N
48	Bed	344	20	36625454 E 4396431 N
49	Bed	150	46	
50	Bed	155	37	36624617 E 4396964 N
51	Bed	8	46	36623303 E 4399493 N
52	Bed	11	34	36623160 E 4399436 N
53	Bed	42	14	36623614 E 4400102 N
54	Vein	242 232 237	73 64 66	
55	Bed	65	6	36621681 E 4400292 N
56	Bed	266	24	36624397 E 4395802 N
57	Bed	285	20	36624130 E 4396376 N
58	Bed	246	36	36623992 E 4396406 N
59	Bed	254	24	36623814 E 4396448 N
60	Bed	262	25	36623375 E 4396258 N

61	Bed	260	20	36623099 E 4396096 N
62	Bed	241	13	36620950 E 4395445 N
63	Bed	150	31	36620753 E 4395409 N
64	Bed	213	6	36620718 E 4395582 N
65	Bed	115	66	36620838 E 4395856 N
66	Bed	235	31	36620063 E 4396724 N
67	Bed	62	63	36619925 E 4397724 N
68	Bed	118	54	36619925 E 4397892 N
69	Bed	108	40	36619988 E 4398012 N
70	Bed	98	51	36619995 E 4398162 N
71	Bed	118	20	36619907 E 4398361 N
72	Bed	167	19	36620407 E 4398646 N
73	Bed	155	9	36620571 E 4398951 N
74	Bed	103	25	36620535 E 4399336 N
75	Bed	165	15	36620250 E 4399239 N
76	Bed	156	20	36619730 E 4399473 N
77	Bed	92	46	36620585 E 4397608 N
78	Bed	307	32	36620860 E 4396475 N
79	Bed	51	73	36621014 E 4396654 N
80	Bed	138	39	36620476 E 4397629 N
81	Bed	18	63	36621015 E 4396654 N
82	Bed	77	22	36622611 E 4398209 N
83	Bed	45	74	36622364 E 4397921 N
84	Bed	62	53	36621959 E 4397484 N
85	Bed	131	41	36617329 E 4396067 N
86	Bed	227	28	36615185 E 4398005 N
87	Fold	351 342 155 171 176 147 328 336 344 343	73 77 75 58 71 77 70 76 77 69	Fold ***a1***
88	Bed	321	74	36616718 E 4397247 N
89	Bed	327	68	36616617 E 4397104 N
90	Bed	126	70	36616687 E 4396991 N
91	Bed	331	78	36617370 E 4397223 N
92	Bed	303	78	36617445 E 4397652 N
93	Bed	321	84	36617225 E 4397652 N
94	Bed	325	72	36616997 E 4397730 N
95	Bed	20	27	
96	Bed	170	15	36614913 E 4408466 N

97	Bed	47	86	36605800 E 4398885 N
98	Bed	117	48	36619792 E 4396007 N
99	Bed	76	54	36620024 E 4395932 N
100	Bed	74	46	36620153 E 4395956 N
101	Bed	108	25	36620158 E 4395937 N
102	Bed	138	50	36620399 E 4398078 N
103	Fault	342	87	36620412 E 4398079 N
104	Bed	121	30	36620379 E 4398237 N
105	Bed	104	27	36620456 E 4398281 N
106	Bed	130	23	36620406 E 4398424 N
107	Bed	140	43	36620092 E 4398374 N
108	Bed	53	58	36621231 E 4396618 N
109	Bed	45	56	36621311 E 4396599 N
110	Bed	241	69	36621338 E 4396635 N
111	Bed	57	73	36621432 E 4396642 N
112	Bed	64	63	36621565 E 4397270 N
113	Bed	43	63	
114	Bed	57	4	36622735 E 4398589 N
115	Bed	314	43	36622484 E 4398827 N
116	Bed	268	3	36622261 E 4398646 N
117	Bed	233	8	36622290 E 4398575 N
118	Bed	234	15	36622289 E 4398544 N
119	Bed	240	14	36622282 E 4398502 N
120	Bed	248	4	36622302 E 4398400 N
121	Bed	197	5	36622406 E 4398398 N
122	Bed	22	10	36622511 E 4398374 N
123	Bed	42	6	36622559 E 4398329 N
124	Bed	46	10	36622544 E 4398199 N
125	Bed	41	11	36622514 E 4398161 N
126	Bed	48	20	36622492 E 4398072 N
127	Bed	66	56	36622134 E 4397803 N
128	Bed	82	53	36622090 E 4397775 N
129	Bed	53	56	36622002 E 4397679 N
130	Bed	60	12	
131	Bed	58	42	36621967 E 4397579 N
132	Bed	247	88	36622160 E 4397371 N
133	Bed	216	57	36622176 E 4397596 N
134	Bed	86	57	36622871 E 4397559 N
135	Bed	73	62	36622789 E 4397700 N
136	Bed	54	62	36622779 E 4397781 N

137	Bed	84	72	36622778 E 4397799 N
138	Bed	74	78	36622837 E 4397796 N
139	Bed	62	83	36623000 E 4397856 N
140	Bed	68	66	36623023 E 4398034 N
141	Bed	67	66	36623141 E 4397914 N
142	Bed	141	42	36616935 E 4395673 N
143	Bed	108	41	36617165 E 4393970 N
144	Bed	264	25	36616863 E 4393773 N
145	Bed	114	16	36607636 E 4395782 N
146	Bed	126	30	36608476 E 4394400 N
147	Bed	151	26	36614494 E 4394633 N
148	Bed	280	15	36615982 E 4393654 N
149	Joint	41 40	85 16	36626667 E 4381360 N
150	Joint	129 164 126 129 144 158 149 122 26 255 5 352	21 26 39 26 32 24 35 30 64 84 60 58	36626671 N 4381300 E
151	Plumose	228	77	36626705 E 4381550 N
152	Joint	77 88 75 81 90 93 62 73 58	75 67 74 75 90 90 75 69 78	
153	Plumose	356	87	36626705 E 4381550 N
154	Joint	164 194 157 162 192 192 182 179	41 33 35 42 29 32 36 36	
155	Joint	32 37 42 53 114	31 44 41 34 30	36626710 E 4381854 N
156	Shear Plane	274 283 274 272 277	64 84 69 71 46	36627173 E 4382113 N
157	Joint	146 159 164 151 145 153	56 77 66 62 64 72	36627173 E 4382113 N

158	Joint	208 176 171 168 228	41 66 63 63 48	
159	Joint	131 124 136 135 122 112 133 126 133 124 129 136	44 35 43 48 37 38 34 45 49 33 46 46	36627082 E 4381582 N
160	Shear Plane	124 125 130 309	86 81 82 82	36628433 E 4380534 N
161	Joints	130 129 127	86 88 83	36628433 E 4380534 N
162	Joints	107 108 109 120	70 62 55 56	36628421 E 4380703 N *
163	Joints	87 126 127 135	38 36 34 35	36628421 E 4380703 N *
164	Vein	111	54	36629978 E 4380387 N
165	Joint	105	73	36629994 E 4380236 N
166	Joints	138 206 143 143 164 151 145 148 165 163 179 153 150 156 156 157 147	60 87 85 75 67 64 82 76 73 78 60 64 67 61 67 85 73	36630400 E 4380357 N
167	Foliation	122	90	36628699 E 4377226 N
168	Fold	151 143 146 169 192 206 206 222 233 241 247	74 72 71 75 77 71 74 71 66 78 83	36629557 E 4376509 N
169	Bed	148	77	36629557 E 4376509 N
170	Bed	300	86	36629627 E 4376448 N
171	Bed	326	52	36629880 E 4376220 N
172	Bed	320	41	36629767 E 4376170 N
173	Bed	136	82	36629747 E 4376149 N
174	Bed	147	32	36629749 E 4376150 N
175	Bed	337	90	36629822 E 4376000 N

176	Bed	336	83	36629930 E 4376075 N
177	Bed	332	79	put on tne map
178	Foliation	133	57	36630018 E 4375744 N
179	Bed	142	55	36629707 E 4376167 N
180	Homocline	185 173 178 172 176 160 152 150 130	39 67 34 50 61 48 44 69 81	
181	Fold	156 138 126 138 283 289 272 265	69 57 67 72 70 63 66 58	
182	Bed	143	69	36630571 E 4375508 N
183	Foliation	119	66	36630609 E 4375681 N
184	Bed	118	71	36630507 E 4375755 N
185	Bed	150	74	36630477 E 4375780 N
186	Bed	155	69	36630441 E 4375774 N
187	Bed	323	68	
188	Bed	285	90	36632179 E 4374008 N
189	Bed	123	66	36631587 E 4374477 N
190	Bed	173 116 98 126 142	44 47 47 39 30	Keçikalesi hill
191	Bed	138	39	36631511 E 4374392 N
192	Fold	171 144 152 162 146 139 122 152 128 116 113 100	23 26 24 24 29 26 34 29 50 73 77 85	
193	Bed	180	18	36631387 E 4374407 N
194	Joint	119 129 127 127 112 123 131 118 113 125 115 109 118 117	66 62 66 73 70 67 57 43 45 56 55 57 62 66	36629205 E 4390262 N

195	Joint	106 109 124 130 70 73 92 80 118 119 112 109 199 202 109 108 200 114 137 113	60 58 54 60 68 54 60 63 46 54 58 62 83 80 64 59 76 68 65 71	36629205 E 4390262 N
196	Joint	347 71 66 339 90 341 75 334 254 74 341 282 302 272 250 79 339 332 332 83 325 338 79 64 63 273 266 282	74 71 70 90 85 83 90 83 25 79 84 23 19 24 24 69 82 87 83 73 90 88 90 89 80 74 23 20	36633548 E 4390195 N
197	Mineral Foliation	261 273 273 293 294 292	14 26 14 18 26 20	36633548 E 4390195 N
198	Fault Plane	125	87	36620800 E 4395318 N
199	Bed	92	79	36623929 E 4397234 N
200	Bed	98	63	36623742 E 4397139 N
201	Bed	85	31	36623661 E 4396976 N
202	Bed	77	43	36623513 E 4396942 N
203	Bed	77	31	36623386 E 4396909 N
204	Bed	48	25	36623236 E 4396779 N
205	Bed	57	31	36623102 E 4396639 N
206	Bed	56	26	36622956 E 4396523 N
207	Bed	31	46	36622810 E 4396446 N

208	Bed	312	41	36623056 E 4396939 N
209	Bed	49	15	36623251 E 4397042 N
210	Bed	194	4	36625521 E 4377347 N
211	Bed	143	12	36625363 E 4376926 N
212	Bed	307	54	36625396 E 4376798 N
213	Bed	94	10	36625504 E 4376719 N
214	Bed	138	23	36625353 N 4376604 N
215	Bed	135	17	36625194 E 4376918 N
216	Bed	173	26	36625341 E 4377280 N
217	Bed	165	9	36625088 E 4377622 N
218	Bed	113	8	36624862 E 4376959 N
219	Bed	122	20	36624836 E 4376593 N
220	Joint	323	90	36624740 E 4376776 N
221	Bed	133	15	36624742 E 4376787 N
222	Bed	142	12	36624254 E 4377340 N
223	Bed	195	13	36624102 E 4377503 N
224	Bed	248	14	36623295 E 4376630 N
225	Bed	261	5	36622989 E 4376809 N
226	Bed	290	5	36622640 E 4377476 N
227	Bed	210	8	36622732 E 4377815 N
228	Bed	194	14	36622817 E 4378027 N
229	Bed	353	11	36622882 E 4378151 N
230	Bed	266	17	36622585 E 4378636 N
231	Bed	202	5	36623030 E 4379076 N
232	Bed	168	11	36623030 E 4378438 N
233	Bed	88	43	36623191 E 4378586 N
234	Bed	92	18	36623609 E 4378737 N
235	Bed	130	29	36623964 E 4378725 N
236	Bed	119	30	36623037 E 4381382 N
237	Bed	70	12	36622504 E 4381014 N
238	Bed	342	58	36622924 E 4380843 N
239	Bed	331	59	36622956 E 4380843 N
240	Bed	158	59	36623282 E 4380719 N
241	Bed	77	58	36623219 E 4380599 N
242	Bed	148	69	36623222 E 4380625 N
243	Bed	297	88	36623192 E 4380569 N
244	Bed	258	43	36623139 E 4380552 N
245	Bed	293	19	36622941 E 4380659 N
246	Bed	242	26	36622907 E 4380403 N
247	Bed	232	78	36623042 E 4380290 N

248	Bed	5	55	36623035 E 4380248 N
249	Bed	315	33	36623207 E 4380243 N
250	Bed	67	15	36623191 E 43780190 N
251	Bed	40	38	36623200 E 4380167 N
252	Bed	304	58	36623264 E 4380217 N
253	Bed	338	61	
254	Bed	12	44	36623246 E 4380198 N
255	Bed	354	36	36623248 E 4380207 N
256	Bed	0	36	36623254 E 4380220 N
257	Bed	332	32	36623252 E 4380223 N
258	Bed	358	49	36623254 E 4380223 N
259	Bed	351	63	36623257 E 4380227 N
260	Bed	351	64	?
261	Bed	48	42	36623205 E 4380171 N
262	Bed	48 51 50 46 57	34 29 43 36 57	36623211 E 4380177 N
263	Bed	56	36	36623179 E 4380155 N
264	Bed	49	30	36623036 E 4380060 N
265	Bed	66	27	36622978 E 4380019 N
266	Bed	91	58	36622840 E 4379974 N
267	Bed	88	60	36622762 E 4379965 N
268	Bed	92	55	36622626 E 4379952 N
269	Bed	58	61	36622462 E 4379966 N
270	Bed	270	49	36622757 E 4380363 N
271	Bed	92	51	36622409 E 4380021 N
272	Bed	87	55	36622575 E 4380186 N
273	Bed	133	66	36622631 E 4380210 N
274	Bed	293	50	36622624 E 4380288 N
275	Bed	274	40	36622579 E 4380481 N
276	Bed	251	31	36622409 E 4380512 N
277	Bed	64	26	36622328 E 4380587 N
278	Bed	152	14	36621598 E 4381011 N
279	Bed	285	55	36622096 E 4380574 N
280	Bed	78	18	36621929 E 4380430 N
281	Bed	69	41	36621931 E 4380432 N
282	Bed	67	45	36622124 E 4380235 N
283	Bed	70	36	36622131 E 43799911 N

284	Fold	334 331 335 342 345 349 2 108 129 146 122 128 88 106	57 46 39 37 42 33 22 21 19 17 16 13 9 14	36622110 E 4379906 N
285	Bed	58	33	36622108 E 4379986 N
286	Bed	79	75	36621313 E 4380020 N
287	Bed	78	78	36621315 E 4379633 N
288	Bed	336	54	36621320 E 4380197 N
289	Bed	72	55	36621331 E 4380232 N
290	Bed	96	45	36621528 E 4380153 N
291	Bed	106	24	36626464 E 4375879 N
292	Bed	116	27	36626308 E 4375951 N
293	Bed	117	27	36626175 E 4376056 N
294	Bed	116	23	366260533 E 4376161 N
295	Bed	130	26	
296	Bed	146	36	36626755 E 4375586 N
297	Bed	145	6	36627827 E 4374842 N
298	Bed	129	9	36627967 E 4374634 N
299	Bed	151	10	36627891 E 4374433 N
300	Bed	148	13	36627925 E 4374325 N
301	Bed	122	12	36627937 E 4374192 N
302	Bed	182	11	36627907 E 4373990 N
303	Bed	207	12	36627663 E 4373809 N
304	Bed	282	13	36627398 E 4373483 N
305	Bed	271	6	36627280 E 4373497 N
306	Bed	275	10	36627182 E 4373500 N
307	Bed	304	7	36627090 E 4373463 N
308	Bed	276	6	36627012 E 4373525 N
309	Bed	276	9	36626832 E 4373525 N
310	Bed	309	10	36626638 E 4373593 N
311	Bed	242	14	36626420 E 4373574 N
312	Bed	282	7	36626238 N 4373731 N
313	Bed	346	12	36625749 E 4373839 N
314	Bed	305	14	36625178 E 4374048 N
315	Bed	290	10	36624801 E 4374145 N
316	Bed	308	14	36624245 E 4374356 N
317	Bed	321	12	36623545 E 4375101 N

318	Bed	296	10	36623353 E 4375244 N
319	Bed	310	13	36623171 E 4375412 N
320	Bed	319	19	36622998 E 4375521 N
321	Bed	312	11	36622800 E 4375798 N
322	Bed	316	7	36622763 E 4376126 N
323	Bed	297	16	36621681 E 4376581 N
324	Bed	293	16	36621341 E 4376661 N
325	Bed	292	12	36621029 E 4376704 N
326	Bed	288	14	36620757 E 4376823 N
327	Bed	198	28	
328	Bed	228	20	
329	Bed	112	20	36623740 E 4383800 N
330	Bed	84	44	36621981 E 4379875 N
331	Bed	345	55	36623110 E 4380568 N
332	Bed	232	16	36623081 E 4381485 N
333	Bed	46	52	36623071 E 4380244 N
334	Bed	92	63	36620262 E 4380078 N
335	Bed	92	62	36620346 E 4380024 N
336	Bed	144	42	36619334 E 4396249 N
337	Bed	134	43	Near Süleymanlı v.
338	Bed	6	26	36627879 E 4367002 N
339	Joint	21	43	36627026 E 4366477 N
340	Bed	43	42	36627026 E 4366358 N
341	Joint	328 331 330 332 337 304 301 311 332 336 303 300 337 301 302 299 282 324 303 308 303 300 304	84 87 87 87 72 64 65 60 58 70 76 66 90 58 61 62 49 70 65 76 68 64 67	36627557 E 4385988 N
342	Joint	146	25	36630770 E 4384649 N
343	Joint	93	68	36631269 E 4383778 N

344	Joint	187 187 143 131 120 134 139 134 135 169 168 150 154 153 165 160	46 51 41 39 49 43 41 56 44 29 35 49 48 50 63 57	36631260 E 4383656 N
345	Mineral Foliation	260 267 302 312 324 328 347 346 333 346	62 56 85 43 64 40 53 45 60 53	36631260 E 4383656 N
346	Bed	92	20	Put on the map
347	Bed	179	9	36621786 E 4398505 N
348	Bed	176	8	36621631 E 4398460 N
349	Bed	90	2	36621530 E 4398645 N
350	Bed	132	2	36621330 E 4398408 N
351	Bed	111	11	36621135 E 4398055 N
352	Bed	33	56	36622744 E 4398192 N
353	Bed	12	81	36623037 E 4398539 N
354	Bed	333	13	36624832 E 4368471 N
355	Bed	284	29	36621259 E 4371717 N
356	Bed	277	9	36621264 E 4371470 N
357	Bed	271	13	36621546 E 4371972 N
358	Bed	213	35	36631699 E 4373784 N
359	Contact Plane	30	52	36631536 E 4374791 N
360	Bed	313	73	36630968 E 4375481 N
361	Bed	127	77	36630780 E 4375452 N
362	Bed	228	58	36630661 E 4375485 N
363	Bed	145	74	36630589 E 4375455 N
364	Foliation	222	59	36630589 E 4375455 N

365	Deformation Band	309 253 262 262 306 285 247 253 304 296 287 255 265 271 264 270 339 236 268 237 262 250 288 276	74 58 66 63 50 60 66 65 76 77 50 58 67 68 50 58 29 28 62 45 50 57 52 52	along ***r7***
366	Bed	123	90	36631096 E 4375242 N
367	Bed	112 80	14 4	near Mahmutlu
368	Bed	18 30	9 0	near Greenhouses
369	Bed	283	35	36620700 E 4372014 N
370	Bed	269	61	36620564 E 4372011 N
371	Bed	262	25	36620424 E 4372033 N
372	Bed	95	75	
373	Bed	76	90	
374	Bed	113	31	36618920 E 4396581 N
375	Bed	132	39	3661884 E 4396705 N
376	Bed	109	33	36618435 E 4396738 N
377	Bed	90	58	36618669 E 4396974 N
378	Bed	105	85	36618473 E 4396967 N
379	Bed	297 344	11 4	Near KRC
380	Bed	270	90	36618352 E 4397174 N
381	Bed	279	88	36618474 E 4397274 N
382	Bed	271	77	36618575 E 4397614 N
383	Bed	134	47	
384	Bed	138	39	36619225 E 4396324 N
385	Bed	152	45	36619477 E 4399302 N
386	Bed	143	38	36619431 E 4399401 N
387	Bed	153	34	36619578 E 4399097 N
388	Bed	132	38	36619635 E 4398708 N
389	Bed	30	44	36625369 E 4398181 N
390	Bed	286	12	36621760 E 4400077 N
391	Foliation	282	27	36621729 E 4400905 N
392	Foliation	279	12	36620728 E 4400525 N

APPENDIX B: RESULTS OF PALEOSTRESS ANALYSIS

5

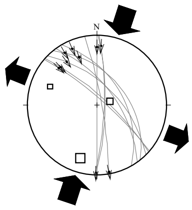

σ_1=198°/13°
σ_2=74°/68°
σ_3=292°/18°
Φ = 0.4
Δ=6°

11

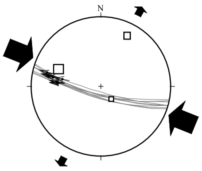

σ_1=293°/23°
σ_2=27°/11°
σ_3=141°/64°
Φ = 0.2
Δ=6°

6

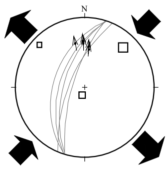

σ_1=44°/12°
σ_2=192°/76°
σ_3=313°/6°
Φ = 0.6
Δ=3°

12

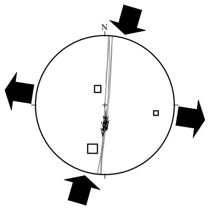

σ_1=196°/23°
σ_2=336°/61°
σ_3=99°/17°
Φ =0.5
Δ=6°

7

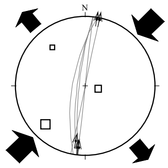

σ_1=225°/13°
σ_2=102°/68°
σ_3=319°/18°
Φ = 0.3
Δ=6°

14

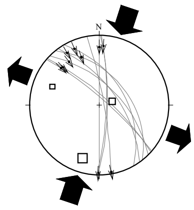

σ_1=164°/23°
σ_2=23°/61°
σ_3=261°/17°
Φ = 0.5
Δ=8°

8

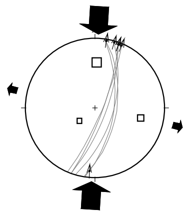

σ_1=2°/23°
σ_2=102°/22°
σ_3=231°/57°
Φ = 0.2
Δ=3°

15

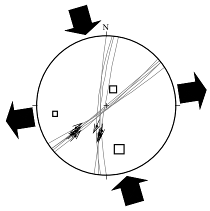

σ_1=196°/23°
σ_2=287°/2°
σ_3=21°/67°
Φ = 0.1
Δ=5°

8

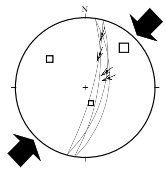

σ_1=44°/12°
σ_2=309°/23°
σ_3=160°/63°
Φ = 0.4
Δ=4°

16

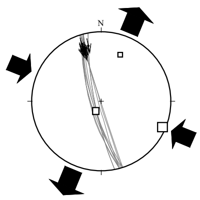

σ_1=113°/2°
σ_2=209°/72°
σ_3=22°/18°
Φ = 0.6
Δ=3°

9

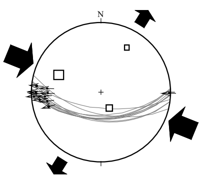

σ_1=293°/23°
σ_2=152°/61°
σ_3=30°/17°
Φ = 0.1
Δ=7°

17

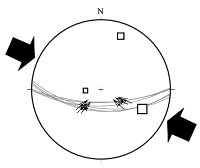

σ_1=115°/23°
σ_2=21°/11°
σ_3=267°/64°
Φ = 0.3
Δ=10°

10

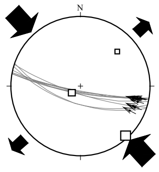

σ_1=138°/2°
σ_2=234°/72°
σ_3=47°/18°
Φ = 0.1
Δ=3°

18

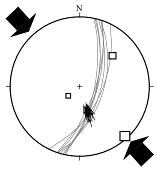

σ_1=138°/2°
σ_2=47°/24°
σ_3=232°/66°
Φ = 0.6
Δ=4°

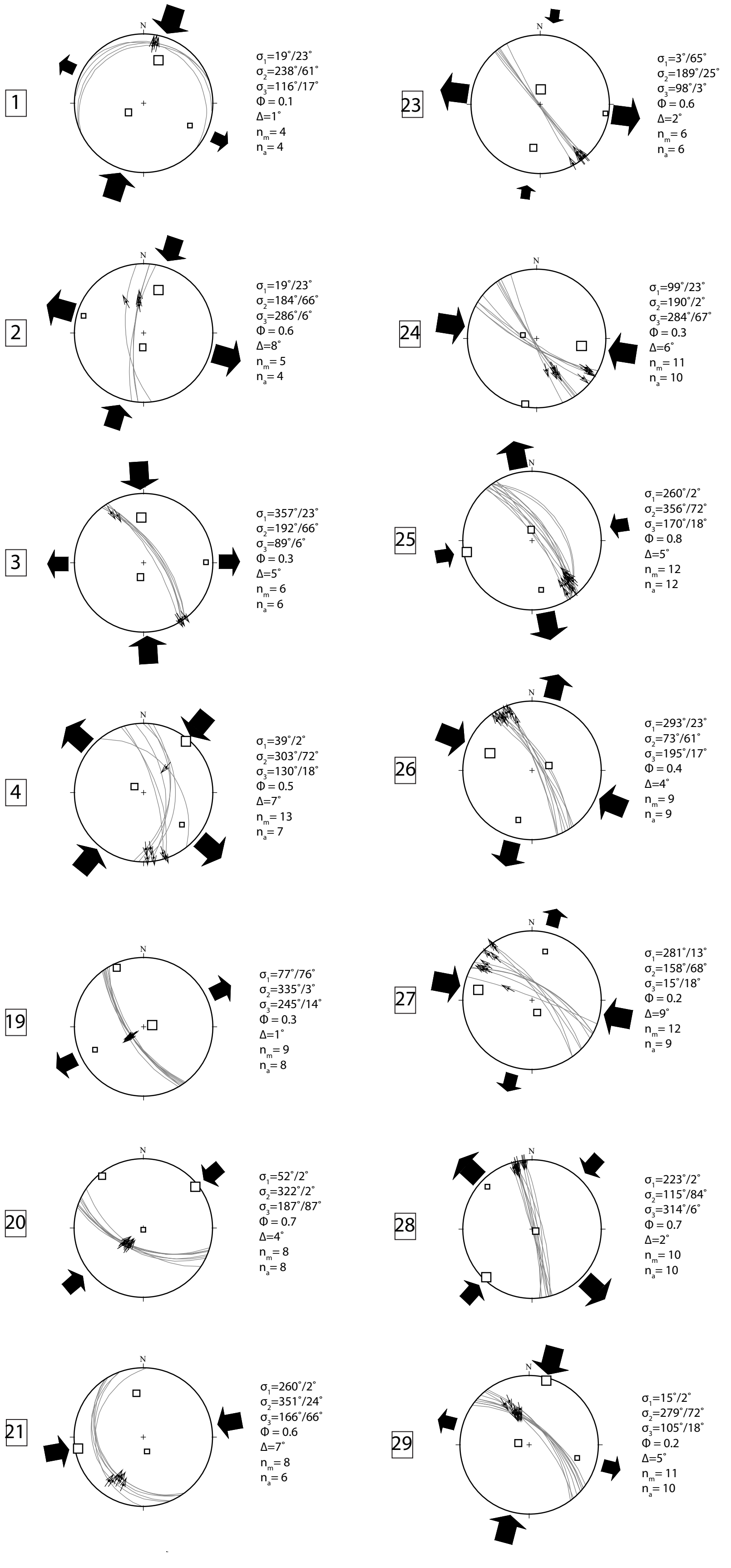
1
σ_1=19°/23°
σ_2=238°/61°
σ_3=116°/17°
Φ = 0.1
Δ=1°
n_m= 4
n_a= 4
23
σ_1=3°/65°
σ_2=189°/25°
σ_3=98°/3°
Φ = 0.6
Δ=2°
n_m= 6
n_a= 6
2
σ_1=19°/23°
σ_2=184°/66°
σ_3=286°/6°
Φ = 0.6
Δ=8°
n_m= 5
n_a= 4
24
σ_1=99°/23°
σ_2=190°/2°
σ_3=284°/67°
Φ = 0.3
Δ=6°
n_m= 11
n_a= 10
3
σ_1=357°/23°
σ_2=192°/66°
σ_3=89°/6°
Φ = 0.3
Δ=5°
n_m= 6
n_a= 6
25
σ_1=260°/2°
σ_2=356°/72°
σ_3=170°/18°
Φ = 0.8
Δ=5°
n_m= 12
n_a= 12
4
σ_1=39°/2°
σ_2=303°/72°
σ_3=130°/18°
Φ = 0.5
Δ=7°
n_m= 13
n_a= 7
26
σ_1=293°/23°
σ_2=73°/61°
σ_3=195°/17°
Φ = 0.4
Δ=4°
n_m= 9
n_a= 9
19
σ_1=77°/76°
σ_2=335°/3°
σ_3=245°/14°
Φ = 0.3
Δ=1°
n_m= 9
n_a= 8
27
σ_1=281°/13°
σ_2=158°/68°
σ_3=15°/18°
Φ = 0.2
Δ=9°
n_m= 12
n_a= 9
20
σ_1=52°/2°
σ_2=322°/2°
σ_3=187°/87°
Φ = 0.7
Δ=4°
n_m= 8
n_a= 8
28
σ_1=223°/2°
σ_2=115°/84°
σ_3=314°/6°
Φ = 0.7
Δ=2°
n_m= 10
n_a= 10
21
σ_1=260°/2°
σ_2=351°/24°
σ_3=166°/66°
Φ = 0.6
Δ=7°
n_m= 8
n_a= 6
29
σ_1=15°/2°
σ_2=279°/72°
σ_3=105°/18°
Φ = 0.2
Δ=5°
n_m= 11
n_a= 10

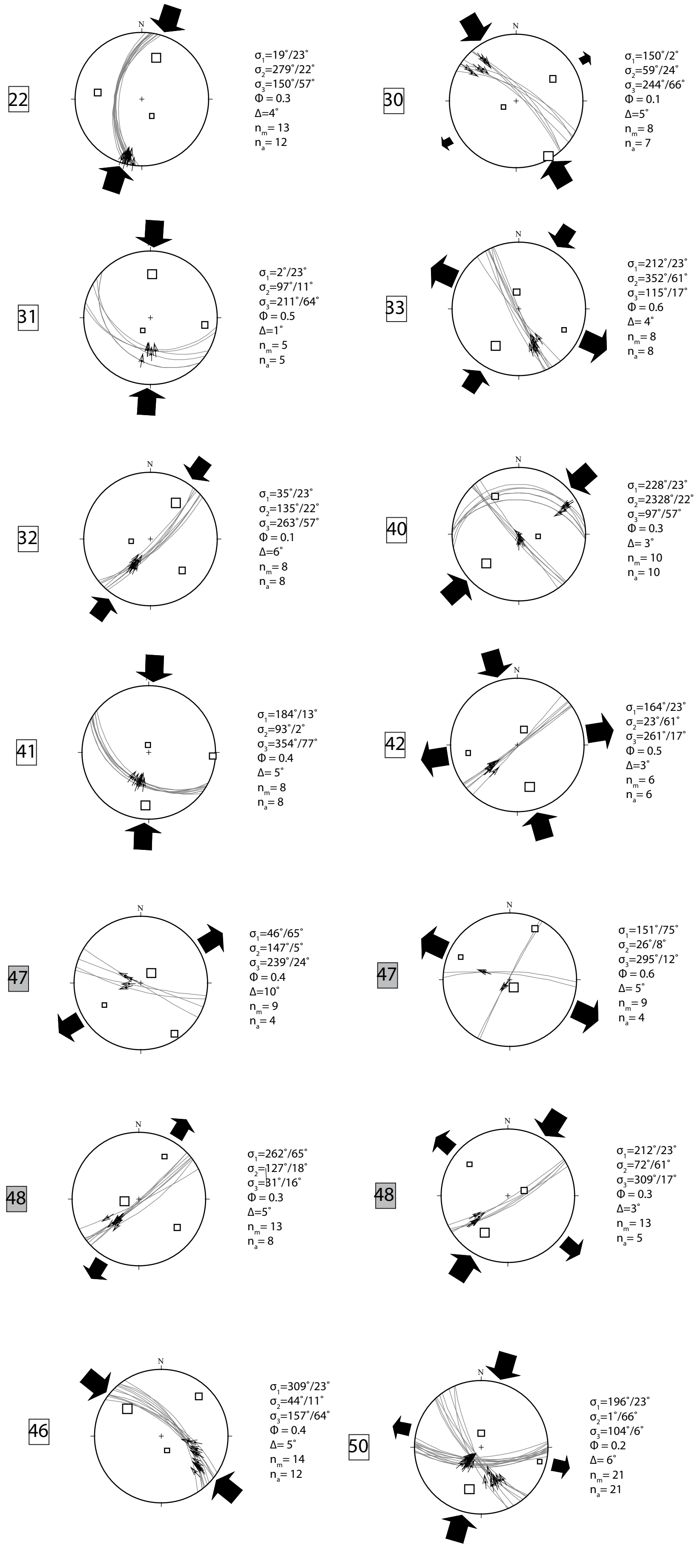
22
σ_1=19°/23°
σ_2=279°/22°
σ_3=150°/57°
Φ = 0.3
Δ=4°
n_m= 13
n_a= 12
30
σ_1=150°/2°
σ_2=59°/24°
σ_3=244°/66°
Φ = 0.1
Δ=5°
n_m= 8
n_a= 7
31
σ_1=2°/23°
σ_2=97°/11°
σ_3=211°/64°
Φ = 0.5
Δ=1°
n_m= 5
n_a= 5
33
σ_1=212°/23°
σ_2=352°/61°
σ_3=115°/17°
Φ = 0.6
Δ= 4°
n_m= 8
n_a= 8
32
σ_1=35°/23°
σ_2=135°/22°
σ_3=263°/57°
Φ = 0.1
Δ=6°
n_m= 8
n_a= 8
40
σ_1=228°/23°
σ_2=2328°/22°
σ_3=97°/57°
Φ = 0.3
Δ= 3°
n_m= 10
n_a= 10
41
σ_1=184°/13°
σ_2=93°/2°
σ_3=354°/77°
Φ = 0.4
Δ= 5°
n_m= 8
n_a= 8
42
σ_1=164°/23°
σ_2=23°/61°
σ_3=261°/17°
Φ = 0.5
Δ=3°
n_m= 6
n_a= 6
47
σ_1=46°/65°
σ_2=147°/5°
σ_3=239°/24°
Φ = 0.4
Δ=10°
n_m= 9
n_a= 4
47
σ_1=151°/75°
σ_2=26°/8°
σ_3=295°/12°
Φ = 0.6
Δ= 5°
n_m= 9
n_a= 4
48
σ_1=262°/65°
σ_2=127°/18°
σ_3=31°/16°
Φ = 0.3
Δ=5°
n_m= 13
n_a= 8
48
σ_1=212°/23°
σ_2=72°/61°
σ_3=309°/17°
Φ = 0.3
Δ=3°
n_m= 13
n_a= 5
46
σ_1=309°/23°
σ_2=44°/11°
σ_3=157°/64°
Φ = 0.4
Δ= 5°
n_m= 14
n_a= 12
50
σ_1=196°/23°
σ_2=1°/66°
σ_3=104°/6°
Φ = 0.2
Δ= 6°
n_m= 21
n_a= 21

49

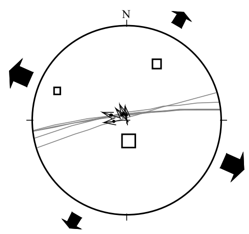
N
σ_1=175°/65°
σ_2=28°/21°
σ_3=293°/12°
Φ = 0.3
Δ=7°
n_m= 5
n_a= 5

51

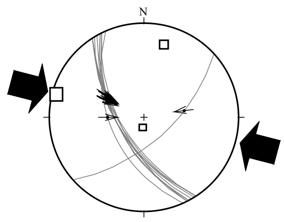
N
σ_1=285°/2°
σ_2=15°/12°
σ_3=185°/78°
Φ = 0.4
Δ=5°
n_m= 11
n_a= 11